Pergamon

Prog. Crystal Growth and Charact. Vol. 29, pp. 85–159, 1994
Copyright © 1995 Elsevier Science Ltd
Printed in Great Britain. All rights reserved
0960–8974/94 $26.00

0960–8974(95)00008–9

MOLECULAR BEAM EPITAXY OF $Hg_{1-x}Cd_xTe$: GROWTH AND CHARACTERIZATION

Jean-Pierre Faurie

Physics Department, University of Illinois at Chicago, IL, U.S.A.

CONTENTS

1. INTRODUCTION

$Hg_{1-x}Cd_xTe$ alloys have heen extensively studied for the last thirty years for infrared device applications. Due to its technological importance, $Hg_{1-x}Cd_xTe$ has motivated numerous studies regarding its growth. Although the growth of bulk material has been improved and provides high quality material, epitaxial growth methods have been developed in response to device construction requirements.

Among these epitaxial growth techniques, Liquid-Phase Epitaxy (LPE), which has established very high standards, is challenged by Molecular Beam Epitaxy (MBE) and Organo-Metallic Vapor Phase Epitaxy (OMVPE). LPE and OMVPE growth techniques are treated in detail elsewhere in this volume.

MBE, which has been developed to grow $Hg_{1-x}Cd_xTe$ since 1981 [1] is the epitaxial technique using the lowest growth temperature for this alloy. In MBE, the growth temperature never exceed 200°C, whereas much higher temperatures (400°C and above) are used for LPE or OMVPE. Thus in MBE, interdiffusion processes are very limited. Many experiments have been carried out, mostly in HgTe-CdTe superlattices, in order to determine the extent of the interdiffusion at the interface. Without entering into the detail of such studies, where parameters such as the crystallographic orientation and the nature of the ternary alloys involved are playing a role, it has been shown that in the MBE growth temperature range (170-190°C) the interdiffusion is, in the worse scenario, limited to a few monolayers. Actually, in most studies it was undetected [2-5]. Obviously, this is no longer the case when the growth temperature is raised to 250°C and above. The diffusion is for example utilized during the OMVPE-IMP technique in order to alloy the HgTeCdTe multiple layer structure. Therefore, MBE has a much higher potential than LPE or OMVPE in the fabrication of heterostructures, due to its potential in the control of composition and doping profiles.

Another important advantage is the possibility of controlling the different steps of the growth *in situ* since MBE occurs in an ultra-high vacuum environment.

In addition, MBE which can be used to grow very large area epilayers on alternative sustrates such as GaAs and silicon with excellent thickness and composition uniformity has the capability of a full *in situ* growth process from substrate to passivating layer which should eliminate the surface-interface contamination problem. In summary, MBE is the most appropriate technique to achieve bandgap and interface engineering. This represents a distinct advantage in terms of flexibility, performance and cost. However, several problems have been encountered during the development of MBE as applied to HgCdTe which have delayed its full implementation.

Mercury has a very low condensation coefficient. At 185°C, the Hg-flux required to grow $Hg_{1-x}Cd_xTe$ (x = 0.22), on (211)B CdZnTe substrate, suitable for IR photodiodes is in the mid 10^{16} at cm^{-2} s^{-1} which is between 20 to 50 times higher than the amount of mercury incorporated in the epitaxial film. Furthermore, this condensation coefficient decreases exponentially when the growth temperature increases. Hence the growth should occur at low temperature. However, the growth temperature should not be too low in order to obtain a good crystallinity. Therefore, the growth by MBE is limited to a very narrow range in temperature. In addition, MBE growth demands that the couple Mercury flux (F_{Hg}) and surface temperature (T_s) be very precisely controlled and stabilized during growth.

Formation of microtwin and point defect, which might have their specificity for MBE grown material because of low growth temperature, has also been a major hurdle regarding the growth in the (111)B direction.

Lack of understanding of the residual doping and difficulties in the control of p-type doping are still important problems to be solved. However, it should be mentioned that the lack of understanding concerning background doping is not specific to MBE.

In recent years, the growth of HgCdTe by MBE has made impressive progress towards a solution to the problems arising from structural, electrical and optical properties. Infrared photodiodes with excellent performance are currently fabricated on MBE grown layers.

MBE has now reached a stage where it will be utilized in the manufacturing of Focal Plan Arrays (FPA). The purpose of this review paper is to give an updated overview of the main problems and of the major accomplishments regarding the growth and characterization of $Hg_{1-x}Cd_xTe$ alloy by MBE. Heterostructures, superlattices, alternative substrates and device fabrication, which all are important MBE related topics, are not discussed in this chapter.

2. EVAPORATION OF II-VI SEMICONDUCTOR COMPOUNDS

Although it is often stated that kinetics controls MBE, thermodynamics still control several growth parameters such as fluxes from effusion cells and also plays a role in the reevaporation from the growing layer. On the other hand, only experiments will indicate if the P-T phase diagram calculated under equilibrium for HgCdTe can be used to predict intrinsic doping, due to stoichiometric deviation, in MBE as-grown layers.

The evaporation of II-VI compounds with a zinc-blende structure depends on the presence or the absence of mercury in the semiconductor. The wide gap materials such as CdTe or ZnTe present a congruent evaporation whereas the Hg based compounds experience a gross incongruence. This is due to the fact that mercury is weakly bonded to the tellurium and consequently it is preferentially reevaporated. This well-known phenomena has been experimentally proven by Farrow *et al.* for $Hg_{1-x}Cd_xTe$ [6].

The knowledge of the evaporation of the semiconductor is important since the growth process depends on the incoming flux of atoms and molecules, surface kinetics, desorption and reevaporation. Both incoming flux and reevaporation should be known from equilibrium vapor pressure curves. Incoming atoms or molecules can be generated from the compound itself or from the constituent elements.

The evaporation of elements such as cadmium, tellurium and mercury along with the sublimation of semiconductor compounds such as CdTe, HgTe and $Hg_{1-x}Cd_xTe$ is briefly presented in this chapter.

2.1. *Elements*

Group II elements are evaporated as individual atoms whereas for group VI elements polyatomic molecules are found in the gas phase. Concerning tellurium, Te_2 is the dominant species but the polymerization degree is higher for selenium and sulfur. For a given range of temperature, the vapor pressure over a pure element can be calculated from a relation such as:

$$\log P^\circ = a - bT^{-1} \text{ where } P^\circ \text{ is in atmosphere} \qquad (1)$$

Table 1 shows the values of coefficients a and b for Cd, Te and Hg.

Table 1: Evaporation of the chemical elements, $\log P^\circ(\text{atm}) = a - bT^{-1}$

Elements	Species in gas phase	a	b	Comments	Reference
Cd	Cd	5.96	5808	T<321°C	7
Cd	Cd	5.12	5317	T>321°C	8
Te	Te2	6.87	7594	T<487°C	9
Te	Te2	4.72	5960	T>487°C	10
Hg	Hg	5.03	3157	—	11

2.2. *Compounds*

The evaporation of most II-VI compounds as mentioned previously with the exception of the Hg-based compounds is nearly congruent [12]. Congruency represents an isothermal equilibrium since the ratio between the species evaporated is identical to the composition of the solid within the solid field (i.e. 10^{-3} % for CdTe). In MBE, congruent compounds can be grown in principle from a single effusion cell. However depending on the growth temperature, the crystallographic orientation and the stoichiometry targeted a second cell containing one of the elements might be necessary.

The equilibrium relation for II–VI as well as for III–V compounds can be written as follows:

$$AB(s) \leftrightarrow A(g) + 1/n\ B^n(g) \qquad (2)$$

where s and g denote respectively solid and gas phases and n the polymerization degree of B in the vapor phase. The equilibrium constant Kp for the reaction is related to the partial pressure of gas species by the mass action relation

$$Kp = P_A \,.\, P_{Bn}^{1/n} \qquad (3)$$

In addition, P_A (P_{Bn}) should be less than the vapor pressure over the pure species $P_A{}^o$ ($P_{Bn}{}^o$) otherwise A(B) would condense as a new phase. This constraint implies that when PA (PB) is at its maximum value then $P_B(P_A)$ is minimum

$$P_A^o\, P_{Bn\,\min}^{1/n} = Kp \qquad (4)$$

$$P_{A\,min} \cdot P_{Bn}^{o1/n} = Kp \qquad (5)$$

The equilibrium pressures over a compound are controlled and linked by relations (3,4 and 5) For each element, the equilibrium pressures are found inside a domain delineated by the log P vs 1/T plot.

2.2.1. *CdTe*

The evaporation of CdTe, which is congruent, gives cadmium atoms and tellurium molecules:

$$CdTe(s) \rightarrow Cd(g) + 0.5\ Te_2(g) \qquad (6)$$

II-VI compounds are well-known to present much larger stoichiometry deviation than III-V compounds because of their larger ionicity character. For CdTe this stoichiometry deviation is in the range [13] of 10^{-5} and accounts for the large change of several orders of magnitude in pressure for an element at a given temperature between the rich and the poor phase boundary.

2.2.2. *HgTe*

In contrast to CdTe, the sublimation of HgTe is highly non congruent [14], Hg being the dominant species in the vapor phase. Upon heating HgTe the compound preferentially loses its mercury. It has been observed that after 1 hour of heating at 210°C, a porous Te layer 5 µm thick is left on the surface of the compound [15]. The reaction of sublimation can be described by:

$$HgTe(s) \rightarrow Hg(g) + (1-\varepsilon)Te(s) + \varepsilon/2\ Te_2(g) \qquad (7)$$

where ε is very small at low temperature. Hence HgTe could be used as a mercury source. However the Hg flux, which is not constant due to its diffusion process through the tellurium porous layer, is getting slower with time. Therefore, a decrease in the Hg flux is observed at a constant temperature making a mercury cell containing HgTe, a highly unreliable Hg source.

There is no overlap between log P vs 1/T diagrams of Hg and Te. A difference of several orders of magnitude is observed between P_{Hgmin} and P_{Temax} which explains the highly non congruent evaporation of HgTe.

2.2.3. *$Hg_{1-x}Cd_xTe$*

The evaporation of $Hg_{1-x}Cd_xTe$ is also highly non congruent [6]. It has been shown that the activity of CdTe and HgTe compounds in the alloy is practically equal to x and (1-x) within the whole range of composition [11,16]. In other words, $Hg_{1-x}Cd_xTe$ can be considered as an alloy of (x)CdTe and (1-x)HgTe. Therefore, it can be written that:

$$K_{CdTe/Hg_{1-x}Cd_xTe} = P_{Cd} \bullet P_{Te_2}{}^{1/2} = (x)K_{CdTe} \qquad (8)$$

$$K_{HgTe/Hg_{1-x}Cd_xTe} = P_{Hg} \bullet P_{Te_2}{}^{1/2} = (1-x)K_{HgTe} \qquad (9)$$

where K_{CdTe} and K_{HgTe} are respectively the equilibrium constants of CdTe and HgTe.

It is also required that the pressure of an element cannot exceed the pressure over the pure element. From relation (8) and (9), when $P_{Hg} = P^{o}_{Hg}$ then P_{Cd} also reaches also its maximum because P_{Te_2} is minimum. However, P_{Cdmax} is much lower than P^{o}_{Cd} when $x < 1$. Due to its important loss in mercury $Hg_{1-x}Cd_xTe$, which should be written $(Hg_{1-x}Cd_x)_{1-\delta}Te_{1+\delta}$, in order to take into account the stoichiometry deviation 6, will be evaporated under Te rich conditions. Therefore P_{Te2} is maximum, i.e. P^o_{Te2} during $Hg_{1-x}Cd_xTe$ evaporation and then P_{Hg} and P_{Cd} are minimum and close to their values over HgTe and CdTe respectively.

The pressure limits of Hg, Cd and Te over $Hg_{0.78}Cd_{0.22}Te$ and $Hg_{0.67}Cd_{0.33}Te$ alloys displayed in Figs 1 and 2 have been calculated between 100 and 300°C, which is the useful temperature range for MBE growth using the relation

$$\log K_p = \log P_A \bullet P_{Te_2}{}^{1/2} = c - dT^{-1} \qquad (10)$$

Table 2: Compound coefficient values (pressures in atmosphere)

Compound	c	d	Reference
CdTe	9.82	15,000	17,18,19
HgTe	9.33	9106	14

It is important to point out that these values have been calculated from thermodynamic data experimentally determined at higher temperatures. The extrapolation at low temperature, where MBE is carried out, is therefore questionable in terms of accuracy and also suitability for the MBE growth process (see Section 5.1).

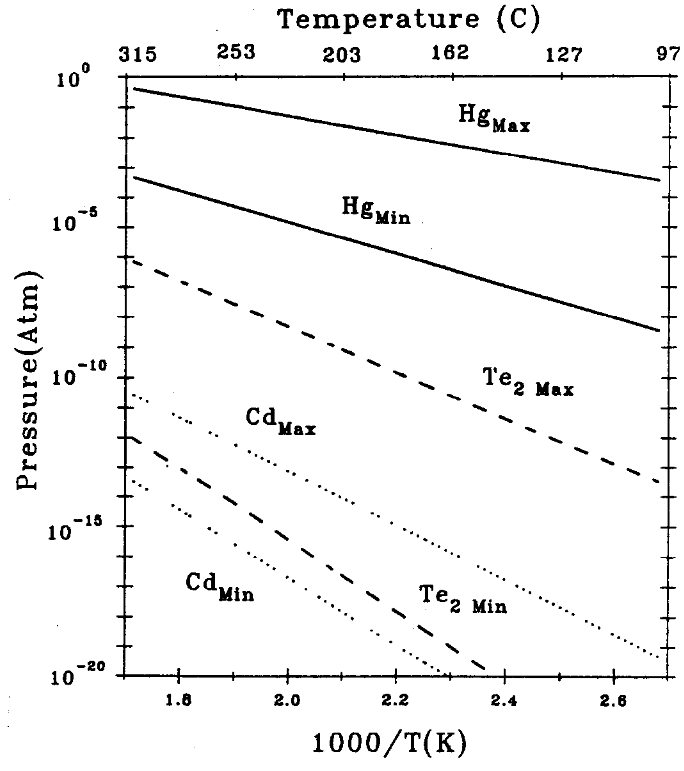

Figure 1: Partial pressure of Hg, Cd, and Te_2 along the three-phase lines for $Cd_{0.22}Hg_{0.78}Te$

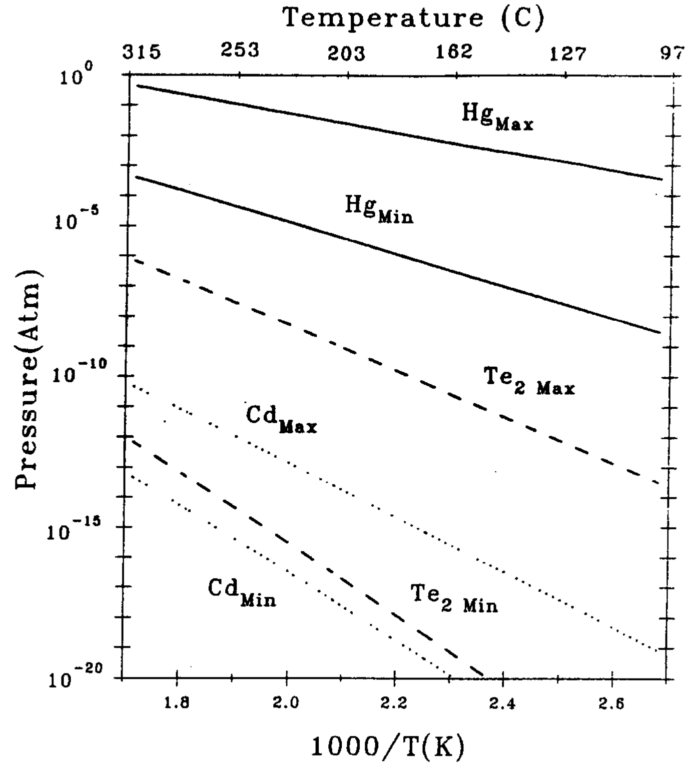

Figure 2: Partial pressure of Hg, Cd, and Te_2 along the three-phase lines for $Cd_{0.33}Hg_{0.67}Te$

2.3. *p-T Diagram and Isohole Concentration Lines for $Hg_{0.8}Cd_{0.2}Te$*

The limits of partial pressure of Hg within which the $Hg_{0.8}Cd_{0.2}Te$ solid coexists in equilibrium with its vapor, are shown in Fig. 1 between 100-300°C, and have been determined up to the melting point as it is shown in (Fig. 3). This figure also shows the calculated isohole concentration lines for native acceptor (doubly ionized Hg vacancies) defect concentrations. Figure 4 is an Arrhenius plot of the Hg vacancy concentration in the $Hg_{0.8}Cd_{0.2}Te$ crystals as a function of inverse T $(K)^{-1}$ under Hg- and Te-saturated conditions.

Needless, to say that these curves have been calculated using equilibrium constants and electrical data have been measured on annealed LPE grown HgCdTe films, where temperature equilibration is supposed to have been reached. In MBE growth, very important differences in Hg condensation coefficient have been observed for different crystallographic orientations [21]. Therefore, it will be very interesting to compare electrical data of MBA layers with hole concentrations shown by these curves. These points will be discussed in 5.1 and 6.2.

3. MBE EQUIPMENT

The large lack of congruency observed for both HgTe and $Hg_{1-x}Cd_xTe$ has important consequences concerning the growth of these semiconductor compounds by MBE. Because Hg tends to reevaporate quickly, the Hg condensation coefficient will be low at the growth temperature. Therefore, a large flux

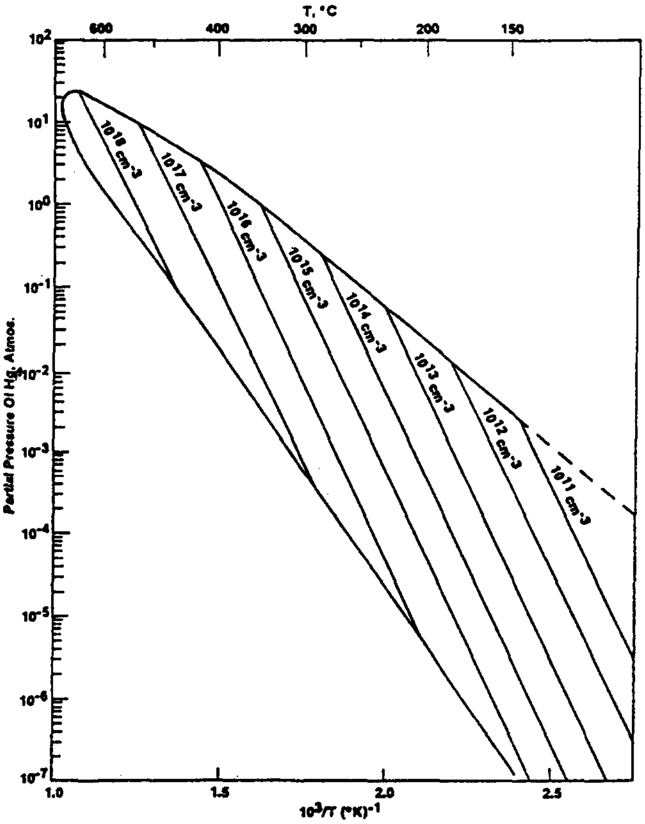

Figure 3: P-T curve and isohole concentration lines for $Hg_{0.8}Cd_{0.2}Te$ from T = 150 to 655°C.

of mercury will be necessary to grow this material. This affects the design of specific parts of the growth apparatus due to the mercury such as the effusion cell, the mercury trap and also the installation in the MBE growth chamber of an effective pumping system.

As it will be discussed later, the control in temperature of the substrate and of the cells should be very accurate and very reliable. Therefore, special attention should be also devoted to this control.

3.1. *Pumping—Mercury Removal*

The pumping of our MBE growth chambers is performed by two cryo pumps which have a special liquid nitrogen (LN_2) trap between them and the chamber. More detail on the amount of mercury required to grow these Hg based structures will be given later. However, it should be pointed out that on average 100 g of mercury are evaporated per growth run. In order to keep a low background pressure in the chamber, mercury should be removed when the gauge used to monitor the Hg flux appears to be influenced by the Hg background pressure. In the RIBER 2300 system, this situation happens when about 2 kg of mercury has accumulated. To remove mercury, the chamber is baked while the trap is kept cold. After that, pump and trap are isolated, warmed up and the mercury is collected in a reservoir located under the trap. The yield of recuperation is between 90-100%. The cryo pump is then recycled. This process can be fully automated and take at least 24 hours. In our system, after the removal and when all the LN_2 shrouds are cold, the growth chamber exhibits a background pressure in the low 10^{-9} torr range with Hg as the dominant peak.

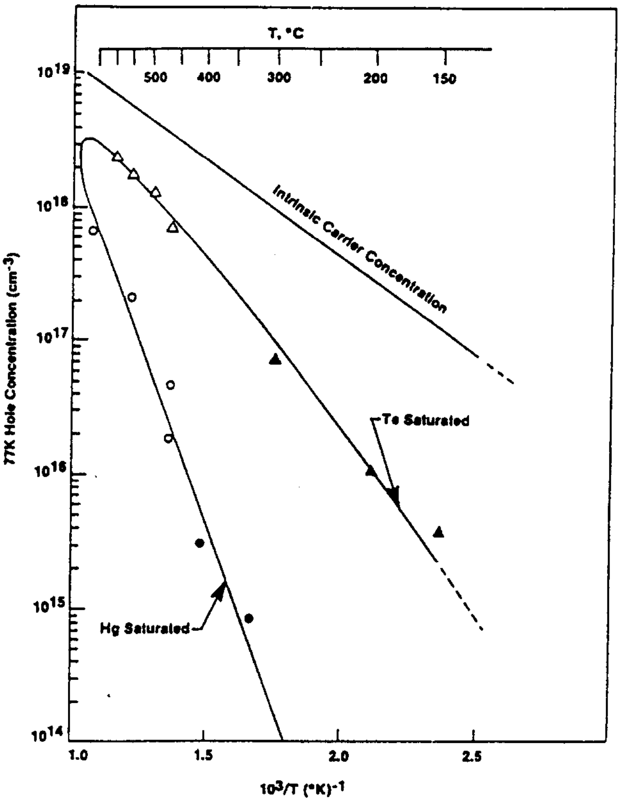

Figure 4: Hole concentration under Hg- and Te- saturated conditions as a function of temperature for $Hg_{0.8}Cd_{0.2}Te$; open symbols represent experimental data for bulk crystals and closed symbols for epitaxial films.

During growth, the pressure measured by the ion gauge which is not directly exposed to the Hg flux is in the low to mid 10^{-7} torr range.

The trap in front of the cryo pump is kept cold 24 h a day. The use of two cryo pumps is very useful. Only one pump is operating at a given time while the other is in the recycling process or on a self pumping mode i.e. ready to be used after the Hg removal.

A light Hg removal can also be carried out for a few hours after each growth run. In this case, only the bottom of the chamber is heated at about 100-150°C. Such a procedure is quite helpful since complete Hg removal process can be done less often.

The Hg removal procedure described here above is very reliable since it has been employed for more than 10 years on the systems at the University of Illinois at Chicago, where excellent $Hg_{1-x}Cd_xTe$ layers and heterostructures are still currently grown.

Hg diffusion pumps can also be used for the same purpose but it has not been demonstrated that this pumping system is more efficient than cryo pumping. In addition, the development of Hg diffusion pump technology is not making progress unlike cryo pumping. Also, a mercury diffusion pump which has an exhaust might not be suitable if safety is a concern.

3.2. *Hg Cell*

The mercury flux can be provided by an effusion cell containing either pure mercury or a mercury compound such as HgTe. The first HgCdTe layers were grown at 120°C using HgTe[1]. With HgTe, the mercury pressure is limited and changes continuously due to mercury loss in the layer making growth above 120°C almost impossible. In addition, it has been shown that layers grown at a temperature of 120°C were not of good crystalline quality. Also since the condensation coefficient for mercury experiences a drastic decrease when the substrate temperature is raised it is evident that HgTe is not suitable as a mercury source. Hence, it was necessary to develop an effusion cell containing pure mercury.

A suitable mercury cell is required to deliver a mercury flux which should be:

(i) constant during a growth of ten hours or more,

(ii) reproducible from layer to layer,

(iii) easy to change in a short period of time and

(iiii) free from impurities.

In addition to this, since a hundred grams or more of mercury is used per growth run, the cell should have a large capacity or should be connected to a mercury reservoir. It is also desirable that the cell can be replenished without breaking the vacuum.

Several kinds of Hg cells have been developed. In the Microphysics Laboratory, two different Hg cells have been designed and are currently utilized. Both have a constant Hg level in a regular cell which is connected to a large reservoir. The level can be kept constant in different ways such as by gravity or by pressure. The first cell presented in (Fig. 5) has been developed in collaboration with ISA RIBER. It uses the gravity to maintain the Hg level constant between the effusion cell and the

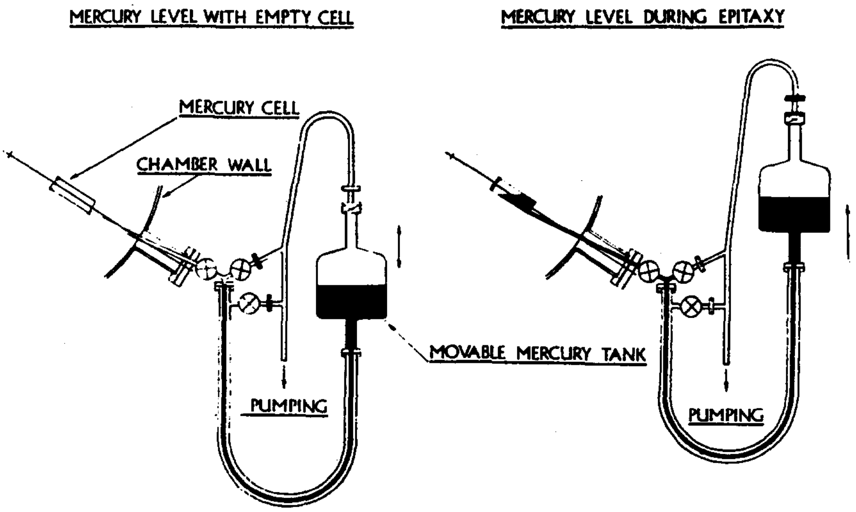

Figure 5: Moveable constant level mercury cell

reservoir. The motion of the reservoir is monitored by a sensor located in the effusion cell in order to keep the level constant. Due to the large difference in the areas of the mercury surfaces in the cell and the reservoir, 10 µm of HgCdTe grown at 185°C in the (111)B or (211)B orientation changes the mercury level by less than 1 mm. Thus, the reservoir is not moved during growth since very small height changes do not affect the mercury flux.

With the help of the sensor, the level is always the same when a new experiment starts, hence the reproducibility of such a cell is achieved which allows a good knowledge of the real value of the Hg pressure. Such knowledge is important for thermodynamic considerations. This effusion cell is small thus its temperature can be changed within a few minutes. This property can be useful for applications which require a specific grading in doping or composition. The quartz is known to have a very low reactivity with mercury. A Hg cell can be built entirely in quartz, but such a cell will have no mobile parts and no ultra high vacuum valve to isolate the external part of the cell from the growth chamber.

The Hg cell just described and developed with ISA RIBER is not entirely in quartz. In the laboratory, a quartz cell has been designed [22]. The internal part i.e. the effusion cell is identical to the one of the first cell. The external part is also entirely in quartz. The level of the mercury in the cell can be changed by acting either on a plunger (P) or on the pressure over the mercury surface in the intermediate reservoir by using an inert gas. Therefore during the growth, the level is kept constant in the cell. After the growth, the mercury is removed from the cell insuring that only a negligible amount of mercury is evaporated in the growth chamber. Obviously, this cell is more fragile than other cells and to disconnect it from the growth chamber the vacuum has to be broken.

Electrical and structural characterizations carried out on numerous layers grown either with the first cell or with the quartz cell have shown no difference. The similarity of $Hg_{1-x}Cd_xTe$ layers grown in either of these two cells in terms of impurity distribution has been confirmed by T. Magee [23].

These two cells are currently used in the Microphysics Laboratory at the University of Illinois and since results are identical, no distinction between them will be made and no mention of the cell used will be given later in this paper.

A cell in which mercury is in contact only with fused silica (excepted perhaps for the three way valve) has been designed at LIR [24] (Fig. 6). This cell allows a nearly constant Hg-level, however the mercury reservoir as well as the mercury cell are feed. Flux reproducibility and stability respectively better than 5% and 1% have been reported.

The other category of mercury cell is basically made in stainless steel with two Hg reservoirs (one internal and one external), a long tube and two UHV valves. The internal reservoir and the tube are heated. The stability of the mercury flux is due to the large inertia of the system, but no information has been reported regarding the rate of change in the mercury flux and the reproducibility between experiments. Such a Hg source has been designed and built at North Carolina State University 25 (Fig. 7) [25].

A fast-response Hg vapor source (Hg-PCVS) has also been built [26]. The design principles of the Hg furnace are based on the fact that for choked flow conditions across an orifice, the gas flow on the low-pressure side is directly proportional to the pressure on the upstream side of the orifice [27]. In this cell (Fig. 8), Hg vapor is generated in a heated stainless-steel Hg reservoir. The vapor flows through a control valve into a plenum where the upstream pressure is maintained by a capacitance manometer/control valve feedback loop to ± 0.002 Torr. After expanding through the orifice, the Hg vapor flows into a heated nozzle, where it is directed onto the substrate. To shutter the beam and prevent flux transients, a vent run valve system is placed just after the orifice.

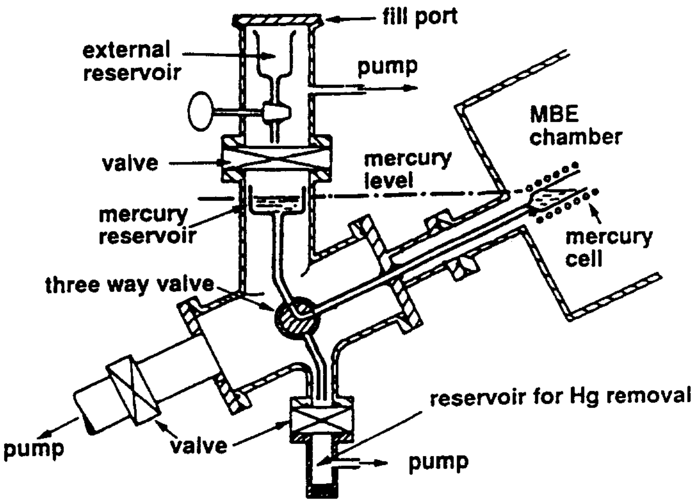

Figure 6: Diagram of the constant level mercury cell.

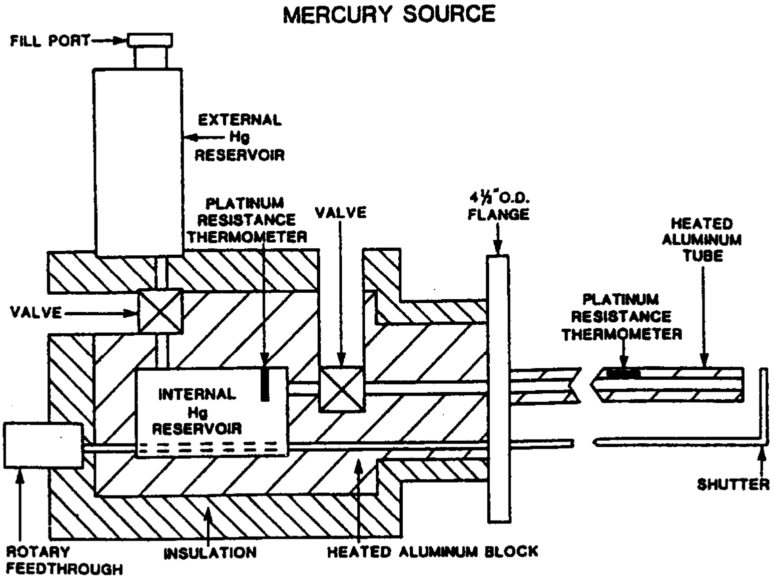

Figure 7: Mercury MBE vapor source.

It is reported that this system has a response time of 10^{-6}, and a dynamic range of 10^{-6} to 10^{-3} Torr. A constant flux output for reservoir temperature changes of 20°C, a stability of 0.1% over 3h and setpoint repeatability of 0.1% have been reported.

The use of stainless steel has been questioned due to a possible reaction of this material with mercury and subsequently a possible contamination of the $Hg_{1-x}Cd_xTe$ layers. T. Magee has reported that layers grown using a stainless steel cell exhibited a much higher density in impurities such as Fe, Ni, Mn, Ti than those grown with a quartz cell [23]. Inductively, coupled plasma emission spectroscopy and neutron activation measurements have been carried out on various samples of Hg collected from a

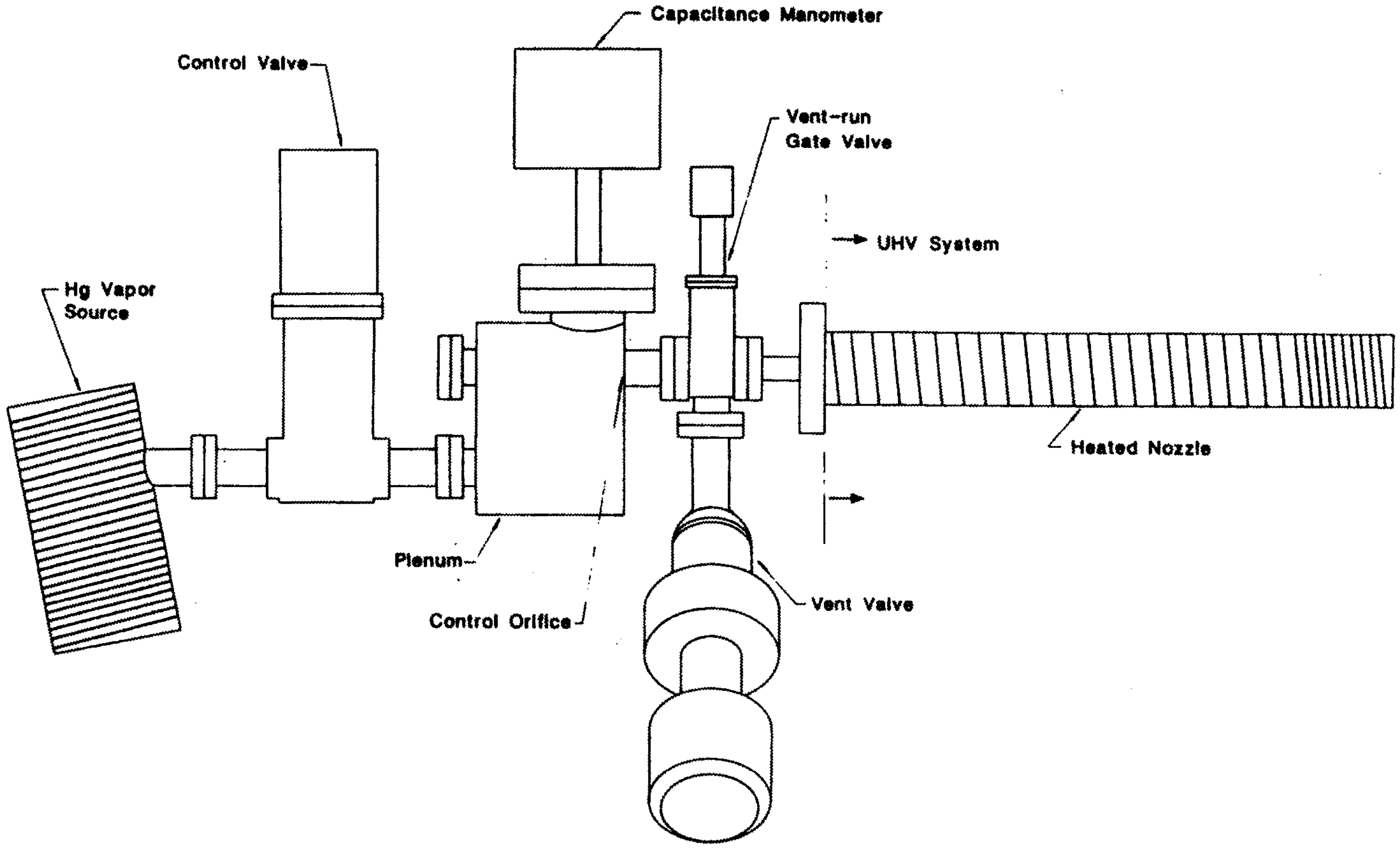

Figure 8: Diagram of Hg-pressure controlled vapor source (Hg-PCVS)

custom-made Hg source based on NCSU design. The detectable (<0.1 ppm) trace metal content of Hg in these samples is reported no to be different from the highest purity Hg commercially available [28].

3.3. *Te and CdTe Cells*

A standard MBE effusion cell is basically made with a crucible in pyrolytic boron nitride heated by a refractory metal wire wound spirally around it, the thermocouple is placed at the bottom of the crucible and held against the base. With its orifice completely open, a large gradient in temperature exists along the axis of the cell. Such a gradient is a problem for the evaporation of tellurium and of CdTe since tellurium is deposited at the lip of the cell which is cold. After a while condensed tellurium obstructs the cell.

This deposit is detrimental to the growth because when the surface area of evaporation is changing, the growth rate and the composition of the alloy are changing too. Thus special attention has to be given to the design of these cells in order to avoid this gradient problem. Good results have been obtained by acting on the spacing of the heater metal wires. In the case of CdTe, due to the higher temperature, a dual filament cell approach is more suitable.

Zinc, cadmium and the other elements used for the doping such as indium are currently evaporated in standard MBE effusion cells however specific design is required if large diameter cells are used. Regarding arsenic, a valved cracking effusion cell is the most suitable.

3.4. *Flux Measurement*

As discussed in section 2.2, the atomic or molecular flux (atoms or molecules .$cm^{-2}s^{-1}$) at the orifice of an effusion cell where a quasi-equilibrium is reached, is given by:

$$J = P(2\pi mkT)^{-1/2} = 3.513 \times 10^{22} P(MT)^{-1/2} \qquad (11)$$

At the substrate, the atomic or molecular beam flux (atoms or molecules $cm^{-2}s^{-1}$) is given by:

$$J = 1.12 \times 10^{22} \frac{AP}{L^2 (MT)^{1/2}} \cos\theta \qquad (12)$$

where A is the area of the orifice of the Knudsen cell (cm^2), P is the pressure in the cell (torr), L is the source substrate distance (cm), M is the atomic or molecular mass (g), T the cell temperature (K) and θ is the angle between the normal of substrate and the direction of the molecular beam.

It is important to point out that a MBE cell is not an ideal Knudsen cell since the orifice is large and the distance between the evaporating surface inside the cell and the orifice is changing with time.

In addition to that, the temperature measured in the back of the cell is not precisely the temperature of the material inside the cell. Therefore, the flux arriving at the substrate cannot be accurately estimated. Several methods are used to determine the beam fluxes: crystal quartz monitor, thickness determination, ion gauge and quadruple mass spectrometer. The first and the last methods are not currently used in the growth of $Hg_{1-x}Cd_xTe$ by MBE because Hg does not stick on the quartz monitor and the mass spectrometry method was found to be unreliable in the Hg background pressure. Thickness measurements are performed by using a step profiler or calculated from the interference fringes of infrared transmission measurement by using the relation:

$$e = \frac{1}{2n\Delta v} \qquad (13)$$

where e is the thickness (cm), n is the refractive index and Δν is the separation between two consecutive maxima (cm^{-1}). If an accurate refractive index is used, then the thickness can be measured within ± 1%.

But for very thin layers (<2 μm) or when x is close to 0.15, this method is less accurate because in the first case, the peak maxima are vanishing and in the second case, the refractive index is too much energy photon dependent.

This approach can be implemented *in situ* through the use of an IR pyrometer but the reaction time is slow since Δν has to be determined before acting on the growth parameters.

A movable ion gauge can also be used *in situ* to determine the relative fluxes from the relative beam equivalent pressure [BEP] according to [29]:

$$\frac{J_x}{J_y}=\frac{P_x}{P_y}\times\frac{\eta_y}{\eta_x}\left(\frac{T_x M_y}{T_y M_x}\right)^{1/2} \qquad (14)$$

where J_x is the flux of species x, P_x is the measured pressure, T_x is the absolute temperature and M_x is the molecular mass of species x. η is the ionization efficiency relative to nitrogen (N_2) and is given by:

$$\eta/\eta_{(N_2)} = [(0.4\ Z/14) + 0.6] \qquad (15)$$

where Z is the atomic number.

In MBE systems very often, the ion gauge is placed in the back of the substrate holder so that it can be easily rotated in order to be exposed to the beams.

In the Hg cell, the pressure is close to equilibrium conditions since the orifice is small and the level constant. The temperature is known accurately thanks to the position of the thermocouple. Therefore, a fairly accurate determination of the Hg flux arriving on the substrate is possible using the Knudsen formula.

In fact, one has to be careful in applying the formula when θ is different than zero. Due to the high effusion rate required for Hg, the cosine distribution obtained for the free flow regime is not valid. In this case, the flux distribution is better described by the transition or laminar flow regime. From Jackson *et al.* calculations for Zn [30], it would be more appropriate to assume a $\mathrm{Cos}^{3/2}\,\theta$ distribution near the axis of the cell. Therefore, this more forward-directional flux for Hg will make uniformity and composition difficult to control on large area substrates in the case of $Hg_{1-x}Cd_xTe$.

3.5. *Band Gap Control*

The standard expression for energy gap Eg of $Hg_{1-x}Cd_xTe$ alloy vs x and T as proposed by Hansen *et al.* [31] is as follows:

$$Eg = -0.302 + 1.93x + 5.35 \times 10^{-4}\,T\,(1-2x) - 0.810x^2 + 0.832x^3 \qquad (16)$$

valid from x = 0.0 to 0.6 and 4 to 300K.

To convert Eg(eV) to cutoff wavelength λ_c (μm), the following expression is used

$$\lambda_c = hc/Eg = 1.24/Eg \qquad (17)$$

To grow HgCdTe by MBE, it is possible to use two different sets of effusion cells. The first set uses cells containing elemental Hg, Cd and Te. The second set uses cells containing elemental Hg and Te along with a cell containing the compound CdTe. It is somewhat important to determine which set is the most appropriate i.e. which set allows the best composition (cutoff wavelength) control. The two sets will have different values for the dispersion of $\Delta\lambda_c$ for the same fluctuation ΔT and will be considered separately.

For the purpose of this calculation [32], we will assume that the variation in the temperature of the effusion cells (ΔT) is 0.1°C. Also we will assume that ΔT for each cell is independent of all the other cells. For this value ΔT of 0.1°C, we have found experimentally from growth rates, and theoretically from formulas given for the flux from an effusion cell operating at a temperature suitable for growth (see section 2.2) that the change in flux is about

$$\frac{\Delta F_{Te}}{F_{Te}} \cong 0.005 \qquad \frac{\Delta F_{Cd}}{F_{Cd}} \cong 0.007 \qquad \frac{\Delta F_{CT}}{F_{CT}} \cong 0.003$$

for Te, Cd, CdTe (CT) respectively.

Changes in Hg flux are not considered in this calculation because the composition of $Hg_{1-x}Cd_xTe$ alloy grown by MBE is to a first approximation mostly controlled by the Cd/Te flux ratio. This is obviously a direct consequence of its low condensation coefficient.

It is easy to calculate the dispersion of $\Delta\lambda_c$ for the first set of cells since the change in x due to changes in the Cd cell (Δx_{Cd}) is just $x(\Delta F_{Cd}/F_{Cd})$. A similar expression is true for the change in x due to changes in the Te cell (Δx_{Te}). Because of the assumption of independence,

$$\begin{aligned} \Delta x_1 &= [(\Delta x_{Cd})^2 + (\Delta x_{Te})^2]^{1/2} \\ &= x[(\Delta F_{Cd}/F_{Cd})^2 + (\Delta F_{Te}/F_{Te})^2]^{1/2} \\ &= 0.0086\ x \end{aligned} \qquad (18)$$

For the second set of cells, the result is somewhat different since the congruent evaporation from the CdTe cell gives a self compensation of the flux. One finds that $\Delta x_{CT} = x(1-x)(\Delta F_{CT}/F_{CT})$. A similar expression holds for Δx_{Te}

$$\begin{aligned} \Delta x_2 &= [(\Delta x_{CT})^2 + (\Delta x_{Te})^2]^{1/2} \\ &= x(1-x)\ [(\Delta F_{CT}/F_{CT})^2 + (\Delta F_{Te}/F_{Te})^2]^{1/2} \\ &= 0.0058\ x(1-x) \end{aligned} \qquad (19)$$

Using equations (18) and (19) along with Hansen's formula for Eg(x,T) and the relation $\lambda(\mu m) = 1.24/E(eV)$ one can find $\Delta\lambda_c$ for HgcdTe alloy grown with either of the two sets of effusion cells. The results are shown in Figure 9. It is quite clear from the curves in Figure 9 that HgCdTe grown using Hg, Te and CdTe (second set) has a much smaller dispersion $\Delta\lambda_c$ than if Hg, Te and Cd (first set) are used.

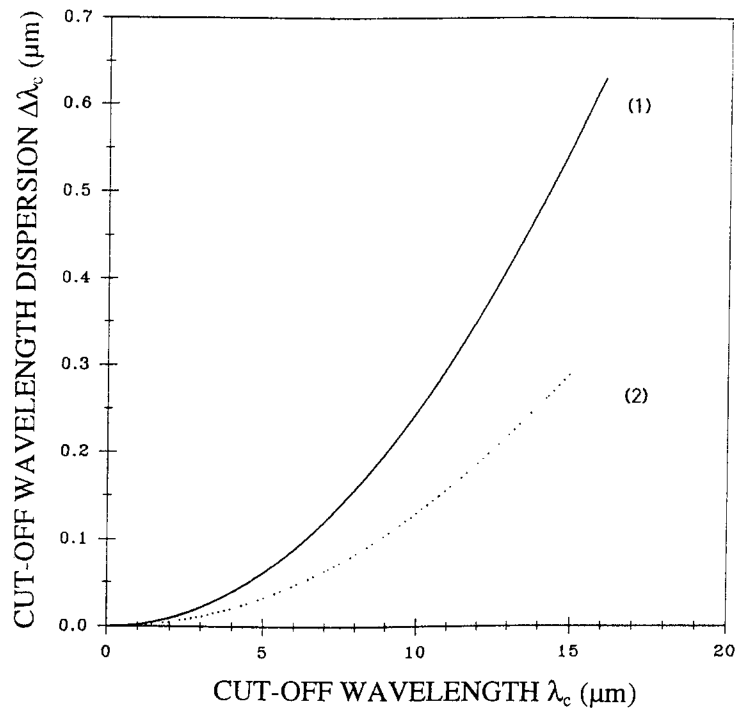

Figure 9: Variation in the cut-off wavelength as a function of the cut-off wavelength for (1) HgCdTe grown with effusion cells containing Hg, Te and Cd; (2) HgCdTe grown with effusion cells containing Hg, Te and CdTe.

At 10 µm, it can be seen that $\Delta\lambda_c$ = 0.13 µm is obtained for the second set of effusion cell (vs 0.25 µm for the first set). This is better than what is required for infrared detector technology. **Thus it appears that alloy composition is better controlled using a CdTe cell instead of a Cd cell.** The other advantage is related to the potential cross reaction of tellurium with cadmium in the cadmium cell, reaction which does not exist when CdTe is employed. There is one disadvantage though, it concerns the purity of CdTe which might not be as good as that of cadmium, but such a problem does not currently appear to be a limitation, since very pure CdTe is commercialized.

3.6. *Substrate Temperature Control*

The control of the substrate temperature T_s is the most difficult task because what has to be controlled is, in fact, the temperature of the surface of the substrate T_{ss} during the growth. We have verified that the temperature indicated by the thermocouple located in the back of the substrate which rotates (1) does not give an accurate reading of the substrate temperature (Tss) and (2) does not account quickly for surface temperature changes.

The use of an IR pyrometer does not present an ideal solution either.

T_{ss} can be kept constant by using a frontal thermocouple imbedded in gallium. Such a thermocouple, that we have installed in order to determine and explain the pyrometer (Tp) and the back thermocouple behaviours, has proven to provide very accurate temperature control, even over the course of several hours of growth when Tss is kept constant at 190°C by using this frontal thermocouple.

3.6.1. *Substrate mounted with gallium on a molybdenum block*

The conclusion of this section involves measurement during MBE of $Hg_{1-x}Cd_xTe$ onto (111)B and (211)B CdTe or CdZnTe substrates mounted with Ga on a molybdenum block, acting as the substrate heater.

At the initiation of growth (Tss = 190°C), a jump of approximately 25°C (in our MBE configuration) occurs in T_p as illustrated in Figure 10. This is due to scattered IR radiation, primarily from the CdTe effusion cell, and secondarily from the Te_2 effusion cell. Immediately, T_p falls steeply. This is due to both the rapid decrease in reflectance resulting from absorption in the thickening $Hg_{1-x}Cd_xTe$ coverage, and the fall toward the first minimum in the interference pattern related to the presence of a thin HgCdTe layer.

Upon reaching the first minimum, T_p rises again toward the next maximum. Several more oscillations in T_p of decreasing amplitude follow. This decrease in amplitude is due to attenuation of the internally reflected IR radiation within the $Hg_{1-x}Cd_xTe$ layer as it grows thicker. After about 2 μm of growth, the oscillations disappear almost completely. At this point, T_p is approximately 15°C higher than the reading before growth. This increase is primarily due to the higher emittance of $Hg_{1-x}Cd_xTe$ and second to a small but nonvanishing contribution from scattered effusion cell radiation.

As the $Hg_{1-x}Cd_xTe$ layer grows, its greater emittance leads to an increasing heat loss from the front of the sample and block, which results in an increasing temperature gradient within the sample and block. This same behaviour has been previously reported for III-V MBE by Heiblum *et al.* [33], and Hoke *et al.* [34].

Therefore, in order to keep the surface temperature constant, the heater must provide greater power to the back of the block. The rear thermocouple (T_r) registers this higher power input by showing an increase in T_r, with respect to T_{ss} as the growth proceeds. That is, the thermal gradient within the block and sample indeed becomes greater as the emittance of the front becomes increasingly larger than that of the back. During the course of a 10 μm $Hg_{1-x}Cd_xTe$ growth, the difference between T_r and T_{ss} increases to greater than 60°C. In other words, if T_r is kept constant, T_{ss} decreases. In this case, a constant Hg flux will become too high, since the Hg sticking coefficient changes drastically with temperature, and reflection twins visible in the RHEED pattern will be formed. From these experiments it appears that the control of the substrate surface temperature T_{ss} which is a key parameter and should be kept constant within ±0.5°C is an extremely difficult task.

The differing emittances among $Hg_{1-x}Cd_xTe$, HgTe, CdTe, Ga and Mo within the 2.0 to 2.6 μm band affect the pyrometer. CdTe and $Hg_{1-x}Cd_xTe$ have higher emittance than the reflective Mo and highly reflective molten Ga metals it covers. However, the gray deposit of polycrystalline $Hg_{1-x}Cd_xTe$ on the molybdenum block surrounding the substrate has a higher reflectance than the epitaxial layer. Therefore, although the pyrometer is focused on the sample, the surrounding of higher reflectance might contribute significantly to Tp, since it is impossible for the pyrometer optics completely to exclude emissions from this nearby region. Such a contribution would diminish for larger-sized samples and this has been proven experimentally.

We have found also that during rotation of smaller sized samples, fluctuations in Tp (as large as ±10°C) are sometimes observed upon rotation during the first 0.5 μm of growth due to a scattering problem cause by excess Ga surrounding the substrate.

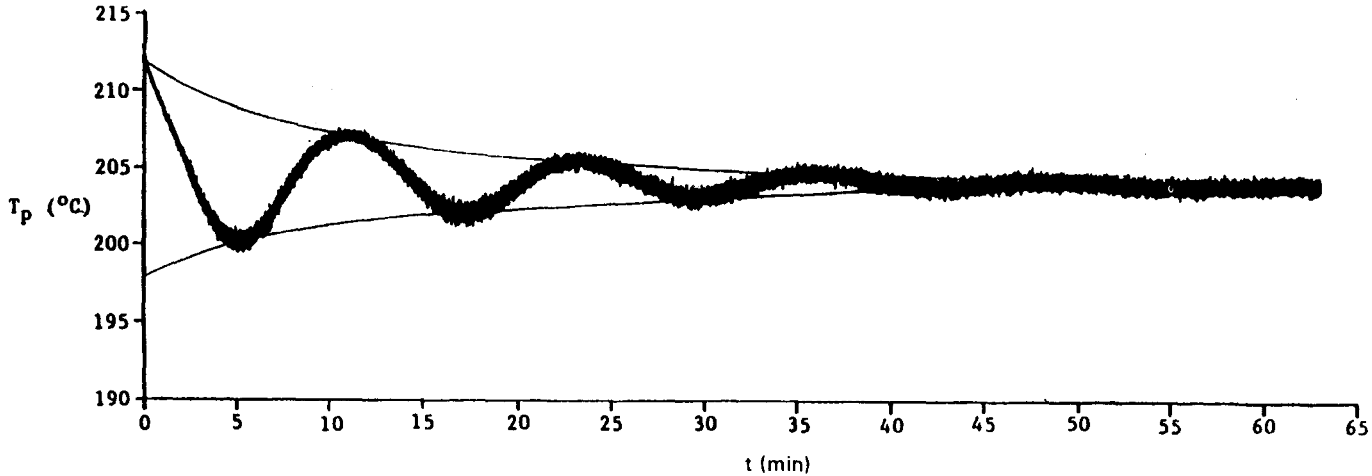

Figure 10: Plot of the temperature pyrometer reading T_p versus time for $Hg_{1-x}Cd_xTe$ ($x = 0.26$) grown on CdTe (111)B. During the experiment, the surface temperature of the substrate Tss is kept constant at 190°C.

We have observed many other subtle effects in pyrometry experiments showing that this technique could be sensitive to crystallographic orientation, crystalline quality and surface roughness if suitably implemented. The detail of experiments carried out in the Microphysics Laboratory has been given in M.D. Lange's thesis dissertation [35].

3.6.2. *Gallium free mounting*

Pyrometer behaviour has been also recorded during growth of $Hg_{1-x}Cd_xTe$ on CdTe-buffered GaAs and Si substrates mounted **without** Ga (Ga free) in the ISA RIBER OPUS 45.

Doped substrates are vital in order to prevent huge changes in absorption during the early portion of growth. This was found to be essential because the thermal inertia of the substrate heater is too great to permit sufficiently rapid adjustment for growth on semi-insulating substrates. Above all, doped substrates also prevent the pyrometer from being overwhelmed by radiation from the substrate heater during the early portion of $Hg_{1-x}Cd_xTe$ growth. Semi-insulating GaAs is an inefficient absorber of heater radiation. Heavily doped substrates block most of the substrate heater radiation from reaching the pyrometer, because they absorb the heater radiation much more effectively. Substrate thickness is a second factor affecting T_p because the absorption of heater radiation increases with the thickness of the substrate. Another factor is the lateral size of the substrate. This affects the substrate heater power requirements because, all else being equal, larger substrates permit greater transmission radiation loss than do smaller substrates, for which the substrate holder blocks some transmission radiation loss.

Once the initial temperature (190°C) is established and the $Hg_{1-x}Cd_xTe$ growth commences, a jump occurs in T_p due to scattered effusion cell radiation which is smaller than was observed in the pyrometry experiments carried out on substrates mounted with Ga. Whereas the smaller jump in T_p is due in part to the different geometry of the ISA RIBER OPUS 45, it is mainly attributable to the fact that the scattered effusion cell radiation is outshone by the transmitted substrate heater radiation.

As the $Hg_{1-x}Cd_xTe$ layer thickens, eventually it completely absorbs any substrate heater radiation (in the 2.0 to 2.6 μm band) that has penetrated it after traversing the substrate and buffer. This causes an overall decline in T_p early in the growth as illustrated in Figure 11 which is the opposite of what is observed on substrates mounted with Ga. The reason is that the contribution from the decreasing transmitted substrate heater radiation is greater than that from the increasing $Hg_{1-x}Cd_xTe$ emissions.

Such as in the previous section regarding the pyrometry experiments on substrates mounted without Ga, the initial setpoint requirements for the rear thermocouple depend on the doping, dimensions, and rear surface condition of the substrate. The setpoint for the rear thermocouple must generally be ramped downward during the first 1.5 μm of the growth.

3.6.3. *Discussion*

The need to Ga-free mounting for the setpoint to be ramped downward early in the growth is opposite to that revealed by the rear thermocouple experiments conducted on substrates mounted with Ga. Both cases are similar in that the thickening $Hg_{1-x}Cd_xTe$ leads to increased emittance of the surface itself. The difference stems from the way the substrate and $Hg_{1-x}Cd_xTe$ layer are heated in each case. For substrates mounted with Ga, radiation from the substrate heater is absorbed by the block. Heat from the block is then passed to the substrate by thermal conduction through the Ga and to the layer by a combination of thermal conduction through the substrate, and radiation which, emitted from the Ga, traverses the transparent substrate. Because the block is opaque, no substrate heater radiation is lost to transmission in this case.

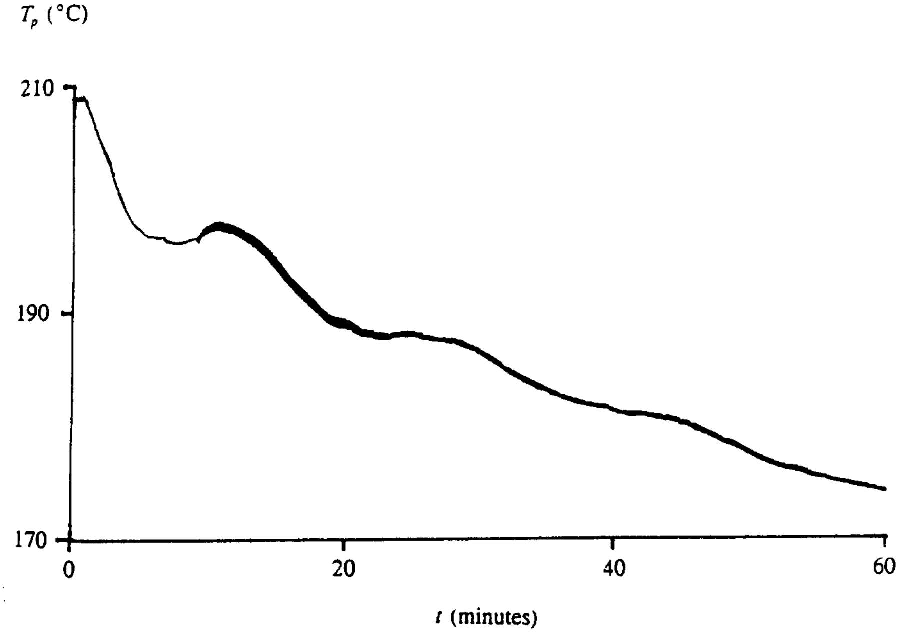

Figure 11: Plot T_p versus time (t) for $Hg_{1-x}Cd_xTe$ grown on CdTe(111)B-buffered GaAs mounted **without** Ga. During the experiment, the surface temperature was kept at about 190°C.

On the other hand, for substrates mounted without Ga, during the early part of the growth only a portion of the radiation from the substrate heater is absorbed directly by the substrate and layer. (And some of the heat absorbed in the substrate passes through to the layer by thermal conduction as well). The rest of the radiation from the substrate heater is lost to transmission through the substrate and layer. (As mentioned earlier, despite its doping, the substrate is semitransparent at the approximately 180°C $Hg_{1-x}Cd_xTe$ growth temperature).

Therefore in this case, unless and until the substrate and growing layer are opaque, some of the heating power is lost to this transmission.

Radiation supplied by the substrate heater during the early portion of the growth is therefore used more efficiently for substrates mounted with Ga than for those mounted without it. As a result, less power is required in the former case to maintain the proper growth temperature. In both cases, when the layer reaches a thickness of about 1.5 μm, essentially all the radiation leaving its surface is emitted from the $Hg_{1-x}Cd_xTe$ itself, and the rear thermocouple requires no more ramping.

The substrate heater power required to maintain the optimal surface temperature during MBE on GaAs or Si substrates depends on their doping, thickness, lateral size, and the smoothness of their rear surfaces. Due to the position of the rear thermocouple, its reading is affected more by radiation from the substrate heater than from the sample. Therefore, calibration of the temperature differs among the various substrates, because for the same T_r, the surface temperatures of the various substrates will differ.

3.6.4. *Optimal combination of thermocouple and pyrometer*

The previously discussed investigations have greatly improved understanding of both pyrometer and rear thermocouple behaviour for $Hg_{1-x}Cd_xTe$ growth by MBE. Based on these improved understandings, it has become apparent that the best temperature control of the substrate during such growth can be achieved through combined utilization of both temperature measurements methods. The thermocouple is most advantageous during the early portion of the growth, when the pyrometer is still affected by thin-film interference effects. The pyrometer then becomes more advantageous for the subsequent portion of the growth, because of its sensitivity to T_{ss}, which permits it to remain unaffected by gradients in the substrate bulk and the sample holder.

The switching from thermocouple to pyrometer could be further implemented by a computerized temperature-control process. Such a process could automatically switch the controller's input signal from the rear thermocouple to the pyrometer at the appropriate point in the growth. Also, as Wright *et al.* [36] have previously proposed for III-V MBE, the process potentially could ramp the setpoints as necessary.

4. DEFECT FORMATION

Microtwins and hillocks are commonly observed in zinc-blende crystals grown in gas phase techniques such as MBE or OMCVD. The (111) orientation is particularly vulnerable to twin formation, but other orientations are also sensitive to twinning. Hillock formation, observed during the growth in the (100) orientation is also associated with microtwins. It is well established that the presence of microtwins or hillocks is highly deleterious for devices such as photodiodes and their formation should be prevented both in the CdTe or CdZnTe buffer layer and in the HgCdTe layer.

While the presence of microstructural defects in MBE layers has been established for several years, information regarding their elimination has been scarce because such elimination is not a trivial problem. Only a few groups have reported some success in the elimination of twins in the (111) orientation [37-40]. Harris *et al.* [39] using photo-assisted MBE on a non-rotating substrate under very demanding parameter control have obtained a twin-free material yield of less than 20%. A clear improvement in structural properties is shown when twins are avoided but no information has been given about change in electrical properties.

Therefore, the question is: why growing in the (111)B orientation if it is so difficult? The (111)B orientation, despite its propensity to form twins is a very important orientation because the mercury consumption is lower than for the (100) orientation [21]. Interfaces are usually very smooth in the (111)B plane, CdTe and CdZnTe substrates are obtained in high yield in this orientation and it is so far the most favorable orientation for growth on GaAs (100) and Si(100) substrates.

Although this problem seems to be less dramatic or at least can be more easily solved, in other directions such as (211)B, (311)B and (100), the progress achieved towards the control of twinning in the (111) should be beneficial for the other orientations. In the (100) orientation, the formation of facets and hillocks is a major problem for focal plane arrays and MIS structures; also hillocks are twin-related defects [39]. Therefore, the identification and control of twin formation is probably the most difficult and the most important problem in the MBE growth of HgCdTe. The presence of twins in CdTe and HgCdTe epilayers can be revealed by detailed investigations involving electron microscopy, cathodoluminescence, chemical etching, and X-ray diffraction as well as electron channeling pattern (ECP).

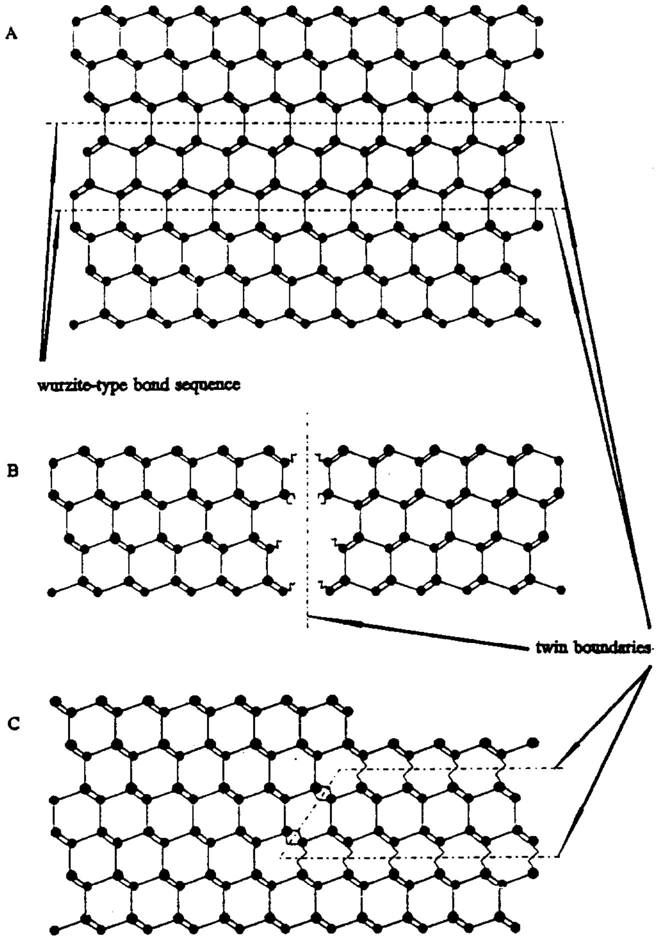

Figure 12: Schematic illustrations of three different kinds of twinning: (A) Lamellar rotation-type twinning, (B) Double-positioning rotation-type twinning, and (C) Reflection -type twinning.

In the zinc-blende structure, there are three types of twinning illustrated in Figure 12 which are very often observed. In Figure 12a, a "rotation" type of twin corresponding to a 180°C rotation about the <111> growth direction is shown. The stacking of (111) plane in the fcc structure changes from the abc type I configuration to acb type II configuration, which involves the presence of one wurtzite bond sequence at the interface. The two stackings are equivalent, the change requires very low formation energy since the Cd(Hg)-Te bonds are preserved. This change can therefore occur several times during the growth. This kind of twinning is sometimes called lamellar twinning. It can be clearly observed by transmission electron microscopy.

During the first step of epitaxial growth, islands can be formed which will grow and coalesce to form the epitaxial film. These islands may be of type I or type II configuration since they are energetically almost equivalent (Fig. 12b). Therefore, twin boundaries will exist after island coalescence and twin domains will grow in a columnar form. This kind of twinning which is also of a rotation type, is sometimes called double positioning twinning.

These two kinds of rotation twins can coexist in the crystal, but one or both can disappear during the growth. It is difficult to observe rotation twins during MBE growth by electron diffraction because the streaked (2D) patterns of the type I and type II configuration are identical to twin-free streaked patterns, and sometimes roughening of the surface, which allows 3D diffraction, is not large enough. The twinned domains present in the crystal are visible on the surface of the crystal under scanning electron microscopy or cathodoluminescence investigations in the form of close loops as illustrated in Figure 13 for a CdTe layer.

Electron channeling patterns (ECP) can also help in the discovery of twins. Figs. 14a and 14b show two simulated ECPs of a twin-free and a twinned crystal. The (113) plane family has a 3-fold symmetry revealed in the form of a regular triangle in the twin-free configuration whereas in a twinned configuration, a second inverted triangle is revealed. Fig. 14c shows the ECP pattern of a twinned CdTe layer similar to the one illustrated in Fig. 14b.

These two kinds of twinning can occur in both CdTe and HgCdTe. In HgCdTe, however, due to the high mercury flux used during the growth, we think that a third kind of twinning illustrated in Figure 12c can occur. This reflection type twin is formed by a mirror reflection with respect to the (111) twin plane.

This produces a change in the polarity of the face by creating an anti-phase boundary. As shown in Fig. 12c, Hg-Hg bonds which usually require high formation energy, occur at the plane of the reflection twin when the Hg flux is too high. This twinning does not occur across the entire area of the wafer; therefore, the growing surface exhibits (111)B and (111)A orientation simultaneously. The growth rate of (111)B and (111)A faces being very different [21], surface roughening allows the observation of extra dots in the RHEED pattern associated with this kind of twinning.

A decrease in the Hg flux or an increase in the substrate temperature produces a rapid change in the RHEED pattern. The extra dots are disappearing and the spotty pattern is transformed into a streaky one. This is as expected, since a (111)A face is a Hg unstable terminated face, which requires a high Hg flux. A new antiphase boundary with Te-Te bond is created reverting the (111)A to a (111)B face (Fig. 12c).

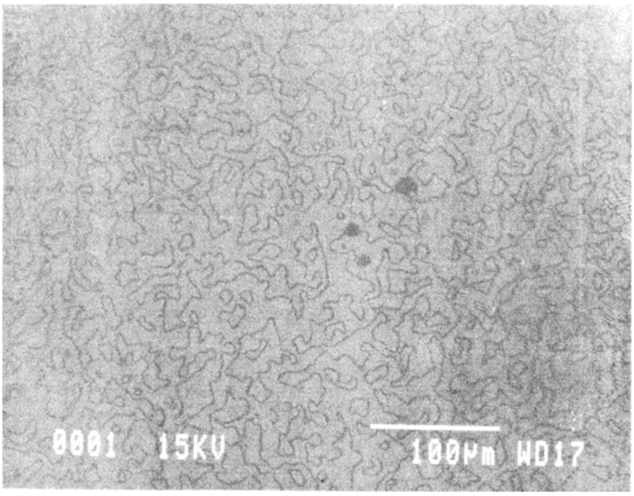

Figure 13 : Cathodoluminescence image of a twinned CdTe(111)B epilayer.

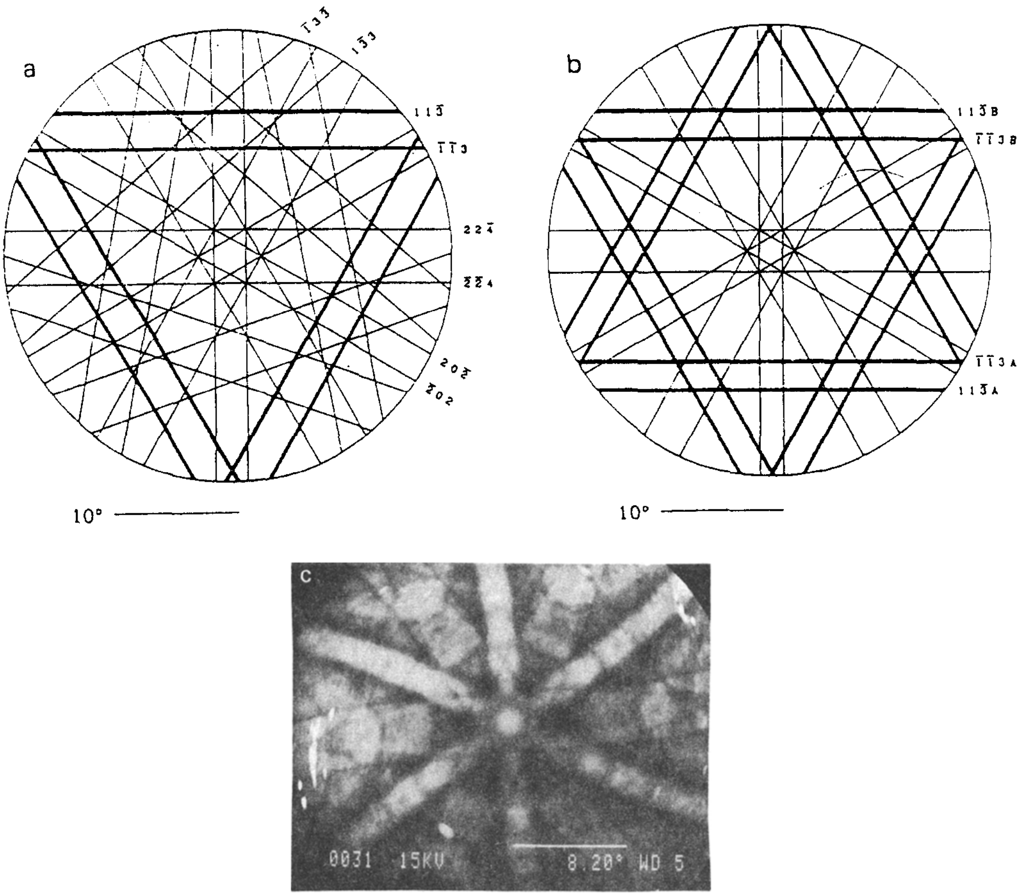

Figure 14 : Electron channeling pattern simulation of a CdTe crystal along the (111) axis: (a) twin-free cystal, 15.0 kV, fcc lattice, a = 6.481 Å. (b) twinned crystal, 25.0 kV, fcc lattice, a = 6.481 Å. (c) ECP pattern of a twinned CdTe crystal.

Figure 15 is a TEM picture of a HgCdTe (111)B layer grown on a CdTe(111)B/ GaAs(100) substrate. It can be seen that the CdTe layer grown on GaAs is full of lamellar twins. At the initiation of HgCdTe growth twins were visible on the RHEED pattern. The growth conditions were kept the same for a while and then the substrate temperature was increased by 5°C. Almost instantaneously the RHEED changed to a twin-free related electron diffraction pattern. The TEM micrograph confirms our *in situ* observation, since a twin is visible in the HgCdTe layer and the position where the twin has disappeared, corresponds very precisely to the changes both in the substrate temperature and the RHEED pattern. High resolution transmission electron microscopy (HRTEM) has not been able to confirm the "reflection" nature of the twin since it is extremely difficult to reveal fine details of atomic structure. However, it is highly probable that this kind of twinning occurs when the Hg flux is too high.

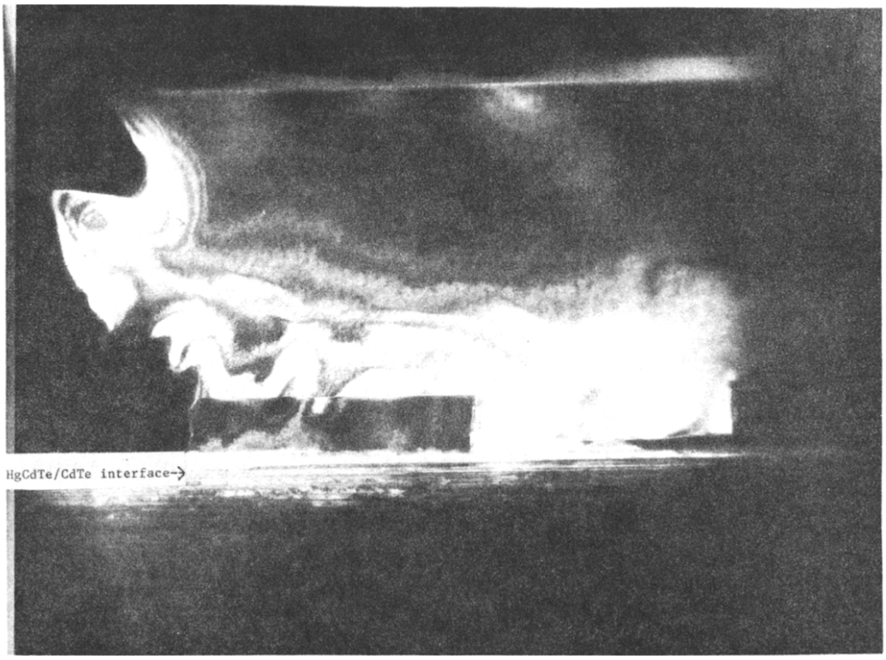

Figure 15 : Transmission electron microscopy of a HgCdTe(111)B/GaAs(100) substrate. Only CdTe epilayer exhibiting numerous lamellar twins and HgCdTe epilayer are visible.

4.1. *CdTe (111)B Twin-tree Epilayers*

Surface cleaning and growth parameters have been thoroughly investigated in order to prevent twinning. Concerning CdTe, "reflection" type twinning is very unlikely to occur when using a single effusion source which delivers a highly constant Cd/Te flux ratio. Therefore, in the case of CdTe, only the formation of the two kinds of "rotation" type twins has to be prevented. Double-positioning twinning which starts at the substrate epilayer interface seems to be related to the surface preparation of the substrate. Regarding lamellar twins, which are formed during the growth, we have not yet precisely identified which parameter is triggering their formation. Concerning CdTe (111)B homoepitaxial growth, it has been found that twinning does not occur when the growth temperature is around 335°C, nor does it occur if the CdTe substrate is cleaned at 335°C before growth at 250°C. The heteroepitaxial growth of CdTe (111)B on GaAs or Si substrates is also subject to twinning. The twinning in CdTe(111)B/GaAs(100) heteroepitaxy has been the object of investigations during the last few years. It has been found that twinning can be avoided by using GaAs substrates cut a few degrees off nominal (100) towards [110] [41-42] so as to exhibit Ga atoms at step edges [43].

CdTe(111)B grown on Si(100) is also subject to twinning. A systematic study on the growth of CdTe (111)B layers on misoriented Si(001) substrates with various tilt angles (θ) and tilt direction (ϕ) [44-45] has been conducted. The formation of double domains and twins in CdTe (111)B layer is related to the surface structure of Si(001) substrate. CdTe(111)B layer grown on nominal Si(001) substrate always exhibits a double-domain and twinned structure. A single-domain and twin-free CdTe(111)B layer can be grown on slightly misoriented Si(001) substrate. The tilt angle (θ) of the substrate plays an important role in suppressing the formation of double-domains. The angle should be optimized in such a way that it is large enough to suppress the formation of double-domains, and as small as possible in order to minimize the introduction of misfit dislocations at the interface due to large vertical lattice mismatch between CdTe(111)B and Si(001) [44]. The tilt direction (ϕ) of the substrate also plays a crucial role in suppressing the formation of twin [45]. Twinned CdTe(111)B layer is always obtained, when it is grown on Si(001) tilted towards [110] ($\phi = 0$) or towards [010] ($\phi = 45°$) It has been found that θ of about 1° and ϕ of about 35° are optimized tilt parameters in order to grow single-domain twin-free CdTe(111)B epilayers on Si(001) substrates.

4.2. *HgCdTe Twin-free Layers*

4.2.1. *Growth in (111)B orientation*

The growth of twin-free (111)B HgCdTe represents a real challenge. In addition to rotation type twins, reflection type twins have been observed as reported in Section 4.1. First of all, the substrate or the buffer layer should be twin-free. Therefore, great care must be taken during substrate preparation and buffer layer growth as discussed before. The same precautions must be observed during the first steps of the HgCdTe growth in order to prevent double position twin formation. During the growth, we have seen that an increase in the Hg flux or a decrease in the substrate temperature can trigger the formation of antiphase boundaries. The control of the Hg flux is achieved through the use of a constant level Hg cell described in part 3.2. During the growth and also from run-to-run, the Hg flux, monitored by an ion gauge, is kept within less than ±2,5% fluctuation. The control of the substrate temperature T_{SS} has been discussed in detail in section 3.6.

Microtwin formation can be avoided in CdTe(111)B buffer layer when a proper thermal cleaning of the substrate and a suitable growth temperature are applied. In order to prevent microtwin formation in MBE HgCdTe layers, a stringent control is required in the stability of Hg (±2.5%), Te, and CdTe fluxes and in the surface substrate temperature (±0.5°C)[40]. Exacting control is particularly difficult to achieve when the substrate is rotating during the growth.

$Hg_{1-x}Cd_xTe$ **twinned layers** grown by the Microphysics Laboratory in the (111)B orientation usually exhibited a p-type character with hole mobility approaching or even exceeding $10^3 cm^2V^{-1}s^{-1}$ [46] and excess carrier lifetime in the range of (20-100) × 10^{-9}s [47]. An excellent electrical mobility is often considered to be associated with excellent crystal quality. It turned out that is was not precisely the case here. All the layers exhibiting 10^3 cm^2 V^{-1} s^{-1} were investigated using X-ray diffraction. X-ray rocking curves recorded for (422) reflections have shown for every layer 6 peaks when rotating the sample about the (111) axis, whereas only three peaks should have been observed in a twin-free epilayer. These findings were confirmed by ECP experiments. The first thought was that the presence of twins did not degrade the hole mobility. In order to confirm this, two HgCdTe epilayers (x = 0.25) were grown under the same growth conditions, except that the Hg flux was increased several times for several minutes during the growth of layer A, whereas for layer B the twin-free growth conditions were applied. X-ray diffraction confirmed that layer B was twin-free and layer A was twinned. Both layers showed a p-type character. However, layer A exhibited a hole mobility of 900 cm^2 V^{-1} s^{-1} whereas layer B had only a hole mobility of 300 cm^2 V^{-1} s^{-1} at 23 K. All the twin-free (111)B p-type layers grown so far have a hole mobility not exceeding 500 cm^2V^{-1} s^{-1}.

In addition, the carrier concentration N_A-N_D for p-type twinned layers has consistently been found to be in the (2-5) × 10^{16} cm^{-3} range and from Hall data curve fitting N_A has been calculated to be in (5-8) × 10^{16} cm^{-3} range, as reported before [48]. For p-type twin-free layers, the carrier concentration is much lower; N_A-N_D is in the low 10^{15} cm^{-3} range. The decrease in N_A-N_D is so marked for twin-free layers that many of them are n-type. Hence, the lower hole mobility in twin-free layers cannot be explained by an increase in scattering due to a larger acceptor concentration since it is the opposite. Therefore, it is concluded that electrically active acceptors and high hole mobility are related to the high Hg flux during growth, which has triggered the formation of reflection twins and of Hg-rich alloy zones in the crystal.

$Hg_{1-x}Cd_xTe$ grown at 185°C under Te-rich conditions (such as MBE) but under thermal equilibrium conditions (unlike MBE) should produce an intrinsic hole concentration due to Hg vacancies in the mid to high 10^{15} cm^{-3} range [20,49] as presented in section 2.3 and discussed in section 5.1. It appears that in the (111)B orientation MBE grown twinned layers have p-type doping levels exceeding the level expected from growth under thermodynamic equilibrium. In addition, the fact that fast low temperature isothermal (mercury-rich) anneals make the (111)B materials even more p-type leads us to believe that extended defects are mostly responsible for the electronic activity in the as-grown material. The increase in the acceptor level could be explained by the presence of numerous (111)A planes in the twin boundaries and antiphase boundaries. As reported before [21], a (111)A plane which is Hg terminated is very unstable and thus should have a Hg-vacancy density higher than the one thermodynamically calculated for a bulk crystal. The existence of Hg-rich alloy zones might also explain a higher Hg vacancy concentration.

Concerning the high hole mobility, no clear explanation has been found yet. However as already discussed, the excess of mercury induces the formation of Hg antiphase boundaries, as well as Hg-rich alloy zones. Therefore, numerous Type III (semimetal-semiconductor) interfaces exist within the crystal. It has been discovered and explained [50,51], that a high hole mobility due to light heavy hole effective mass is associated with type III interface. However, it is possible that with the presence of Hg-rich antiphase boundaries and therefore the existence of Type III (semimetal-semiconductor) interfaces, similarities with the high hole mobility observed in Type III HgTe-CdTe superlattices exist.

Another important difference related to etch-pit density (EPD) has been found between twinned and twinfree layers in good agreement with ref. 39. EPD count which is related to dislocation density, is determined using a defect chemical etching solution suitable for the investigated crystallographic orientation. One can see in table III that by eliminating twins, EPD drops tremendously, indicating a drastic improvement in the crystal quality. This improvement however is unexpectedly associated with a decrease in the measured hole mobility as already discussed.

Table 3 provides also a brief summary of the main differences between (111)B twinned and twin-free layers grown by MBE.

Table 3: Main differences between (111)B twinned and twin-free layers grown by MBE.

	Conduction type	N_A-N_D p-type layers (cm^{-3})	Hole mobility ($cm^2V^{-1}s^{-1}$)	EPD (cm^{-2})
Twinned layer	p-type	(2-5) x 10^{16}	800-1600	10^6-10^7
Twin-free layer	p-type or n-type	(1-2) x 10^{15}	300-500	10^4-10^5

4.2.2. *Growth in the (211)B orientation*

The (211)B orientation has been found to be less sensitive to microtwin formation and therefore the growth in this orientation is easier to control[52]. The (211)B orientation has attracted a lot of attention these past years in the MBE community. A series of HgCdTe epilayers has been grown by MBE on (211)B CdZnTe substrate in order to analyze the influence of the growth parameters in view of their optimization. Double X-ray rocking curve (DCRC) FWHM is the selected physical parameter since it provides very useful information about the crystal quality and hence about the dislocation density and of other defects present in the epilayer. Figure 16a illustrates the change in DCRC FWHM vs Hg flux. In these experiments carried out at EPIR Ltd., the growth temperature was 185°C and the growth rate between 4 and 5 Å/sec. The results confirm what has been previously observed and already discussed, i.e. the crystal quality deteriorates when the Hg flux either is too low or too high. It is striking that the Hg flux "window" which allows the growth of the highest crystal quality, is very narrow here, between 4 and 5.5 in arbitrary units. This represents a change in the Hg flux of about 30% which is achieved by a change of only 50 in the Hg cell temperature. The same trend is observed when the growth rate increased but the window is even narrower, whereas the optimum Hg flux is about the same (Fig. 16b and 16c).

Three very important conclusions can be drawn from this study:

1 - under optimized growth conditions, DCRC FWHM of MBE (211)B-$Hg_{1-x}Cd_xTe$ duplicates that of (211)B CdZnTe substrates, i.e. 20-30 arcsec.

2 - the optimum Hg flux is almost constant when the growth rate increases by about 50% which implies that Hg incorporation coefficient increases with the growth rate (at constant growth temperature) *i.e.* Hg consumption decreases with growth rate, and

3 - to the contrary of what was thought in earlier studies, MBE growth does not allow any flexibility in terms of stoichiometry deviation since the Hg flux is strictly determined for a given growth temperature.

4.3. *Dislocation Density Measurement*

It is widely recognized that defects are limiting the performance of HgCdTe devices and therefore FPA operability. Deleterious effects of dislocations on p-on-n double layer heterojunction diodes has been studied [53,54]. It has been shown that at 77K, dislocation densities greater than the mid $10^6 cm^{-2}$ can produce dark current densities in excess of the diode diffusion current. These studies therefore support the requirement, previously accepted, of mid $10^5 cm^{-2}$ or less as the suitable level in terms of dislocation density in HgCdTe material for IR photo diodes. EPD has been so far the screening technique used to qualify HgCdTe epilayers. Unfortunately, EPD is destructive and therefore cannot be a screening technique in a manufacturing process. Thus, a non-destructive technique is required, such as X-ray diffraction, provided that a good correlation could be established with EPD count. EPIR has attempted to establish such a correlation as illustrated in Figure 17. From this curve it can be seen, as expected, that there is a general trend i.e. a decrease in EPD when DCRC FWHM is decreased [55].

As discussed previously, the objective in terms of EPD is mid $10^5 cm^{-2}$ or lower. From this curve it appears that when DCRC FWHM is not larger than 40 arcsec, EPD is mostly in the low-mid $10^5 cm^{-2}$ range. Incidently, the large FWHM's and EPD's reported in this Figure are related to epilayers grown under nonoptimized growth conditions purposely used to study the influence of growth conditions on crystal quality as shown in Figure 16. This study demonstrates that by using a simple, fast and non-destructive technique such as double crystal X-ray diffraction, it is possible to screen with reliability MBE grown HgCdTe epilayers in terms of dislocation density. This represents an important contribution in manufacturing procedure.

This study has also shown interesting features. The spread in EPD's for low DCRC FWHM is not understood at present. Several parameters such as CdZnTe surface preparation, CdZnTe lattice parameter, particle spitting from the effusion cells, minute changes in Hg flux or growth temperature are suspected. This should be investigated thoroughly. A correlation between EPD and macroscopic defect density might explain the spread. Such a correlation would be interesting to establish.

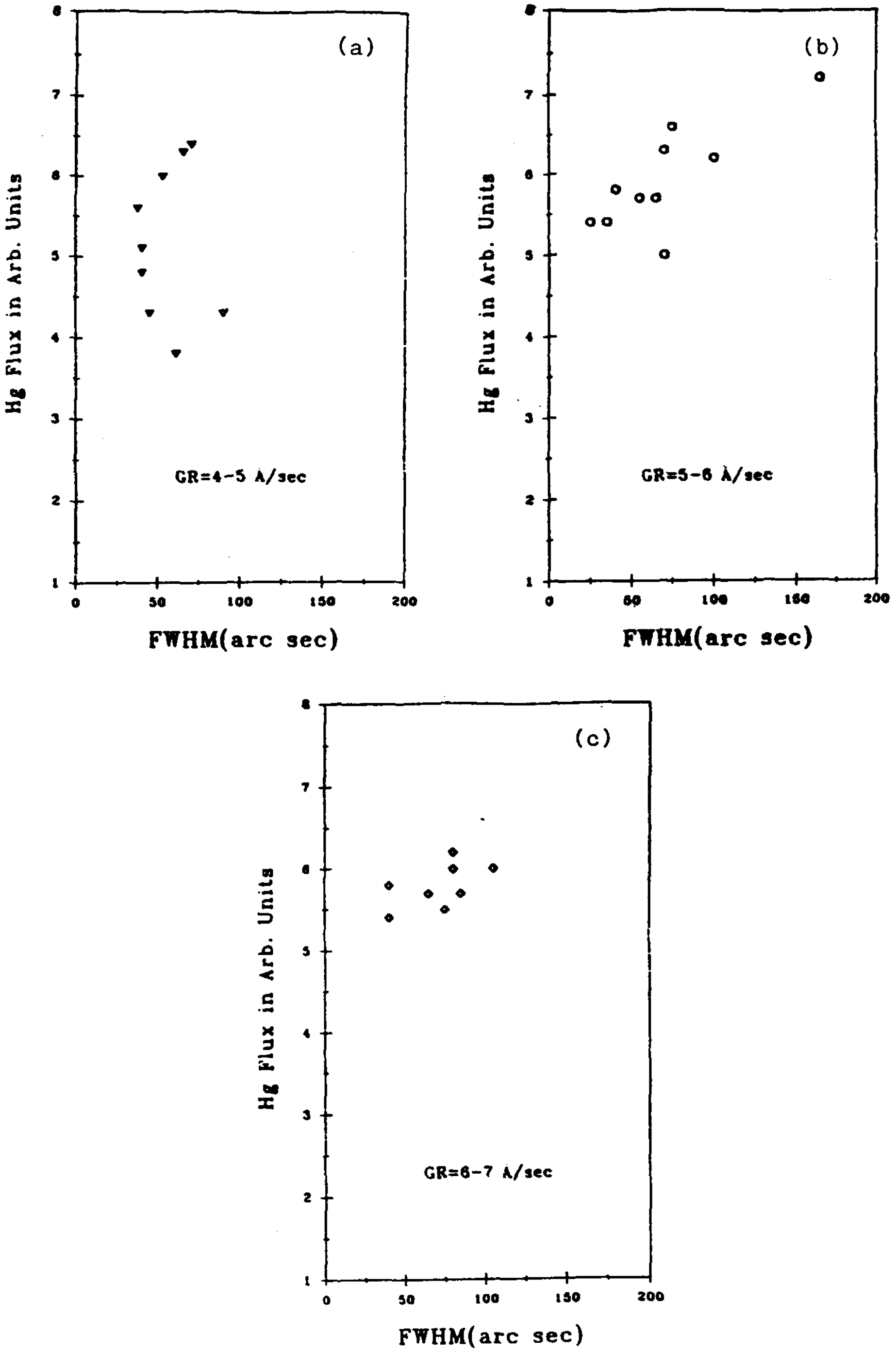

Figure 16: a) DCRC FWHM versus Hg flux for $Hg_{1-x}Cd_xTe$ ($x = 0.22$) epilayers grown at 185°C by MBE with a growth rate of 4 to 5 Å/sec. b) DCRC FWHM versus Hg flux for $Hg_{1-x}Cd_xTe$ ($x = 0.22$) epilayers grown at 185°C by MBE with a growth rate of 5 to 6 Å/sec. c) DCRC FWHM versus Hg flux for $Hg_{1-x}Cd_xTe$ ($x = 0.22$) epilayers grown at 185°C by MBE with a growth rate of 6 to 7 Å/sec.

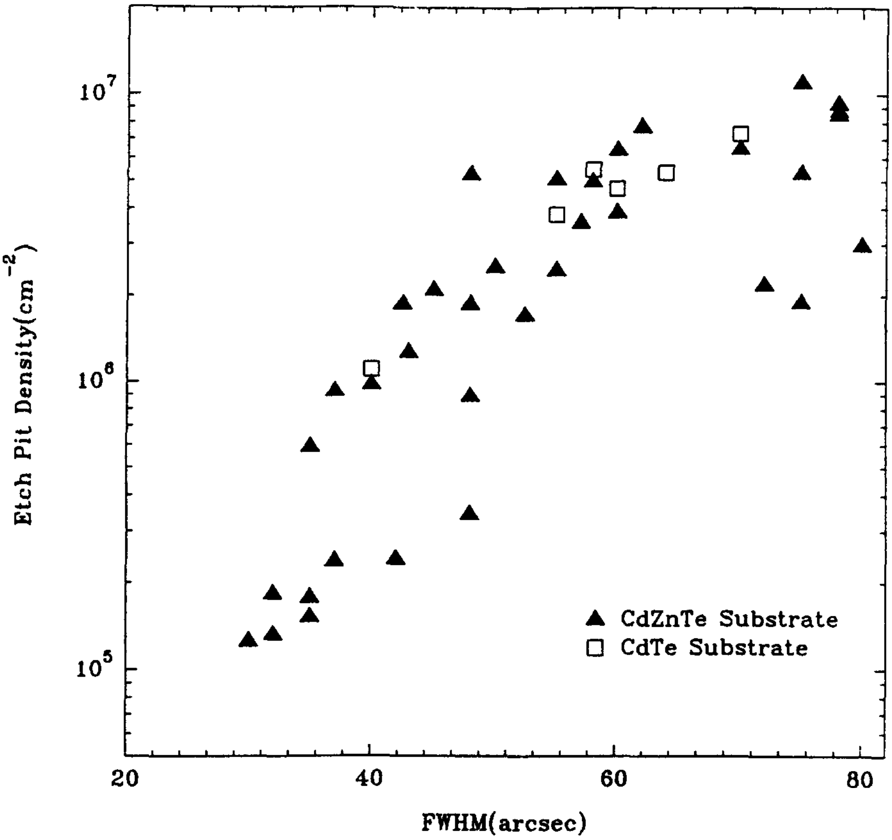

Figure 17: DCRC FWHM vs etch pit density for $Hg_{1-x}Cd_xTe$ (x=0.22-0.23) epilayers grown at 185°C by MBE on CdZnTe and CdTe substrates.

Figure 17 also displays EPD measured on epilayers grown on CdTe(211)B substrates. It appears that on CdTe subtrates, the best FWHM and EPD are 40 arcsec and $1 \times 10^6 cm^2$ respectively. This confirms that a lattice matched substrate such as CdZnTe is more suitable for the epitaxy by MBE of HgCdTe (x = 0.22). This also suggests that if alternate substrates such as GaAs or Si are selected, a CdZnTe lattice matched buffer layer should be more appropriate than a CdTe buffer layer.

In MBE, growth parameters have been optimized as presented hereafter in order to get on a routine basis EPD lower than $5 \times 10^5 cm^2$.

5. OPTIMUM CONDITIONS FOR MBE GROWTH OF $Hg_{1-x}Cd_xTe$

A lot of attention has been given regarding the determination of the optimal conditions about the growth of HgCdTe films by MBE. Many aspects having already been discussed in previous sections, the purpose here is to give an overview of the difficulties, the limits and the solutions related to the growth.

5.1. *Hg Condensation Coefficient* (C_{Hg})

As already mentioned, the MBE growth of HgCdTe is difficult to achieve because the evaporation of this semiconducting alloy is highly non congruent. This is due to the fact that mercury is weakly bonded to tellurium. Thus, the mercury tends to evaporate preferentially from the surface. As a consequence, it has been experimentally shown that the condensation coefficient for Hg is low and decreases when the substrate temperature is raised. The condensation coefficient for a given element is defined as the ratio of the number of atoms incorporated in the layer to the number of incident atoms impinging the surface.

The precise determination of a condensation coefficient actually is quite difficult and the comparison between results is meaningless if several growth parameters are not reported, because it is not a thermodynamic parameter as it will be discussed hereafter.

For a given element, incident flux and amount incorporated have to be known to calculate the condensation coefficient. A direct and precise measurement of the Hg flux striking the surface of the growing film has never been done. The incident Hg Flux is either estimated from Knudsen effusion equation (equation 12) in section 3.4) or from the pressure measured in an ion gauge located at the substrate manipulator. In both cases, the accuracy is not very high. Taking into account, the uncertainties related to the temperature of the mercury inside the cell described in Section 3.2, the area of the aperture and the distance between the cell and the film we have estimated that using the Knudsen formula, the Hg flux is known within a factor of two.

It is important to mention that since the growth of single crystalline HgCdTe can occur for a range of Hg flux (existence field) at a constant temperature, the condensation coefficient should be determined for the minimum amount of Hg flux required to grow the single-crystalline HgCdTe film. Actually, measurement of condensation coefficients implies that specific experiments are carried out since during a typical MBE growth of $Hg_{1-x}Cd_xTe$ it is preferred not to take the risk by growing at the lower limit of achieving polycrystalline growth.

Once the incident Hg flux is known, it is rather easy to determine the condensation coefficient since the amount of Hg incorporated in the film can be calculated precisely once thickness, film composition and growth duration are known.

Hg condensation coefficient C_{Hg} has been estimated several times and different values have been obtained. As a matter of fact, parameters such as growth temperature, crystallographic orientation and growth rate have an influence on the condensation coefficient. The first attempt to determine the Hg condensation coefficient has been carried out in the Laboratoire Infra Rouge (LIR) in 1983 [56]. The experiments were carried out on (111)B $Hg_{1-x}Cd_xTe$ (x 0.2). The determination of C_{Hg} was not precise because the Hg flux had been estimated from the amount of mercury evaporated during several growth runs. In addition, the growth experiments were not carried out under the minimum Hg flux requirement. Hence, the value of 10^{-3} for C_{Hg} at a growth temperature of about 190°C was underestimated. However, it has been found that C_{Hg} decreases **exponentially** when the growth temperature increases. This point, which has never been questioned since then, is extremely important. It shows for example that between 180 and 200°C, CHg decreases roughly by a factor of two i.e. Hg consumption increases by a factor of two. Actually, the pressure over pure Hg has the same rate of increase in the range of temperature investigated (120-200°C). From these experiments, it is concluded that the temperature of the growth has a strong influence on C_{Hg} and we have seen that a precise determination of T_{ss} is difficult (Section 3.6).

The second parameter that C_{Hg} depends on is the crystallographic orientation. The influence of the crystallographic orientation on condensation coefficients has been compared between the (111)A, (111)B, (100) and (211)B orientations [21]. In each case, $Hg_{1-x}Cd_xTe$ growth was closely followed by RHEED. The minimum amount of Hg necessary to maintain the growth was determined by slowly decreasing the Hg flux until difficulties in maintaining monocrystalline growth were observed. The results are reported in Table 4. We have found that among all the orientations investigated (211)B and (111)B are those requiring less mercury and (111)A the one which needs the largest amount.

Table 4: Minimum amount of Hg flux (in arbitrary units) needed to maintain the monocrystalline growth of $Hg_{1-x}Cd_xTe$ at a growth temperature of 185°C.

Crystallographic orientation	(211)B	(111)B	(100)	(111)A
Hg flux (arbitrary units)	1	1.25	5.5	11.25

With all the other growth conditions being the same, including the composition, the minimum amount of Hg necessary to maintain epitaxial growth of $Hg_{1-x}Cd_xTe$ at 185°C, is almost one order of magnitude higher for the (111)A orientation than for the (111)B orientation. The minimum amount of Hg necessary to maintain epitaxial growth along the (100) orientation falls in between that for the (111)A and the (111)B orientations. These results have been explained in terms of the bonding of surface atoms. Hg atoms are more protected from reevaporation in the (211)B and (111)B orientation than in the (100) orientation. A similar but less dramatic tendency has also been observed for Cd.

From another study [57], it has been reported that (211)A has about the same C_{Hg} than (100) regarding the growth of HgTe at 200°C. This indicates that the same important difference observed between (111)B and (111)A exists also between (211)B and (211)A. Regarding (110), it is difficult to determine C_{Hg} from the information reported in the paper published by Arias *et al.* [58] It seems that $C_{Hg}{}^{110}$ is not higher than C_{Hg} [100].

Results regarding the growth parameters for different orientations provide an important means for ascertaining the best orientation for growth. From a Hg consumption point of view, one could conclude that (211)B and (111)B orientations are the best. But it is important that other parameters, such as the ease in the growth control and the achievement of high quality layer are taken into consideration. As already discussed in section 4, (211)B orientation appears to be far superior to (111)B because it is much less sensitive to microtwin formation. This better suitability of (211)B compared to (111)B will be further confirmed by investigating the transport properties.

From these experiments, it is therefore concluded that the crystallographic orientation plays a major role in the value of the mercury condensation coefficient.

The third parameter which has been found to have an influence on C_{Hg} is the growth rate as discussed in Section 4.2.2. According to Figure 16, the optimum Hg flux is almost constant when the growth rate increases. Even though, these experiments have not been carried out in view of the determination of C_{Hg} i.e. under the lowest Hg flux required to maintain the single-crystaline growth, it can be safely extrapolated that C_{Hg} increases almost linearly with the growth rate, at least up to a 50% increase. **These experiments confirm that the condensation coefficient is not an intrinsic or thermodynamic parameter**. Hence, increasing the growth rate presents many advantages such as reducing the mercury consumption and the amount of mercury to be removed per growth run and also the duration of a growth run. This translates to a significant cost reduction in a manufacturing program. However, a drastic increase in the growth rate degrades the crystal quality and therefore device performance. In the (211)B orientation growth rates up to 15 Å/s i.e. 5.4 μm/h have been used to grow good quality $Hg_{1-x}Cd_xTe$ films on GaAs (211)B substrates at 180-185°C [59,60], It seems that 15 Å/sec represents an upper limit in terms of growth rate. However, from the data reported in ref. 58, it is difficult to determine if C_{Hg} has increased compared to a typical growth rate of 5 Å/sec.

In summary, in a RIBER MBE 2300, the incident mercury flux necessary to grow high quality $Hg_{1-x}Cd_xTe$ (x = 0.22) on (211)B CdZnTe substrates at 185°C with a growth rate of 5-6 Å/sec, is estimated to be of (5±2) 10^{16} at(cm^{2}s^{-1} from the Knudsen effusion law. This gives a condensation coefficient C_{Hg} of about 0.01 to 0.03 slightly underestimated since the growth is not carried out under the minimum Hg flux. Therefore 0.02-0.05 is a realistic range value for C_{Hg} under the growth conditions specified hereabove.

A quantity which is much more concrete is related to the amount of mercury required for a complete growth run which include not only the mercury evaporated during growth but also before and after. **Under the growth conditions described above about 100g of mercury are necessary to grow 10-12μm thick (211)B $Hg_{1-x}Cd_xTe$ (x=0.22) films in a RIBER MBE 2300.**

5.2. *Te and Cd Condensation Coefficients*

It has been experimentally shown that above 195°C the evaporation of tellurium from HgCdTe is not negligible and that C_{Te} is no longer equal to one, which is expected since MBE of $Hg_{1-x}Cd_xTe$ occurs under Te saturated conditions. By comparing changes in $Hg_{1-x}Cd_xTe$ composition and growth rate, we have seen that both are due to a change in the growth rate of HgTe but not in that of CdTe [(1-x)HgTe + x CdTe = $Hg_{1-x}Cd_xTe$] when the growth temperature exceeds 195°C [46], Above 200°C, the rapid reevaporation of Hg leaves free Te which is also reevaporated and the film still grows monocrystalline. However, an increase in x value of 1.5% to 2% for a 1°C increase in the substrate along with a rapid change in the growth rate has been observed. The experiments were carried out with a constant Hg flux. The growth of $Hg_{1-x}Cd_xTe$ above 200°C is not recommended for the following reasons

1 - the comsumption of Hg is very high,

2 - the control in composition x is extremely difficult along the growth axis and also across the wafer and

3 - compositional inhomogeneities with an x-value variation of 0.1 over a period of ~1000 Å has been observed for growth in the (100) and (211) orientations[57].

During the growth of $Hg_{1-x}Cd_xTe$ the Hg flux is high compared to the Te flux when the growth occurs at 185°C in the (211)B growth direction however the Te flux produced by the effusion cell and the Te incorporated in the layer are comparable and therefore C_{Te} is close to unity. It is no longer the case when the Hg flux is increased by a factor of ten or more because reaction in the gas phase between Hg atoms and Te_2 molecules occurs. Therefore the determination of C_{Te} is not straightforward since the Te flux impinging the surface cannot be estimated from Knudsen law. As an example during growth in the (100) direction at 190-200°C, we have determined that under our growth conditions (in the (100) orientation, the field of existence of single crystaline $Hg_{1-x}Cd_xTe$ is very large and the Hg flux can be very high) about 40% of the Te evaporated does not reach the substrate. This shows that the growth does not occur under a molecular regime i.e. the growth of HgCdTe under these conditions should not be called MBE.

However, the growth in the (211)B direction at 185°C is under a MBE regime and C_{Te} and C_{Cd} are close to unity. This implies the following:

1 - the growth rate is controlled by the Te flux i.e. primarily by the temperature of the Te cell.
2 - since C_{Hg} is much lower than unity the composition x of the alloy is mostly controlled by the Cd flux i.e. by the temperature of CdTe cell. Changing the composition in $Hg_{1-x}Cd_xTe$ is therefore very easy.

A comparison between the pressures measured in the mercury and tellurium flux with an ion gauge indicates after using relations (14) and (15) that for the growth conditions described in 5.2., the ratio between Hg flux and $Te_{(atom)}$ flux is between 30 and 35. Since the Hg/Te ratio is 0.78 in the alloy, C_{Hg}/C_{Te} is of about 0.025 which is in complete agreement with C_{Hg} found earlier and confirms also that C_{Te} is very close to one under these growth conditions.

5.3. *Temperature and Flux Stability*

As just mentioned, due to its low condensation coefficient mercury does not control the composition. This is accomplished through CdTe and Te effusion cells. However, this does not permit loose control in the temperature of the mercury cell. Indeed, we have reported that microtwin formation can be avoided in CdTe (111)B buffer layer when a proper thermal cleaning of the substrate and a suitable growth temperature are used. We have also shown that in order to prevent microtwin formation in MBE HgCdTe layers a stringent control is required in the stability of Hg flux and in the surface substrate temperature (section 6).

The growth in the (211)B orientation has also shown that for a given growth temperature, $Hg_{1-x}Cd_xTe$ of high crystalline quality is obtained in a very narrow Hg flux window of less than 30% (corresponding to a change ΔT of only 5°C in the Hg cell).

The couple [Hg flux - surface temperature] should be accurately controlled. It should be very stable during the growth, across the wafer which represents a challenge for very large wafers and it should be also reproducible from run to run. In order to achieve these requirements, the temperature in the Hg cell should have a stability of ±0.5°C (flux stability of ±2,5%) and the stability of substrate temperature and its variation across the wafer should not be more than ±0.5°C.

Mercury flux stability better than the gauge sensitivity limit of ±2.5% have actually been observed using the Hg cell described in 3.2. Regarding Te and CdTe flux stability, we have seen in section 3.5 that in order to achieve the requirements in terms of cut-off wavelength for I.R. photodiodes, temperature fluctuation ΔT in CdTe and Te cells should not exceed ±0.1°C which is achieved in current MBE systems.

5.4. *Growth Temperature*

The influence of the growth temperature has already been discussed. It has been found in early experiments [61] and confirmed since then that MBE growth of $Hg_{1-x}Cd_xTe$ ($x=0.22$) should occur between 170 and 200°C. Below 170°C it is difficult, in conventional growth, to obtain a high crystalline quality. Decreasing the growth rate improves the quality but the duration of the growth is too long. At 200°C and above the condensation coefficient for Hg low and the reevaporation of Te complicates the growth as seen in 5.2. This explains why most of the experiments are carried out between 180 and 190°C.

5.5. *Thickness and Composition Uniformities*

Thickness and composition uniformities of $Hg_{1-x}Cd_xTe$ films grown by MBE have been performed in different growth chambers and by different groups. The best results for a given distance between effusion cells and substrates are obviously achieved when the rotation of the substrate is used.

At EPIR in a RIBER 2300 standard deviation for both thickness (σ_t) and composition (σ_x) uniformities measured across 2x2 cm^2 wafer are below sensitivity limits i.e. $\sigma_t<2\times10^{-2}\mu m$ and $\sigma_x<5\times10^{-4}$.

Experiments have been reported on 2-inch GaAs substrates [62] and more recently, on 2, 3 and 5-inch Si substrates [63,64]. In the OPUS 45, where the experiments on Si have been performed, the distance between the front of the Hg-cell and the substrate is 15 cm. The results are presented in Table 5. It can be seen that MBE results are excellent up to 3-inch in diameter. In terms of thickness control, they are one order better than those reported in LPE [65].

Composition uniformity has also been measured along the growth axis [55]. A profile of the absorption coefficient has been determined at different thicknesses through FTIR measurements for a 11 µm-thick sample. A standard deviation $\sigma = 5\times10^{-4}$ i.e. $\sigma/tz = 5\times10^{-5}/\mu m$ which is almost within the measurement uncertainty has been obtained confirming that when MBE growth conditions are stable no change in composition is observed along the growth axis.

Such a control, achieved in MBE in terms of thickness uniformity and composition uniformity both across the wafer and along the growth axis, has never been demonstrated by any other growth technique. Run-to-run reproducibility in composition has started to be measured in MBE manufacturing related programs. In 1992, at EPIR in a Research and Development program, a standard deviation of 0.005 with $x_{mean} = 0.220$ has been obtained on 20 layers. In 1994, a standard deviation of 0.002 with $x_{mean} = 0.225$ has been reported for 25 runs in a MBE manufacturing program [66], these results compare well with run-to-run reproducibilities reported in LPE large volume production [67].

Table 5: Uniformities of HgCdTe epilayers grown by MBE

Diameter		2-inch	3-inch	5-inch
thickness uniformity	σt	0.02 µm	0.05 µm	0.1 µm
standard deviation	σt/t	0.2%	0.5%	1%
Composition uniformity	σx	6.7×10^{-4}	1.3×10^{-3}	5.4×10^{-3}
standard deviation	σx/x	0.3%	0.6%	2.4%
Composition uniformity (Z axis)			$5\times10^{-5}/\mu m$	

5.6. *MBE Growth Modelling—Thermodynamics vs Kinetics*

The discovery of the strong influence of the crystallographic orientation on the condensation coefficient of Hg and to a less extend on that of Cd reported in 1986 [21] and confimed later[57] has important consequences in terms of MBE growth modelling. They confirm that a classical thermodynamic approach using the mass action law which implies that growth occurs under thermodynamic equilibrium, and neglecting surface kinetics is not perfectly adapted for the growth of $Hg_{1-x}Cd_xTe$ by MBE. A pure thermodynamical approach nevertheless can provide suitable information and can be very useful in terms of prediction once the influence of the selected crystallographic orientation has been taken into account. For example, it would have been very interesting to compare the intrinsic doping, due to Hg vacancies, in MBE grown $Hg_{1-x}Cd_xTe$ in different crystallographic orientations and under various growth conditions with the doping predicted by the P-T phase diagram (Figs. 3,4) since this phase diagram has been established for $Hg_{1-x}Cd_xTe$ grown under thermodynamic equilibrium (bulk crystal or LPE material). Unfortunately, this extensive study has not been done for the different orientations discussed above. However, investigations carried out in the (211)B orientation and limited to a very narrow range of growth temperature, have produced interesting information which will be discussed in the following section.

6. ELECTRICAL PROPERTIES: INTRINSIC DOPING

Establishing the behaviour of extrinsic dopants in $Hg_{1-x}Cd_xTe$ is very important. Small concentrations of unintentionally added elements can, if electrically active, affect the properties of the material and influence the performance of devices. More importantly, the need to produce photo diodes with improved performance may ultimately require intentionally doped material with known and controllable concentrations of both donor and acceptor elements on both sides of the junction.

It is obvious that undoped material, both in the as-grown and low temperature Hg-annealed states must be studied before the effect of deliberate doping can be understood. This aspect becomes increasingly important in an epitaxial process such as MBE where growth temperature is low. A complex picture of behaviour has been described [68]. In MBE material, several factors such as substrate orientation, growth temperature, Hg flux and the x value of the layer appear to influence the electrical properties.

From early investigations, it was difficult to determine what controls electronic properties between native defects (Hg vacancy, interstitial Te...) and background impurities. Therefore, a solid understanding regarding intrinsic as well as extrinsic doping in MBE grown layers is absolutely necessary. This can be achieved by investigating electrical properties of as-grown and Hg-annealed of unintentionally as well as intentionally doped material.

6.1. *Transport Properties Measurement*

Electrical properties of doped as well as undoped layers have been measured using the Van der Pauw technique [69]. Hall coefficient [$R_h(T)$] and resistivity [$P(T)$] of the layers were calculated by the van der Pauw technique (typical sample dimension ≈ 5x5 mm^2) for temperatures ranging from 300 to 20K and magnetic fields up to 1.0 T. Great care was taken in contacting the samples in small areas at the corners. This is known to give reliable measurements. Contact resistance was systematically checked.

The lifetime measurements (typical sample dimensions are ≈ 3x3 mm^2) were carried out using the photoconductivity decay technique. All the samples were etched in Br-methanol solution prior to measurement, which was especially important in the latter case. Indium was used to make good ohmic contacts for n-type layers.

A pulsed GaAlAs laser beam ($\lambda = 850$ nm) was focused on the sample to generate the excess carriers. The samples were mounted on the cold finger of a liquid nitrogen variable temperature dewar. Photoconductivity decay signals were amplified with a low-noise cryogenic preamplifier and were measured using a Hewlett-Packard 54100A digitizing oscilloscope. The decay signals obtained were averaged in order to minimize the noise. The noise at zero beam intensity was subtracted from the signal measurements. The biasing was kept low to avoid sweep-out effects, and the light intensity was also kept low in order to satisfy the low injection conditions.

Indium was used to make ohmic contacts for n-type HgCdTe layers. The biasing was kept low to avoid sweep-out effects, and the light intensity also kept low in order to satisfy the low injection condition.

Secondary ion mass spectrometry (SIMS), calibrated with implanted reference samples, was used to evaluate the impurity atomic concentration. It should be pointed out that the apparent doping efficiency defined as the ratio of the carrier concentration (N_D-N_A) measured at low temperature by the Hall technique divided by the impurity atomic concentration measured by SIMS can be misleading in the case of as-grown materials where Hg vacancy concentration cannot be neglected. Actually, in doped $Hg_{1-x}Cd_xTe$ the doping efficiency should be only determined on isothermally annealed material.

6.2. *Doping of Unintentionally Doped Layers*

The doping in unintentionally doped HgCdTe layers is related to

1. Intrinsic doping from point defects (primarily Hg vacancies, Te interstitials...) and

2. Background impurities introduced during the growth and/or diffusing from the substrate.

Since the effect of these two potential sources of doping are combined, their specific contribution is extremely difficult to determine. The analysis of the MBE growth conditions shows the following.

The flux of Hg atoms impinging on the growing epilayer is calculated to be in the (5±2) 10^{16} at $cm^{-2}s^{-1}$ range (a small uncertainty still exists in the precise determination of the Hg temperature inside the Hg cell). This translates to an equivalent pressure P_{eq} of (5±2)10^{-7} atm on the surface of the epilayer which is growing at 185°C.

The Hg partial pressure over a Te saturated $Hg_{0.78}Cd_{0.22}Te$ at 185°C is calculated from relations (8), (9), (10) to be 1.5×10^{-6} atm in agreement with the published P-T phase diagram [see Fig 1] which gives a reevaporating flux of 1.3×10^{17}at $cm^{-2}s^{-1}$. This phase diagram is calculated for bulk $Hg_{0.78}Cd_{0.22}Te$. Obviously, it does not take into account the crystallographic orientation which plays a role regarding species incorporation as well as desorption in the MBE growth process as discussed in section 5.1. Hence, it can be seen that under optimized growth conditions in the (211)B orientation, the incoming Hg flux is found to be at least lower by a factor of 2 than the calculated reevaporating Hg flux. Since it is unlikely that MBE growth can proceed if the reevaporating flux is higher than the incoming flux, this indicates that the extrapolation at low temperature (180-200°C) of the mass action law coefficients determined at higher temperature (section 2.2.3.) does not describe either accurately or correctly MBE growth because the crystallographic orientation is not an input parameter. It is also expected that the discrepancy will be different for another crystallographic orientation. For example, on a (111)A face, the minimum incoming Hg flux, which is more than 10 times higher, will be 5-6 times higher than the reevaporating flux from bulk $Hg_{0.78}Cd_{0.22}Te$. **However, it appears that MBE does occur, for all the crystallographic orientations under Te saturated conditions.** This explains why the crystal quality deteriorates quickly when the Hg flux decreases or when the substrate temperature slightly increases (excess Te) (see Fig. 16a). Impinging fluxes of both Te and Cd are higher than re-evaporating fluxes (several orders of magnitude higher in the case of Cd) which is consistent with usual MBE growth process.

Incidently and perhaps by coincidence, the growth on (211)B proceeds under conditions which can be considered to be close (within a factor of 2) to equilibrium. This is also the case for (111)B. However as discussed in Section 5.6, MBE growth modelling **should** take into account the crystallographic orientation even though for some orientations such as (211)B and (111)B; a thermodynamic model can be used to a good approximation.

This particular situation of quasi-equilibrium does not provide a straightforward answer regarding point defect equilibrium. Can we really consider that CdTe and HgTe are independent sublattices during MBE growth? Such an independence would imply that increasing the Cd flux should increase x with almost no influence on Hg vacancy concentration. Such a detailed study should be carried out in order to predict and control the intrinsic doping in MBE growth of $Hg_{1-x}Cd_xTe$.

Nevertheless, the fact that a change of no more than 30% is possible in the Hg-flux, if one wants to obtain good crystallinity [see Fig. 16], implies that there is almost no flexibility in the control of the intrinsic doping related to Hg vacancies or other point defects for a given growth temperature. Hence, according to P-T phase diagram, $Hg_{1-x}Cd_xTe$ (x=0.22) grown at 185°C should be p-type with a doping level in the high 10^{15} cm^{-3} range [see Figs. 3 and 4] if doping is mainly controlled by Hg vacancies and if MBE on (211)B can be considered to occur near equilibrium conditions. This will be answered in 6.4.

6.3. *Background Impurities*

Unintentionally doped MBE as-grown layer do not always exhibit a p-type character. For several years, erratic behaviour (in terms of electrical properties) of as-grown as well as annealed MBE epilayers was observed in different laboratories, including the Microphysics Laboratory at the University of Illinois at Chicago. It has been found recently that it was not due to a lack of control in MBE growth but to diffusion of impurities from the substrate[70,71]. Convincing evidence which are presented hereafter has been obtained.

• After isothermal anneal, HgCdTe MBE layers should exhibit a residual background level which can be called "genuine" or "intrinsic" MBE background level. In previous studies, an understanding of the "intrinsic', doping was hindered by the presence of twins in (111)B oriented epilayers, and the analysis of a few twin-free (111)B layers had not been conclusive [40] because of what is discussed hereafter and unknown at that time.

• A few years ago, a major study was undertaken of the growth on the (211)B orientation because the twinning problem did not appear as severe as in the (111)B orientation. The (211)B layers were grown under stringent and similar growth conditions for comparison with those grown in the (111)B orientation. However, striking differences in carrier concentration as well as in mobilities appeared for as-grown non intentionally-doped $Hg_{1-x}Cd_xTe$ (x=0.22) epilayers grown under similar conditions on (211)B CdZnTe substrates, bought from various suppliers. After isothermal apneal, large differences remained. Figure 18 illustrates what we consider to be the word case; after n-type anneal; HgCdTe layer is still p-type. These differences have, after tedious investigation, be explained satisfactorily by the diffusion, in the epilayer, of impurities originating from the substrate [70]. SIMS analysis have been performed and impurities such as Li, Ag and Cu have been found. This problem has been observed for all the epilayers, however, the impurity level varies from supplier to supplier and even from lot-to-lot.

Evidence of p-type impurity outdiffusing (copper and silver) from the substrate during anneal has also been observed and reported since then by another group [71].

• The distribution of these impurities strongly depends upon the temperature and the duration of the anneal. It appeared that when the layer is exposed to a high temperature anneal at 400°C or above, the electrical behaviour of the layer is improved. This effect is thought to be due to the segregation of impurities at the epilayer surface. The origin of the contamination and the role played by the tellurium precipitates are still unanswered questions which should be investigated thoroughly.

• Experiments carried out on selected substrates of the same batch have shown that the surface of the substrate might also have accumulated impurities. For a series of expected suitable substrates, a deep etch was necessary to grow a clean HgCdTe epilayer. A 2 µm etch prior to growth was not enough

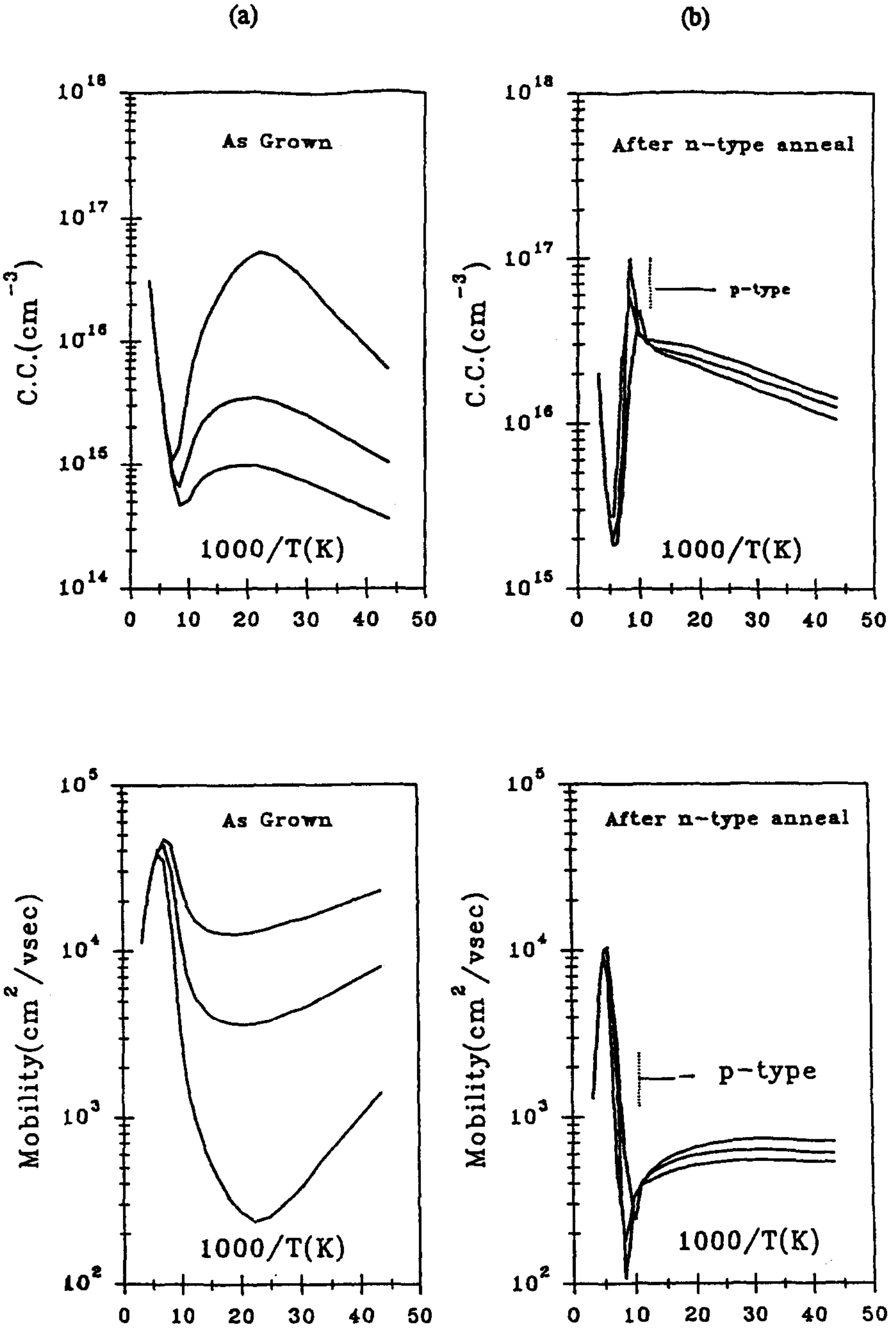

Figure 18: Anomalous Hall behaviour of non intentionally-doped MBE $Hg_{1-x}Cd_xTe$ (x=0.22) grown on a bad (211)B substrate. Magnetic field strength of 0.2, 0.4 and 0.8 Tesla have been used; (a) carrier concentration, (b) mobility of as-grown and after n-type anneal versus reciprocal temperature.

to prevent contamination from substrate surface whereas a 5 μm etch was enough. Therefore, it turns out that even on so-called "good" substrates, the surface preparation has to be carried out with a lot of care.

These problems which are very detrimental in MBE growth are very likely less damaging in LPE growth. Indeed LPE occurs at temperatures above 400°C, therefore impurities can diffuse through the layer into the melt during the growth. In addition at the initiation of the LPE growth, the substrate can be etched by meltback, a step which can eliminate or at least decrease the substrate surface problem. However, according to private information, severe contamination of LPE melts has been observed in the past by several groups.

- Conclusion

This was obviously a critical problem regarding the use of MBE grown HgCdTe for device fabrication. After intensive investigation and numerous experiments, CdZnTe substrates of higher quality have been found. However, non-intentionally doped material grown on these substrates both in the as-grown and Hg anneal states very often exhibit mixed electrical conduction. This indicates that background impurities are competing with native defects to govern electrical properties in the low 10^{15} cm^{-3} range. The shape of carrier concentration and mobility vs 1/T curve determined from Hall measurements can be explained only by nonuniform distribution of carriers. Impurities diffusing from the substrate are obviously non uniformly distributed along the growth axis and very likely also across the epilayer plane. On the other hand, impurities incorporated during MBE process should be uniformly distributed and therefore they should be responsible only for compensation and not for the mixed conduction (Hall anomalous behaviour). This mixed conduction behaviour for which the substrates are responsible, prevents the determination of the genuine background doping level in the MBE-grown HgCdTe layers. The incorporation of indium, during growth, which is reported hereafter, has been carried out not only to control mid to high donor doping concentrations, but also in order to establish a background level. However, as it is discussed in detail hereafter, the lower limit of $\approx 2 \times 10^{15}$ cm^{-3} controlled in In-doped MBE HgCdTe, is still due to impurities diffusing from substrates. Substrate screening and cleaning are therefore two very important steps in a MBE manufacturing programme.

6.4. *Intrinsic Doping related to Hg Vacancies*

With a limited impurity background it is possible to try to determine the intrinsic doping in MBE grown HgCdTe layers for comparison with the predicted intrinsic doping at equilibrium. A study has been carried out on In-doped layers because it has been found that the results are very consistent when N_D is in the 10^{16} cm^{-3} range. Table 6 shows the change in the acceptor level N_A between as-grown and 250°C isothermal Hg-annealed states for HgCdTe material (x=0.22). A decrease in ΔN_A of 5 to 9×10^{15} cm^{-3} is observed in the acceptor level. In these experiments, it is also assumed that the change, if any, in N_D can be neglected compared to ΔN_A. It is supposed that at this temperature, close to the growth temperature, additional electrical activation of impurities can be neglected. Therefore, the difference $-\Delta N_A$ should be equal to the Hg vacancy concentration obtained at the growth temperature since it is generally accepted, that a low temperature Hg anneal fills Hg vacancies. At 250°C, the concentration of Hg vacancies in an isothermal anneal being of $\approx 1 \times 10^{14}$ cm^{-3}, it is reasonable to conclude that this decrease in N_A concentration corresponds roughly to the Hg vacancy concentration produced during MBE growth. Actually, this value ΔN_A compares well with the Hg vacancy concentration expected for a growth occurring at 185°C at equlibrium under Te saturated conditions. This very important point has been investigated in much detail only for the (211)B orientation. Since crystallographic orientation plays a major role in MBE growth, especially regarding mercury condensation coefficient [21], intrinsic doping related to point defects might be very different for other crystallographic orientations (Section 5.1). However, since all the growth runs reported here have been carried out in the (211)B orientation, this represents a solid basis, which has never been established before, towards understanding and control of the doping. **Furthermore, these results prove that regarding Hg vacancy formation, MBE of HgCdTe (x=0.22) in the (211)B orientation is controlled primarily by thermodynamics and confirms that MBE growth in this orientation is described with a good approximation by a quasi-equilibrium approach.**

Table 6: Change in acceptor level NA between as grown and isothermal annealed In-doped $Hg_{1-x}Cd_XTe$ epilayer

Name	N_D-N_A (cm^{-3}) (as grown)	N_D-N_A (cm^{-3}) (n-type annealed)	-ΔN_A (cm^{-3})	Hg flux (arbitrary units)	x %
069	1.3×10^{16}	2.2×10^{16}	9×10^{15}	5.3×10^{-6}	24.4
070	1.8×10^{16}	2.6×10^{16}	8×10^{15}	5.5×10^{-6}	20.5
071	1.6×10^{16}	2.0×10^{16}	4×10^{15}	5.4×10^{-6}	20.5
019	1.1×10^{16}	1.7×10^{16}	6×10^{15}	5.7×10^{-6}	20.5
020	0.75×10^{16}	1.5×10^{16}	7.5×10^{15}	5.8×10^{-6}	20.5
023	0.75×10^{16}	1.9×10^{16}	9×10^{15}	5.7×10^{-6}	19.0
013	0.75×10^{16}	1.4×10^{16}	5.3×10^{15}	5.7×10^{-6}	22.0

7. EXTRINSIC N-TYPE DOPING

We have seen that MBE growth occurs under Te saturated conditions and also that the Hg flux should be kept very constant inside a very narrow window. It has also been observed that when the growth temperature is lower than 160°C, the crystal quality is poor and when it is higher than 200°C, the Hg flux required to grow is too large and the growth is difficult to control. All these constraints, to the contrary to what was thought from early MBE experiments, prevent any flexibility in the control of *in situ* intrinsic doping during MBE growth (section 4.2.2). We have shown that under optimized growth conditions, MBE (211)B HgCdTe epilayers, in agreement with the P-T phase diagram in the as-grown state, have a Hg vacancy concentration of mid to high 10^{15} cm^{-3}.

We have seen also that isothermal annealed «undoped» layers are not reliable in terms of electrical properties since mixed conduction very often occurs due to residual impurities which have diffused from the substrate, even from the best substrates commercially available. However, p-type conversion is usually obtained on undoped layers grown on the best CdZnTe substrates after a suitable p-type anneal. Nevertheless, these limitations obviously require that for optoelectronic device fabrication, extrinsic doping should be developed.

At this point it might be useful to consider the characteristics a good doping impurity should have:

1. easy incorporation in the right lattice site during the growth,

2. electrical activation at the growth temperature,

3. 100% electrical efficiency,

4. associated with a shallow level and responsible for excellent electrical characteristics,

5. no defect creation in the lattice and

6. low diffusion coefficient.

Foreign elements have been found to substitute mostly in the cation site in MBE due to the Te saturated growth conditions. Therefore, if is not surprising that whereas n-type doping is easily obtained, p-type doping is difficult to achieve.

7.1. *Indium Doping—Hall effect*

Among several impurities tested, Indium has been found to be an excellent donor [72]. Indium is easily incorporated during MBE growth using an effusion cell loaded with elemental indium. The amount of indium incorporated was found to increase continuously with the In cell temperature.

Incorporation and electrical activity of indium has been studied for the (111)B, (100) and (211)B orientations in as-grown and annealed MBE grown HgCdTe layers for high doping levels as well as low doping levels [68,72-75]. It was very difficult in the early studies to determine the influence on the doping of the impurities diffusing from the substrate since this effect was discovered later (see section 6.3.). However, regarding the experiments involving the (111)B orientation since they have been carried out in as-grown material and mostly for high doping levels, the following conclusions are relevant.

The set of samples grown for the first MBE experiments using indium as a dopant had Cd compositions varying from 0.2 to 0.31 and therefore were supposed to produce native p-type material if In had not been introduced. Uncertainties apparent in the experimental relation between the doping efficiency and the doping level were then anticipated. Absolute concentration measurements are also known to be difficult to achieve using SIMS technique. Nevertheless, a clear trend was detected, with a maximum around 10^{18} cm^{-3} and a sharp falloff below this value. We concluded that the In incorporation mechanism was not a steep function of the Cd composition in this narrow-band-gap range. The experimental observation could be successfully modeled assuming that a fraction of the In atoms was singly ionized, while the rest was precipitating in the crystal to form In_2Te_3. A fixed 3×10^{17} cm^{-3} acceptor compensation was also assumed for this set of samples. These results were in agreement with a previous study of In doping by diffusion in bulk material [76]. The electrical efficiency reported in our work was higher probably because of the lower MBE growth temperature limiting the In_2Te_3 precipitation. The presence of this constituent in the crystal should actually not be considered as a defect since In_2Te_3 has been shown to form a solid solution with HgTe preserving its sphalerite structure for a composition range of 0 to 0.2 [77]. The fact that the compensation could be assumed constant meant that the interaction between In and the Hg vacancies could be neglected.

In 1986, it was still unclear why a fixed N_A of 1 to 3×10^{17} cm^{-3} was obtained whereas N_A due to Hg vacancies was predicted to be as already discussed, 1×10^{16} cm^{-3}. Two hypotheses could explain this larger "native" acceptor concentration found in these samples. The first one related to the presence of foreign acceptors such as copper diffusing during growth from the substrate since at this time screening of substrates was not applied. The second hypothesis, which has been discussed in section 4.2.1., deals with the experimental evidence that twinning defects observed in as-grown (111)B HgCdTe material doped the material p-type consistently in the high 10^{16} cm^{-3} range. These In-doped HgCdTe (111)B layers analyzed in 1986 were indeed twinned.

In conclusion, from this early study, it has been found that indium is an excellent donor. Up to a level in the 10^{17} cm^{-3} range, indium has an electrical activity of almost 100%. The memory effect which has been reported earlier is fully understood and it was completely eliminated in 1987.

Indium-doped HgCdTe epilayers have been grown at EPIR recently under optimized MBE growth conditions on (211)B CdZnTe substrates in order to establish the lowest n-type background possible and to measure the characteristics of the epilayers and to analyze, if any, the favorable effect of indium.

In order to determine precisely the effect of indium, the layers investigated were annealed under a Hg saturated atmosphere at 250°C. Such a treatment is expected to reduce the Hg-vacancy concentration created during MBE growth down to the low 10^{14} cm^{-3} level, according to the P-T phase diagram. Figure 19 illustrates electrical properties of In-doped $Hg_{1-x}Cd_xTe$ layers with the same composition (x = 0.22) whose carrier concentrations (N_D-N_A) are range from 3×10^{14} cm^{-3} to 2×10^{16} cm^{-3}.

In-doped layers grown on these substrates show excellent electrical properties and they do convert completely p-type after a suitable anneal.

Figure 20 shows the carrier concentration and the mobility versus reciprocal temperature of a typical layer grown on a selected substrate after different annealing conditions. As it can be seen, this

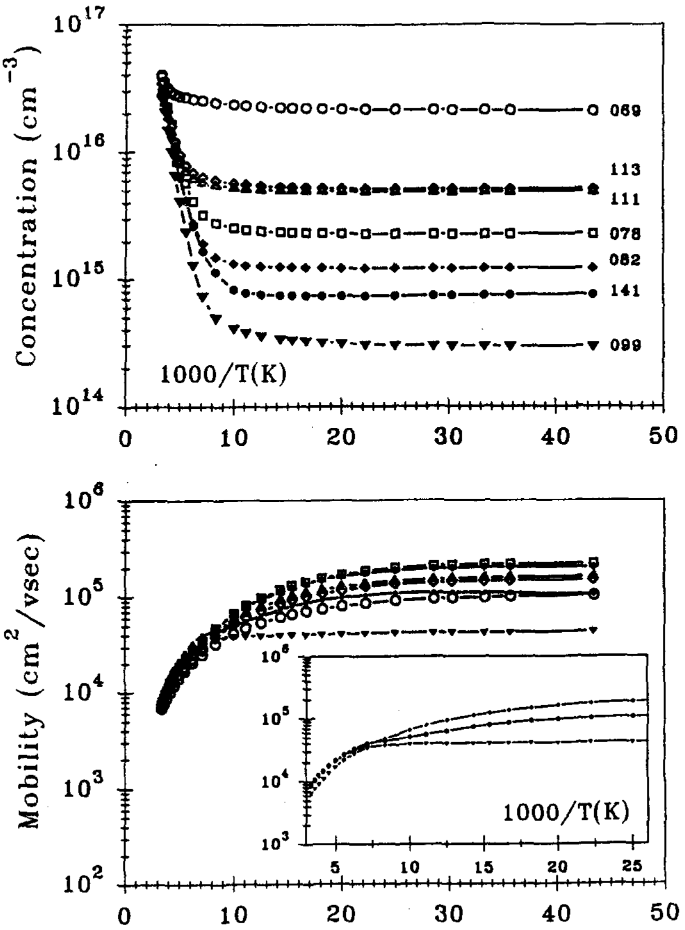

Figure 19: (a) Carrier concentration and (b) mobility versus reciprocal temperature of (211)B Indium-doped MBE grown $Hg_{0.78}Cd_{0.22}Te$ layers grown on selected CdZnTe substrates.

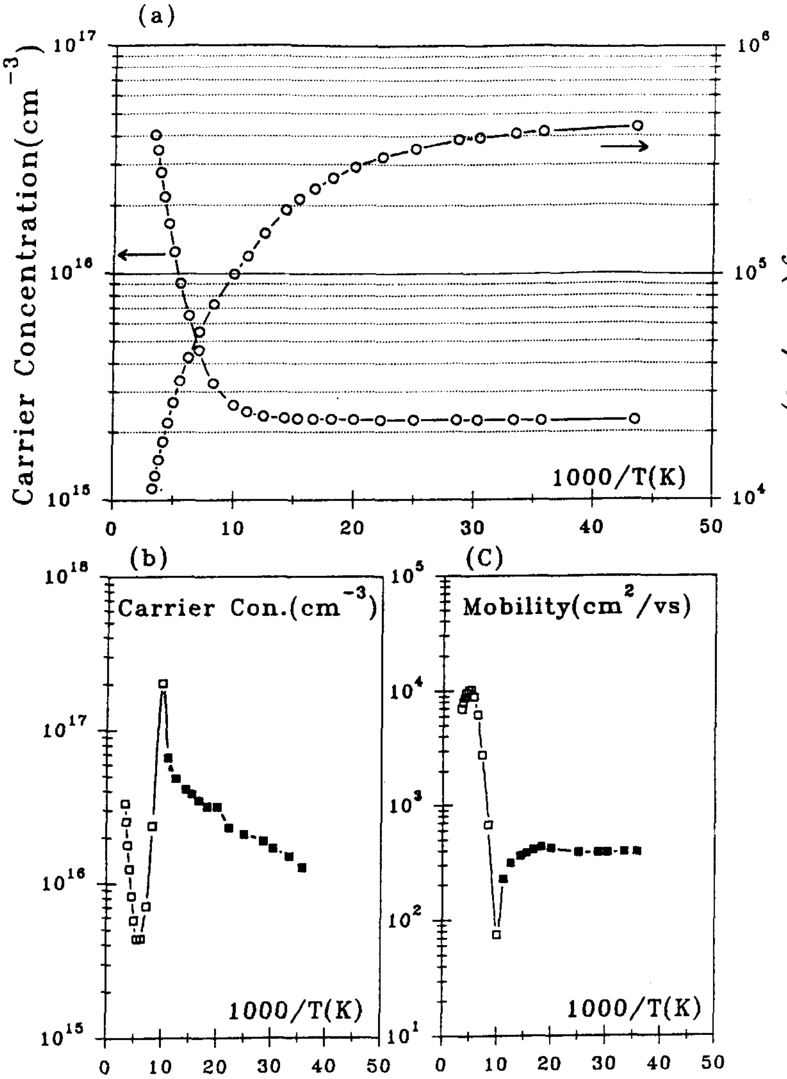

Figure 20: Hall characterization of Indium-doped MBE $Hg_{0.79}Cd_{0.21}Te$ grown on (211)B CdZnTe at magnetic field strength of 0.2 Tesla; (a) carrier concentration and mobility of after n-type isothermal anneal (b), (c) carrier concentration and mobility of after suitable p-type anneal versus reciprocal temperature respectively.

In-doped layer after a n-type anneal exhibits excellent electrical properties. The Cd composition of this layer is 0.21. Electron mobility exceeds $4\times10^5 cm^2/V.s$ at 23K which is outstanding and compares well with the best mobilities reported so far. This layer does convert p-type, after a p-type anneal as illustrated in Fig. 20b and Fig. 20c.

Figure 21 shows the mobility versus doping measured at 23K after isothermal anneal at 250°C. The expected behaviour of increase in mobility with decreasing doping levels can be clearly seen down to $2.0\times10^{15}cm^{-3}$. When the doping level decreases below $2.0\times10^{15}cm^{-3}$, the measured Hall mobility starts to decrease instead of increasing. From Table 7 and Figure 21, it appears that these annealed layers can be classified into two different categories.

I: N_D-$N_A \geq 2.0\times10^{15}$cm^{-3} and

II: N_D-$N_A < 2.0\times10^{15}$cm^{-3}

However, an important remark should be made before the detailed discussion of the results.

A doping level of 2×10^{15}cm^{-3} is low enough and very appropriate for current IR photodiode applications. The targeted doping level on LPE production lines is currently 3×10^{15}cm^{-3} [65]. However, carrier concentration in the mid 10^{14}cm^{-3}, with minority carrier lifetime of several microseconds, have been reported at 77K for LPE HgCdTe material. Hence, it is important to determine what prevents MBE material to exhibit such a low doping level. Mobility vs N_D trend which is illustrated in Figure 21, will be correlated with minority carrier lifetime in Section 7.2.

Table 7: Typical Hall characteristics and lifetime behaviour of selected layers with doping levels ranging from 3×10^{14} to 2×10^{16}cm^{-3}.

Name	Doping N_D-N_A (cm^{-3})	μ at 23 K (cm^2/vs)	Hall data	Lifetime data (SR visible or not)
069	2.0×10^{16}	1.1×10^5	Classical	No
111	4.9×10^{15}	1.6×10^5	Classical	No
078	2.2×10^{15}	2.3×10^5	Classical	No
139	1.4×10^{15}	1.6×10^5	Classical	No
082	1.2×10^{15}	2.0×10^5	Classical	Yes
141	7.6×10^{14}	1.1×10^5	Slightly mixed	Yes
099	2.9×10^{14}	4.4×10^4	Mixed	—

7.1.1. *Category I: N_D-$N_A \geq 2.0\times10^{15}$cm^{-3}*

The layers which fall into this category always show well behaved Hall characteristics (see Fig. 19). Carrier concentration and mobility versus reciprocal temperature curves show no visible mixed conduction effects. Electrical properties are fully explained by the intrinsic material properties. Measured mobility, as expected, decreases when the doping level increases. This is an indication of the scattering due to ionized impurities. The solid line in Figure 21 shows the overall mobility calculated at 23K as a function of the doping concentration by reciprocally combining the mobility due to ionized impurity and that due to lattice scattering:

$$\frac{1}{\mu}=\frac{1}{\mu_{\text{Lattice}}}+\frac{1}{\mu_{\text{Ionized}}} \qquad (20)$$

where μ_{Ionized} is the ionized impurity scattering mobility (assuming no compensation) given by [78]

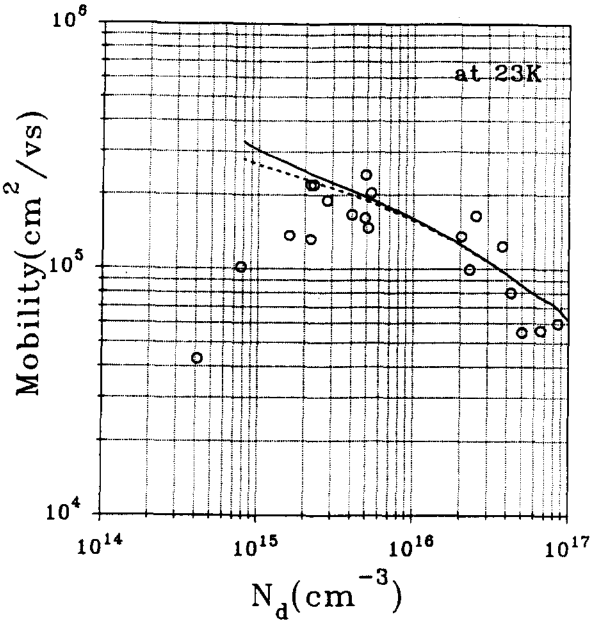

Figure 21: Dependence of mobility versus doping concentration at 23K. The solid line is the theoretical calculation assuming no compensation and the dash line take into account compensation as described in the text.

$$\mu_{Ionized} = \frac{0.20\,\varepsilon}{(m_o^*/m)^2\, g(b)} \frac{E_g}{\left(2E_F + E_g\right)^2} \tag{21}$$

where ε is the dielectric constant[79], $m_0^* = 3\hbar^2 E_g / 4P^2$, $P = 8\times10^{-8}$ eV cm [79], and E_F is the Fermi energy. The screening factor g(b) is given by,

$$g(b) = \ln(1+b) - \frac{b}{1+b} \tag{22}$$

where

$$b = \frac{0.85\,\varepsilon}{(m_o^*/m)^{1/2}} \frac{\sqrt{E_F E_g}\left(E_F E_g\right)^{1/2}}{\left(2E_F + E_g\right)} \tag{23}$$

We have assumed[80] $\mu_{Lattice} = 9\times10^5 cm^2/vs$.

A 250°C isothermal anneal should produce, under Hg saturated conditions, an acceptor level due to Hg vacancies in the low $10^{14}cm^3$ range. Hence, when N_D is above $2\times10^{15}cm^{-3}$, layers can be considered not to be compensated by these Hg vacancies. As can be seen, there is an excellent agreement with the theory by assuming no compensation. The dash line in the Figure 21 was obtained by assuming compensating acceptor concentration of 1.0×10^{14}cm^{-3}. These compensating acceptors start to play a significantly role when $N_D < 2\text{-}3\times10^{15}$ cm^{-3} as seen by the dash line in Figure 21.

7.1.2. *Category II:* $N_D\text{-}N_A < 2.0\times10^{15}cm^{-1}$

In this range, layers are expected to be compensated due to Hg vacancies. However, it can be seen from Figure 21, that there is a substantial discrepancy between the calculated mobility, assuming 1×10^{14}cm^{-3} of compensating acceptors, and the measured mobility at 23K. This drastic reduction in mobility cannot be due to the compensating acceptors. For the lowest doping that we have observed 3.0×10^{14}cm^{-3}, this decrease in mobility is clearly visible.

Layers falling between 1 and 2×10^{15}cm^{-3}, show no mixed conduction effects (see table 7). When the doping is at or below 1.0×10^{15}cm^{-3} level, compensation, but not mixed conduction, should indeed occur after n-type annealed at 250°C. However, mixed conduction effects start to be slightly visible in the mobility versus temperature curve in the extrinsic temperature region (see Fig. 19). This mixed conduction can only be explained by non uniform distribution of carriers. There is no evidence that this mixed conduction, only slightly visible though, is due to non uniformity in Hg vacancy distribution. This point will be discussed later on.

7.2. *Indium Doping: Minority Carrier Lifetime*

Minority carrier lifetime (τ) of the excess photogenerated carriers is one of the most important electrical parameters for HgCdTe when used as an infrared detector [81,82]. Therefore, it is essential to measure this parameter and to understand the factors that limit the recombination mechanism in MBE-grown layers. Here we will only consider n-type In-doped MBE grown HgCdTe (211)B layers. However, we have also reported on (111)B p-type HgCdTe layers grown by MBE [47,83]. The temperature dependence of the lifetime on these p-type HgCdTe layers was explained in terms of the Shockley-Read (SR) recombination mechanisms in the extrinsic temperature region and have shown a deep level close to midgap.

Lifetimes on n-type HgCdTe have been studied by several investigators [84-86] but layers were grown by different growth techniques. In bulk grown crystals at low temperatures, lifetime is controlled by band-to-band recombinations. These include Auger or radiative recombination contributions from both. Compensated layers show SR recombination with energy levels ranging from 10 to 70 meV below the conduction band. On epitaxial layers, very little work has been reported in the literature.

Minority carrier lifetime was measured on epilayers described above in Section 7.1. As already mentioned, all the layers were doped *in situ* during growth with indium. They were annealed under a Hg-saturated atmosphere at 250°C in order to reduce the Hg-vacancy concentration created during the MBE growth. Lifetime measurements were carried out as described in 6.1.

7.2.1. *Theory: Recombination mechanisms in n-type HgCdTe*

Minority carrier lifetime in n-type HgCdTe is determined by several different recombination mechanisms; namely Auger, radiative and Shockley-Read mechanisms and these have been discussed extensively in the literature [84,87,88]. Let us outline briefly the relevant equations under low injection conditions.

In the case of the Auger process, recombination occurs directly between bands which involves two electrons in the conduction band, and a heavy hole in the valence band.

This relevant lifetime is given by:

$$\tau_A = \frac{2n_i^2 \tau_{Ai}}{\left(n_0 + p_0\right)\left(n_0 + \gamma p_0\right)} \tag{24}$$

where n_i is the intrinsic carrier concentration (cm^{-3}) and is given in Ref. 89 to be

$$n_i = (5.585\text{-}3.820x + 1.753x10^{-3}\ T\text{-}1.364x10^{-3}xt)\ 10^{14}\ E_g^{3/4}\, T^{3/2} \exp\left(\frac{E_g}{2KT}\right) \tag{25}$$

Also, E_g is the energy gap (see Ref. 31), n_o is the equilibrium electron concentration, p_0 is the equilibrium hole concentration, γ is the hole-hole collision term, which is negligible for n-type HgCdTe and τ_{Ai} is the Auger lifetime for intrinsic HgCeTe (see Ref. 88), given by

$$\tau_{Ai} = \frac{3.8x10^{-18}\ \varepsilon^2\left(1+\eta\right)^{1/2}\left(1+2\eta\right)}{\left(m_e^* / m_0\right)\left|F_1F_2\right|^2\left(KT / E_g\right)^{3/2}}\ x\ \exp\left(\frac{\left(1+2\eta\right)E_g}{\left(1+\eta\right)KT}\right) \tag{26}$$

In this last expression, $\eta = m_e^*/m_h^*$ and ε is the dielectric constant and is given in Ref. 88 as 20-9.4x. Also, m_e^* and m_h^* are the electron and hole effective masses, m_0 is the electron rest mass, K is the Boltzmann's constant, and T is the absolute temperature. We assumed $m_h^*/m_0 = 0.55$ and $m_e^* = 0.07\ E_g$ (eV). The value for $|F_1F_2|$ varies between 0.1 and 0.3 [90], and in this paper, we assumed a value of 0.2 to fit our experimental data. The radiative recombination lifetime is given by

$$\tau_R = \frac{1}{B\left(n_0 + p_0\right)} \tag{27}$$

where B is given by [84]

$$B = 5.8x10^{-13}\ \varepsilon^{1/2}\left(\frac{m_0}{m_e^* + m_h^*}\right)\left(1 + \frac{m_0}{m_e^*} + \frac{m_0}{m_h^*}\right)x\left(\frac{300}{T}\right)^{3/2} E_g^2 \tag{28}$$

The Shockley-Read lifetime, assuming one single recombination level E_t below the conduction band edge and low density levels, is given by [87]

$$\tau_{SR} = \frac{\tau_{p0}\left(n_0 + n_1\right)}{n_0 + p_0} + \frac{\tau_{n0}\left(p_0 + p_1\right)}{n_0 + p_0} \tag{29}$$

where τ_{n0} and τ_{p0} are the shortest time constant for electron and hole captures, and $n_1 = n_0 \exp(E_t\text{-}E_F)/KT$ and $p_1 = p_0 \exp(E_F\text{-}E_t)/KT$, where E_F is the Fermi energy. The effective lifetime τ is calculated from

$$\frac{1}{\tau} = \frac{1}{\tau_A} + \frac{1}{\tau_R} + \frac{1}{\tau_{SR}} \tag{30}$$

7.2.2. *Experimental*

Measured lifetime at 80K along with carrier concentration and mobility of a few selected annealed In-doped n-type layers are summarized in Table 8. Most of these layers have been presented in section 7.2 and in Figures 19 and 21. These In-doped layers show excellent electrical properties as already discussed. In Table 8, N_D is the doping concentration extracted from the measured Rh(T) data at B=0.4 Tesla, and n_0 is the equilibrium electron concentration extracted from lifetime.

Table 8: Measured and fitted parameters of selected In-doped annealed MBE grown $Hg_{1-x}Cd_xTe$ layers.

Sample No.	x (%)	t (μm)	$N_D \times 10^{15}$ cm^{-3}	$n_o \times 10^{15}$ cm^{-3}	$\mu \times 10^5$ $cm^2/v.s$	τ at 80K (ns)	E_τ (meV)
073	24.6	09.7	03.8	02.7	1.0	560	32.7
072	23.7	11.5	04.0	03.1	1.6	250	—
075	22.0	10.3	02.0	01.8	2.3	580	—
074	25.4	08.5	01.4	01.0	—	1490	38.6
069	24.4	09.5	20.0	10.0	1.0	20	—
078	22.0	10.8	02.3	02.7	2.2	410	—
077	22.2	11.4	02.2	02.9	1.3	220	—
113	22.6	12.1	04.7	03.3	1.6	184	—
111	22.0	12.2	04.9	03.6	1.6	140	—
082	22.1	10.4	01.4	01.4	2.0	780	45.1
139	21.7	08.7	01.4	01.3	1.6	940	—

Concerning lifetime measurements, MBE grown $Hg_{1-x}Cd_xTe$ (x=0.22) epilayers can be classified also (see 7.1.) in two different categories.

I: N_D-$N_A \geq 2\times10^{15}cm^{-3}$

Figure 22 shows the relation between lifetime and electron concentration of Indium-doped $Hg_{0.78}Cd_{0.22}Te$ layers at 80K. Lifetime decreases from ≈1 μsec to ≈20nsec when doping increases from $2\times10^{15}cm^{-3}$ to $1\times10^{16}cm^{-3}$. The solid symbols represents layers grown by MBE at EPIR with Cd composition 0.22. The measured lifetime data can be explained satisfactorily by the intrinsic limited band-to-band recombination processes throughout the temperature region down to 80K (see also in Ref. 91 and 92). We have also included in Figure 22 for comparison purposes lifetime data at ≈80K of Loral LPE- and bulk-grown layers [93]. As can be seen, our MBE grown layers compare very well with the Loral layers with comparable doping densities. Figure 23 shows the lifetime behaviour of layer #075 versus temperature.

Solid circles represents measured experimental data points after anneal at 250°C. The peak lifetime reaches 1.0 μsec at 130K, and at lower temperatures, it decreases exponentially. The solid line represents the theoretical curve, which includes only intrinsic band-to-band (namely Auger and radiative) processes. As can be seen, there is an excellent agreement between the experimental data and the intrinsic material properties of MBE-grown HgCdTe layers. This layer has a doping level of $2.0\times10^{15}cm^{-3}$. Similar behaviour is obtained for higher doping levels. The Auger lifetime dominates throughout the entire temperature region from 300K to 80K. The solid line in Figure 22 shows n_0^{-2}

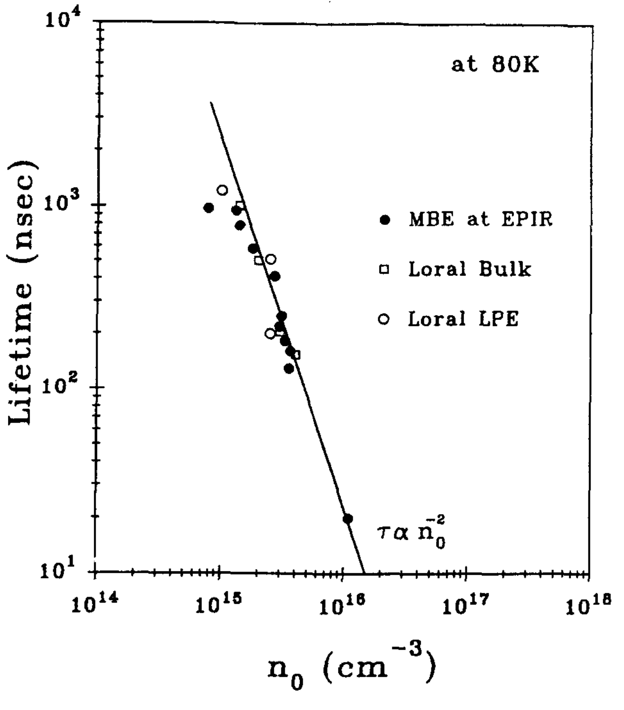

Figure 22: Dependence of minority carrier on electron density measured (solid symbols) at 80K on Indium-doped MBE-grown $Hg_{0.8}Cd_{0.2}Te$ layers. Data also included Loral LPE-grown (O) and bulk-grown (□) $Hg_{0.8}Cd_{0.2}Te$ layers obtained from ref. 93. The solid line shows the calculated Auger lifetime at 80K with $|F_1F_2| = 0.22$.

dependence as expected; and this further confirms that the measured lifetime is limited by the Auger recombination at 80K.

II: N_D-N_A < $2.0\times10^{15}cm^{-3}$

As previously discussed, in this range, layers are compensated due to Hg vacancies. Layers with doping level between 1 to $2\times10^{15}cm^{-3}$ do not show mixed conduction effects (Table 7). Measured lifetime on few of these layers, can be explained by intrinsic band-to-band processes without SR recombination, similar to layers with a higher doping. Figure 24 shows lifetime date on layer #139 which has a doping level of $1.3\times10^{15}cm^{-3}$ after 250°C anneal.

However, measured lifetime on most of the layers (doping between $1\text{-}2\times10^{15}cm^{-3}$) needs SR recombination centers in addition to the band-to-band recombination processes to be explained. Figure 25 shows measured lifetime on layer #082. This layer has a doping level of $1.4\times10^{15}cm^{-3}$. The behaviour of lifetime versus temperature data are similar to those obtained for higher doping levels. The combined Auger and radiative lifetime gives a good agreement with the experimental data in the intrinsic region. But, in the extrinsic temperature region, the data is lower by a factor of ≈1.2 than the theory. In order to obtain a good fit throughout the entire temperature range, we had to assume SR recombination level of 45 meV below the conduction band. This defect level is located $\approx(3/4)E_g$ with respect to the valence band edge. When the doping falls below $1.0\times10^{15}cm^{-3}$, compensation should indeed occur after n-type annealed at 250°C. Measured minority carrier lifetime data does require

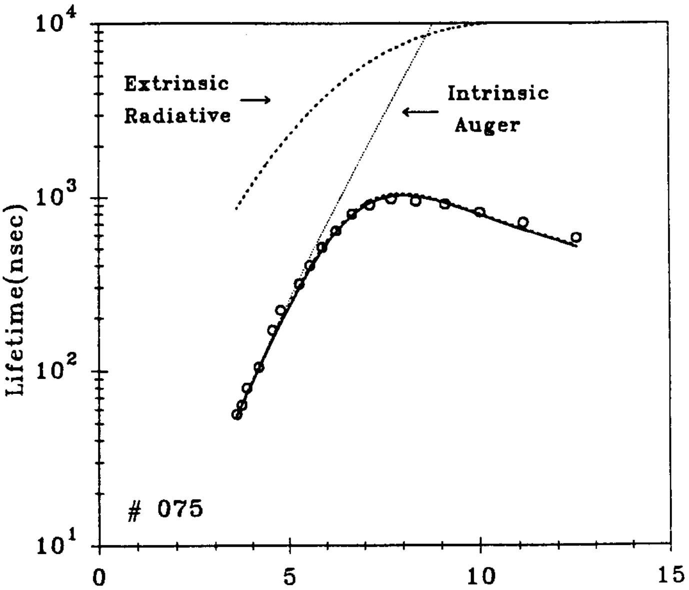

Figure 23. Measured (O) and theoretical minority carrier lifetime on an Indium-doped HgCdTe layer #075 versus reciprocal temperature after anneal at 250°C. Lines show various contributions from radiative (--), intrinsic Auger (···), and combined Auger plus radiative (—)recombination processes.

recombinations from SR centers in order to be fitted throughout the entire extrinsic temperature region. Figure 26 shows the measured lifetime data on layer #141, which has a doping of 7.8x10^{14} cm^{-3}. At 80K, measured lifetime is lower by a factor of 2 than lifetime calculated only from Auger plus radiative processes. The same SR defect level which is located $\approx(3/4)E_g$ with respect to the valence band has to be used. This indicates that it has the same origin than for the layers which have doping level between 1 and 2x10^{15}cm^{-3}. As we have concluded from a previous study [91], we believed that these SR levels are related to the Hg vacancies.

It should be pointed out that this Hg vacancy related SR defect level exists in all the In-doped layers since Hg-annealing conditions are the same. However, the correction factor (1.2 and 2 respectively for layers #082 and #141) decreases when N_D increases (lifetime decreases). Therefore, in layers exhibiting doping levels of 2x10^{15}cm^{-3} and above, it can be neglected which explains why this SR level "is not seen" in these layers.

7.3. *More Discussion about Background Doping*

As pointed out earlier, compensation from Hg-vacancies does show up for low-doped as-grown layers as well as for low-doped annealed layers at 250°C and the observed SR defect level is somehow related to the Hg vacancies. Hence, in order to reduce the Hg vacancy concentration further down, these layers were annealed at 150°C. This study was carried out in order to understand the current lower limit of 2.0x10^{15}cm^{-3}. We concentrated more on the low-doped layers which mostly show SR recombination in the extrinsic temperature region. Table 9 shows the measured electrical data for epilayers annealed at 250°C and post-annealed at 150°C. As can be seen for all the layers, the doping level N_D-N_A increased after the 150°C anneal. The increased in N_D-N_A after 150°C anneal is more

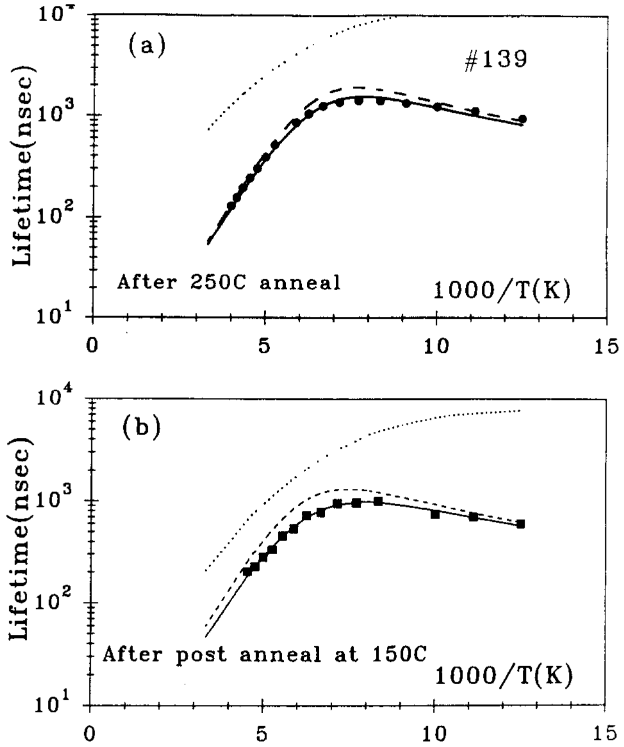

Figure 24: (a) Measured (O) and theoretical minority carrier lifetime on Indium-doped HgCdTe layer #139 versus reciprocal temperature (annealed at 250°C). Lines show various contributions from Auger (--), radiative (···) and combined Auger plus radiative (—) recombination processes. (b) Measured (■) and theoretical minority carrier lifetime for the same layer after a post-anneal at 150°C. Lines show various contributions from Auger plus radiative (--), SR (···) and combined Auger, radiative plus SR (—) recombination processes.

visible as the doping decreases. This is expected since N_A should be lower after anneal at 150°C, but the decrease in N_A being equal for all the layers, this reduction in Hg-vacancy concentration should be less noticable for layers displaying a higher doping level.

This increase N_D-N_A indicates that the compensation has decreased. Therefore, both electron mobility and minority carrier lifetime should increase. But from Table 9, it is clear that on the contrary, a decrease in electron mobility for all the layers is visible except for layer #069 which has the highest doping in this study. Figure 27 shows Hall curves versus reciprocal temperature of three selected layers which fall in the two regions that we discussed in the Figure 21.

Data on Figure 27 compares Hall data after 250°C (O) and post 150°C (☐) anneals. For layer #139, the mobility curve shows mixed conduction effects indicating the presence of a non-uniformity in carrier distribution in the layer after being annealed at 150°C, whereas no non-uniformity is visible after the 250°C anneal. Also, minority carrier lifetime is reduced after a post-anneal at 150°C as illustrated in Figure 24 (b) for layer #139. In addition, the fitting of the lifetime data versus temperature requires recombination from SR centers in addition to the band-to-band recombinations.

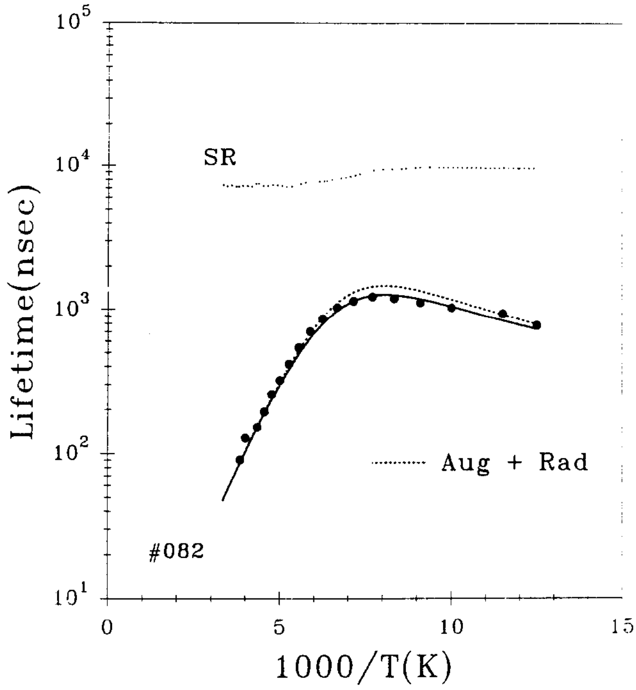

Figure 25: Dependence of minority carrier lifetime versus reciprocal temperature on sample #082. Lines show various contributions; SR recombination (···), combined Auger and radiative recombination (--), and combined Auger, radiative and SR recombination (—).

The obtained SR energy level is very different than that of Hg vacancy related SR centers. We obtained $E_t = 97$ meV which is deep below the conduction band edge, and is about $(1/4)E_g$ with respect to the valence band edge.

Similar behaviour is observed for layer #077 after a post-anneal at 150°C. Lifetime data cannot be explained with only intrinsic band-to-band recombinations.

As the Hg-vacancy concentration falls down to the 10^{12}cm^{-3} range after an isothermal anneal at 150°C, the defect level associated with Hg-vacancies obviously diminished. But now, another defect level, which has a different origin than that of Hg vacancy related defect, emerged. In addition, the non uniformity in carrier distribution slightly visible in some low-doped layers annealed at 250°C is much more pronounced after the post-anneal at 150°C which has markedly reduced the Hg-vacancy density. Hence, this non uniformity is neither due to indium nor to Hg vacancies, but very likely to impurities non uniformly distributed, i.e. introduced by diffusion. Impurities diffusing from the substrates appears to be the best hypothesis which can explain the observed results. However, it is not very clear that why these impurities, associated with defect levels, do not show up after 250°C annealing. After 150°C annealing, the Hg-vacancy related defect level diminished and impurity related defect level started to appear. It seems that these impurities are more electrically active when both Indium- and Hg-vacany concentrations are low. In this case, these non uniformly distributed electrically active impurities give mixed conduction which will dominate the transport properties. Therefore, even after careful screening, it seems that CdZnTe substrates are the source of contamination for low-doped HgCdTe epilayers grown by MBE.

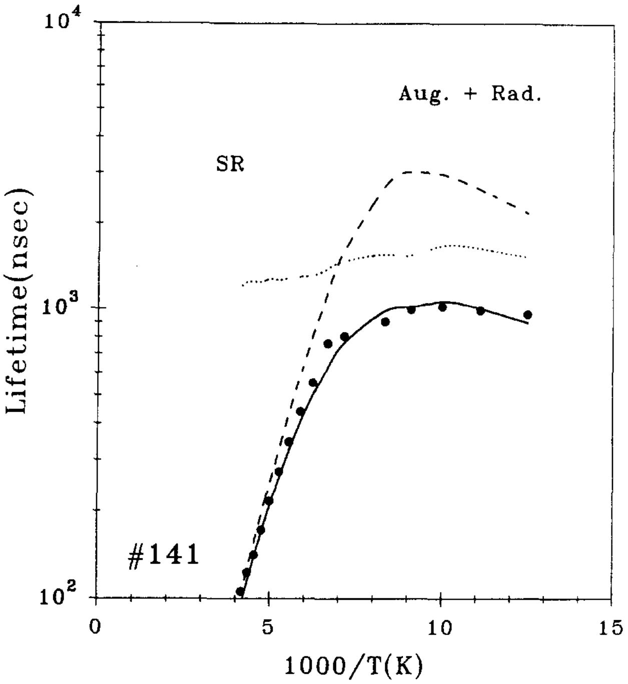

Figure 26: Dependence of minority carrier lifetime versus reciprocal temperature on low-doped layer #141. Lines show various contributions; SR recombination (¨), combined Auger and radiative recombination (--), and combined Auger, radiative, and SR recombination (-).

Table 9: Summary of the measured and fitted parameters of MBE-grown $Hg_{1-x}Cd_xTe$ layers that were annealed at 250°C and post-annealed at 150°C

Name	Anneal at 250°C			Post-anneal at 150°C		
	N_D (cm^{-3})	N_D-N_A (cm^{-3})	μ at 80 K (cm^2/Vs)	N_D (cm^{-3})	N_D-N_A (cm^{-3})	μ at 80 K (cm^2/Vs)
077	2.4×10^{15}	1.9×10^{15}	7.6×10^4	3.1×10^{15}	3.1×10^{15}	5.4×10^4
078	3.0×10^{15}	2.3×10^{15}	9.7×10^4	2.9×10^{15}	2.8×10^{15}	8.8×10^4
139	1.9×10^{15}	1.4×10^{15}	7.0×10^4	2.1×10^{15}	2.1×10^{15}	4.5×10^4
075	2.3×10^{15}	2.2×10^{15}	9.5×10^4	2.7×10^{15}	2.7×10^{15}	8.6×10^4
082	1.4×10^{15}	1.2×10^{15}	9.4×10^4	—	—	1.6×10^4
069	2.2×10^{16}	2.2×10^{16}	5.1×10^4	2.2×10^{16}	2.2×10^{16}	5.3×10^4

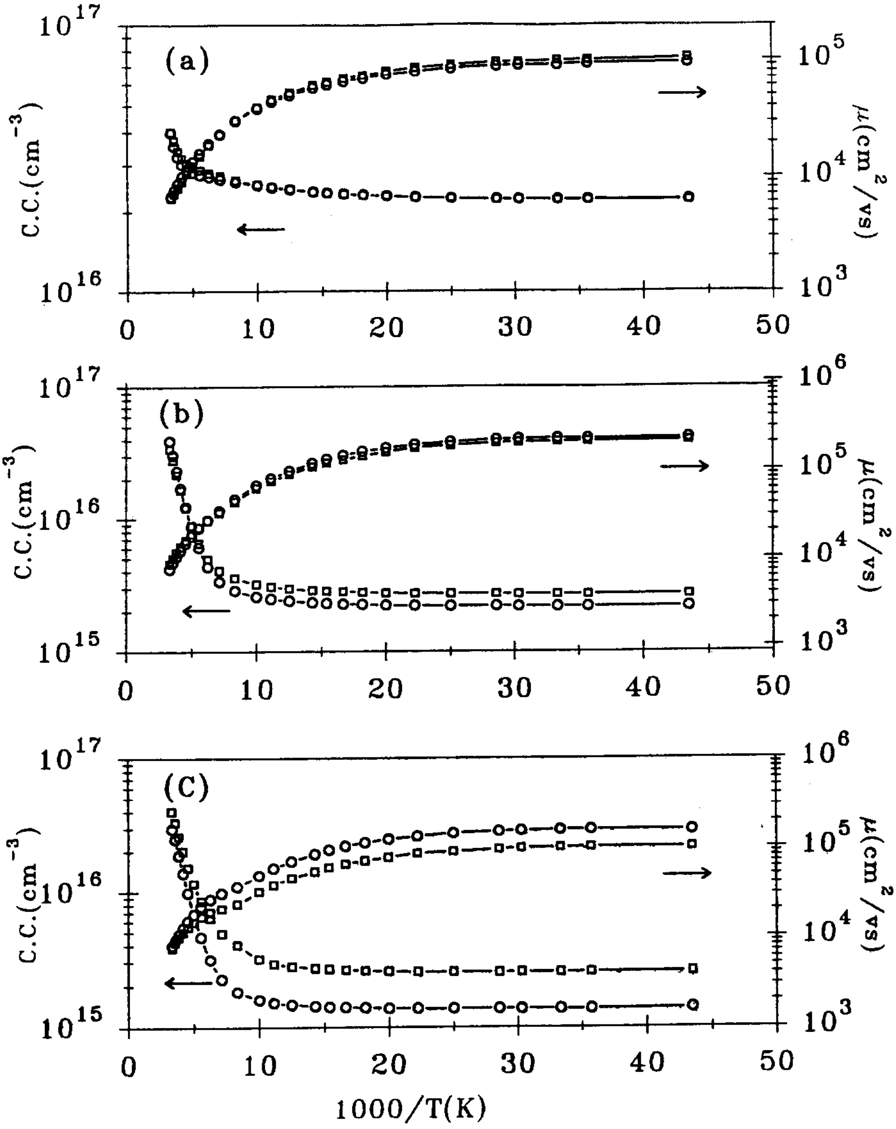

Figure 27: Hall characteristic of layer #069, #078 and #139 (top to bottom) at magnetic field strength of 0.4 Tesla after 250°C and post-150°C anneal.

7.4. *Summary about Indium doping*

In summary, Indium is an excellent n-type dopant which seems to have a favourable effect for establishing a background level in MBE grown $Hg_{1-x}Cd_xTe$.

When the doping level is above $2.0\times10^{15}cm^{-3}$, MBE-grown layers exhibit excellent electrical properties. Electron mobilities are very high and measured lifetime data fits very well with the intrinsic band-to-band recombination mechanisms. **Therefore, the incorporation of Indium during**

the growth of MBE HgCdTe is under control down to doping levels of $2\times10^{15}cm^{-3}$. Hence MBE-grown In-doped $Hg_{1-x}Cd_xTe$, of excellent quality, highly suitable for IR photodiode technology, are obtained on a routine basis.

Below $2.0\times10^{15}cm^{-3}$, compensation occurs after a 250°C anneal. This is mostly due to Hg-vacancies. Often, mobility versus reciprocal temperature curves, start to reflect non uniformity in carrier distribution. Minority carrier lifetime versus reciprocal temperature data requires SR recombination centers to be fitted. A single level located $\approx(3/4)E_g$ with respect to the valence band, is necessary to explain the measured data. This level appears to be related to Hg-vacancies. In order to reduce the Hg-vacancy concentration down to the $10^{12}cm^{-3}$ range, these layers have been annealed at 150°C. When the Hg-vacancy concentration is in the $10^{12}cm^{-3}$ range, mobility and minority carrier lifetime are reduced compared to the properties of layers annealed at 250°C. This can be explained by an increase in the non uniformity of the carrier distribution after the anneal at 150°C. The SR defect level has a different origin than that of Hg vacancy related defect. This defect level is approximately located at $(1/4)E_g$ with respect to the valence band.

Diffusion of impurities from the substrate appears to be the best hypothesis which can explain these experiments. Therefore, even after careful screening, it seems that CdZnTe bought from the best suppliers is still currently a source of contamination for HgCdTe epilayers grown by MBE. From these experiments, two conclusions can be drawn:

1. N_D-N_A=$2\times10^{15}cm^{-3}$ is certainly not the lower limit achievable in terms of doping in HgCdTe grown by MBE and

2. In order to break this lower limit, better substrates have to be grown by manufacturers and/or a specific process has to be implemented.

For example, at EPIR it has been observed that a HgCdTe epilayer grown on a substrate which has already been used (growth of HgCdTe and etching of the epilayer) exhibit better characteristics. The first epilayer acts as a getter for impurities. However, such a cleaning process is obviously costly and in addition it does not completely prevent diffusion of impurities when various anneals are performed.

It is also unclear why non-uniformity and associated SR centers located at $(1/4)E_g$ are revealed when both the Hg-vancancy and In-concentrations are low.

8. EXTRINSIC P-TYPE DOPING

In HgCdTe p-type doping can be controlled either by Hg-vacancies and/or electrically active impurities. In section 7.1. (see Fig. 20), it has been shown that In-doped HgCdTe layers can be converted to p-type after a suitable anneal. Incidentally, this is also the case for undoped layers. These Hg-vacancy p-type single layers exhibit excellent electrical characteristics. In particular, lifetimes at 80K are usually between 50 and 100 nsec which is considered to be very good for Hg-vacancy doped p-HgCdTe. Both, mobility and carrier concentration are excellent. These p-type layers are suitable to fabricate n-on-p photodiodes either by Hg-diffusion or by ion implantation.

However, p-on-n junction is currently the preferred structure by U.S. manufacturers because they offer significantly better performance than n-on-p Junctions for LWIR photodiodes [94]. One important advantage of this configuration is the easier control of low doping ($10^{15}cm^{-3}$ range) in the n-type base layer than in the p-type base layer for the n-on-p junction. Therefore, a longer minority carrier lifetime is achieved in the n-type base layer. The p-side which is a capping layer of x ≈ 0.30, should have an acceptor level in the 10^{17}cm^{-3} range. This requires the use of extrinsic dopant which should have a slow diffusion coefficient.

The other reason to replace the native acceptor (Hg-vacancy) with an external acceptor dopant is that, in principle, it is possible to increase Shockley-Read limited carrier lifetime when energy levels are closer to the valence band edge.

Column I and V elements are expected to act as acceptor impurities in $Hg_{1-x}Cd_xTe$ if they substitute respectively on metallic (column I) or non metallic (column V) sites. Following the previous discussions about the MBE growth process which occurs under Te-saturated conditions, substituting group I elements in Hg(Cd) sites, should be much easier than substituting group V elements in Te sites. This is precisely what has been observed but unfortunately none of the Column I elements are suitable p-type dopants for MBE grown HgCdTe for reasons to be discussed.

8.1. *Lithium Doping*

Li is a column I element and it was considered as a potential p-type dopant. Lithium was incorporated *in situ* during MBE growth of (001) $Hg_{1-x}Cd_xTe$ by using an effusion cell loaded with pure Li. Since it is a very reactive material, great care was needed when loading it into the growth chamber. This was done in an inert atmosphere. The Li-cell temperature range was 205-280°C.

Hole conduction was indeed observed [95]. The doping level increased monotonically with the Li effusion cell temperature and we have obtained doping levels as high as 8×10^{18}cm^{-3}. Since a calibrated sample implanted with Li was not available, the amount of Li incorporated in the layers was estimated from the effusion cell temperature and the growth rate, assuming a sticking coefficient equal to unity. Since very good agreement was obtained with the doping levels measured by Hall above 5×10^{17}cm^{-3}, we have concluded that nearly all the Li was incorporated and was electrically active. The impurity was singly ionized and no evidence of precipitation was detected. The evidence of a compensating donor became clear for Li concentrations in the low 10^{17}cm^{-3} range. Hole freezeout from a shallow acceptor level was only seen once for a doping level of 10^{16}cm^{-3}. For doping levels above 4×10^{16}cm^{-3}, the acceptors were completely ionized (flat curve after the transition region (see Figure 28). The solid line in Figure 28 is the best fit. It was obtained with $N_A=1.89\times10^{16}$cm^{-3}, $N_D=1.05\times10^{16}$cm^{-3}, $\tau = 0.24$, $E_A=8.3$meV and Cd composition = 25.8%.

More detail on the fitting is given in Ref. 95. It is interesting to note that N_D extracted from Hall measurements is approximately equal to the acceptor concentration N_A. Therefore, it is also observed in these experiments that the residual donor concentration in the (100) orientation is of the order of 10^{16}cm^{-3} which is much different than that for the (111)B orientation. Above 2×10^{18}cm^{-3}, the carrier concentration begins again to decrease slightly with temperature along a curved shape, showing the onset of a degenerate quasimetallic behaviour. The hole mobilities were all in the 300-400 cm^2/V.s range at low temperatures. Simple impurity scattering calculations similar to the ones used in Ref. 96 were made. They agree reasonably well with the measured values for the high doping levels in the 10^{17}cm^{-3} range or higher when the lattice mobility (mobility without lithium) is assumed to be 500 cm^2/V.s and the Li is singly ionized.

The same element has also been incorporated successfully as a p-type dopant during the growth along the (111)B face, even for a cadmium composition lower than 0.16 where intrinsic doping alone would produce n-type material. Thus, Li appears to be a very efficient p-type dopant probably substituting with the metal site in the crystal. Unfortunately, we discovered by SIMS profiling that it diffuses uniformly in unintentionally doped layers grown under or above Li-doped regions. Isothermal annealings also demonstrated that Li can diffuse out of the crystals since the annealed layers became

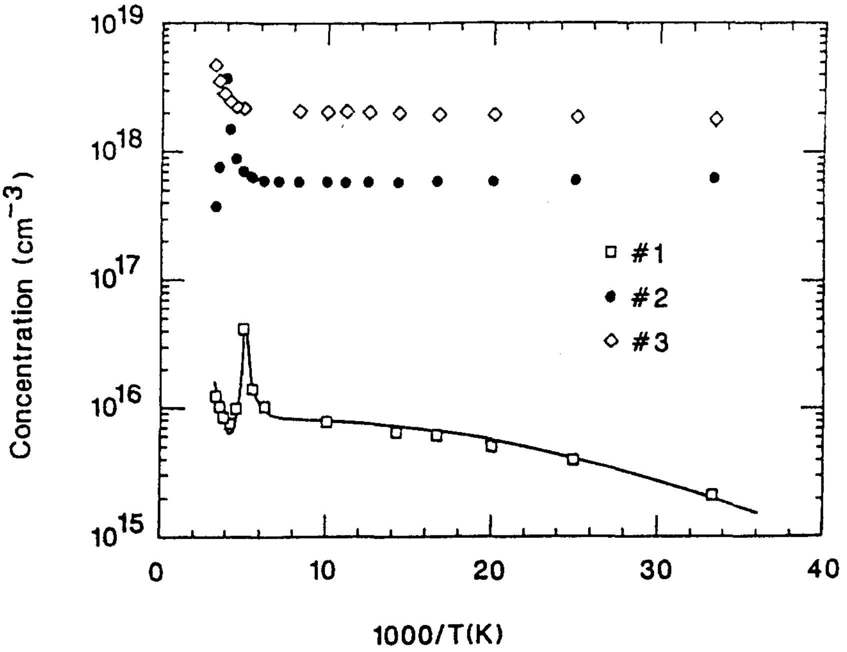

Figure 28: Hole concentration as a function of 1000/T(K) for lithium-doped MCT layers grown by MBE. The solid line for sampe N° 1 is the best fit obtained for the following parameters: $N_A=1.89\times10^{16}cm^{-3}$, $N_D=1.05\times10^{16}cm^{-3}$, $\tau=0.24$, and $E_A=8.3$ meV.

n-type. We also noticed that when the layers with low Li doping levels are stored at room temperature, their electrical properties can evolve slowly with time. Because of its small atomic mass and radius, the Li atom is highly mobile in the MCT material. This behaviour prevents the use of Li as a p-type dopant.

This situation unfortunately, even to a less extent, is the case for all the group I elements investigated such as Cu, Ag and Au. Silver doping has been successfully achieved during MBE growth [97], p-type $Hg_{1-x}Cd_xTe$ (100) and (111) oriented layers have been grown with $0.18 < x < 0.25$ on GaAs substrates. These layers exhibited good electrical properties however the average diffusion coefficient calculated to be of $7\times10^{14}cm^2/s$ at 165°C is too high to produce controlled junctions.

Group I elements are excellent p-type dopants, in terms of electrical properties, for $Hg_{1-x}Cd_xTe$. Copper or gold doped LPE $Hg_{1-x}Cd_xTe$ epilayers exhibit minority carrier lifetimes almost one order of magnitude higher at low doping than that of Hg-vacancy doped epilayers [98]. However, as reported, the large diffusion coefficients limit drastically their use as p-type dopants.

8.2. *Arsenic Doping*

Since group I elements are not suitable acceptors for homo- as well as for heterojunctions due to their large diffusion coefficients in $Hg_{1-x}Cd_xTe$, group V elements are the only remaining solution to the extrinsic p-doping problem.

A group V element has to substitute a Te atom to act as an acceptor.

Most elements are active dopants in accordance with their relative position in the periodic table but several important exceptions exist notably group V elements in Te-rich material. For bulk-grown HgCdTe clearly for elements which are expected to substitute onto Te sites (groups V and VII) electrical activity is only likely for material grown under Hg-rich conditions (e.g. Bridgman), i.e. where Te lattice sites are available for the substitutional atoms [99]. For Te-rich grown bulk material ($x < 0.3$), group V elements have been found to be inactive or amphoteric in SSR (Solid State Recrystallized) and ACRT Bridgman (Accelerated Crucible Rotation Technique). In any case, anneal is necessary to activate or reveal the true nature of the dopant [100-102].

The same contrasted behaviour is seen in LPE growth where both Te-rich [103] and Hg-rich [104] conditions have been used. The most comprehensive study of dopant behaviour has been carried out by Kalisher in Hg-rich LPE [105] and a full account of the growth and doping of Hg-rich LPE layers has been given by Tung [106]. In Hg-rich LPE, it has been reported that As is 100% active over three orders of magnitude in concentration (10^{15} - 10^{18}cm^{-3}).

A detailed study of the behaviour of group V elements in Te-rich LPE ($x \approx 0.24$-0.31) was reported by Vydyanath *et al* [107]. In the as-grown state, P, As, Sb and Bi were inactive. When annealed at 200°C, layers converted to n-type as did undoped layers of similar x. However, when a preanneal at 500°C (in Hg) was used before the 200°C anneal, p-type conduction was obtained for P, As and Sb, but not for Bi. This behaviour was explained by the dopants occupying metal sites in the as-grown state and being moved onto active Te sites by the 500°C anneal.

The same basic problem occurs in MOVPE material. Both P and As were shown to behave similarly $x = 0.26$-0.3 layers [108]. Under normal Te-rich conditions, both elements were electrically inactive but when alkyl ratios were changed to produce metal-rich conditions, both were seen to be 100% active at levels of 6×10^{16}cm^{-3} and 1-2×10^{17}cm^{-3} respectively. The importance of maintaining metal-rich conditions during the CdTe IMP cycle was also stressed [109].

In MBE growth, the primary goal is to obtain p-type doping at the growth temperature or after an anneal at low temperature in order do preserve the integrity of the structure. If a high temperature anneal is requested (>250°C), MBE will lose the advantages attached to its low temperature character, i.e. tailored profile in composition and/or doping as well as fabrication of quantum structures.

This requirement implies that As should be incorporated during growth in Te sites.

But MBE growth as discussed in detail in section 5 cannot occur under Hg-rich conditions in contrast of whatgof can be achieved in LPE, MOVPE or bulk growth. Since MBE growth is carried out under Te-saturated conditions, it is not surprising that As and Sb atoms incorporated during the MBE process have been found to act primarily as donors in as-grown materials [110].

This "intrinsic" difficulty in MBE explains why many approaches have been tried with a view to achieving p-type doping in MBE growth of HgCdTe using arsenic. They can be divided into five categories:

1 - *in situ* doping using As_4, cracked As_4 or arsenic compounds,

2 - arsenic diffusion,

3 - arsenic implantation

4 - arsenic doping in multilayers or superlattices and

5 - delta doping.

However, most of these approaches demand a high temperature anneal (>400°C) in order to activate As.

8.2.1. *High temperature anneal (>400°C) MBE grown layers*

The direct incorporation of arsenic during MBE growth process using As_4 was achieved several years ago [110] and it was found that the as-grown (111)B epilayers exhibited poor n-type characteristics. The doping concentration remained in the low $10^{16}cm^{-3}$ range or lower. The effect was obvious for Cd compositions > 0.3, since the native material would have been p-type. It was also true for low x material, since the carrier concentration remains independent of temperature in the extrinsic region of the Hall curves. After isothermal annealing at temperatures between 200 and 250°C, the samples remained n-type showing that the doping mechanism during growth was stable. We concluded that these impurities interact preferentially with the metal site. We have also noticed that they were self-compensated, since the doping concentrations remained low, and the Hall measurements showed evidence of strong impurity scattering limiting the mobility at low temperature. Illumination of the substrate during MBE MCT growth by ultraviolet light or a green Nd-YAG laser pulsed at 10-kHz repetition rate did not increase substantially the carrier concentration and left the material n-type.

Recently, a series of arsenic doped $Hg_{1-x}Cd_xTe$ x Te films with $x \approx 0.22\pm0.01$ have been grown by MBE on CdZnTe(211)B substrates at the University of Illinois at Chicago in order to analyze As activation

The concentration of arsenic was varied from $5\times10^{18}cm^{-3}$ to $1\times10^{20}cm^{-3}$. After the growth, the epitaxial layers were annealed at various pressures of Hg within the existence region of (Hg,Cd)Te and at temperatures ranging from 400°C to 500°C. Hall effect and resistivity measurements were carried out subsequent to the anneals. 77K hole concentration measurements indicate that for concentrations of arsenic $<10^{19}cm^{-3}$, most of the arsenic is electrically active acting as acceptors interstitially and/or occupying Te lattice sites at the highest Hg pressures. At lower Hg pressures, particularly at annealing temperatures of 450°C and higher, compensation by arsenic centers acting as donors appears to set in and the hole concentration decreases with decrease in Hg pressure.

Based on the information gathered from this data it is clear that arsenic behaves amphoterically in MBE grown (Hg,Cd)Te similar to its behaviour in LPE (Hg,Cd)Te and that of phosphorus in bulk and LPE material [109,112-114]. At high concentrations of arsenic, larger than 10 cm and at an annealing temperature of 450°C and above, the 77K hole concentration in the cooled crystals is less than the total arsenic concentration, suggesting that the crystals are well compensated particularly at low Hg pressures. The behaviour of arsenic as an acceptor at high Hg-pressures and as a donor at low Hg-pressures is also deduced from the results.

Similar experiments have been carried out at Rockwell [115]. Anneal experiments in Hg-rich ambient have been performed on arsenic-doped epitaxial layers of HgCdTe with $0.22 < x < 0.3$ grown by MBE on (211)B CdZnTe substrates. The temperature dependence of carrier concentration indicates that the effect of As compensation is increased as the annealing temperature increases until it converts to p-type. It is suggested that the extremely low n-type mobility of the as-grown sample is due to the formation of As precipitates in the alloy because of the low growth temperature around 190°C.

It was found that As-doped MBE grown HgCdTe epilayers remained n-type after post-growth annealing up to 400°C under Hg-saturated conditions followed by 200°C Hg-annealing. However, the As-doped layer converted to p-type after the 420°C - 30 min Hg-annealing and the *ex situ* 200°C Hg-annealing. These experiments are in complete agreement with the results obtained at the University of Illinois and demonstrate that As-doped $Hg_{1-x}Cd_xTe$ epilayers grown on (211)B CdZnTe substrates can be converted p-type but only after an anneal at a temperature of at least 400°C.

A striking similarity for As activation as a function of temperature with As-doped MBE HgCdTe has been observed for As diffusion into HgCdTe as well as for As implantation. Diffusion of As at 380-450°C from a Hg solution containing As was used [116] to produce p+/n homojunction diodes in $Hg_{1-x}Cd_xTe$ grown by MBE on (211)B CdZnTe substrates.

Planar MBE based HgCdTe heterostructure photodiodes with the p-on-n configuration have been formed by selective pocket diffusion of arsenic deposited on the wide gap surface by ion implantation [117]. In order to fabricate high performance photodiodes, the structure, after the implantation process, has to experience two anneals under Hg overpressure, the first one at 435°C for 20 min. followed by another at 250°C for 24h. High temperature anneal is also required in this technology to achieve p-type conversion. By inducing As diffusion, it allows the pin junction formation in the narrow gap layer away from the damaged wider gap region.
In conclusion, the high temperature anneal necessary to activate arsenic can have positive effect on junction position as well as on crystal quality improvement, and therefore can have an overall positive effect on MBE based infrared photodiode technology.

However, high temperature anneals are obviously very detrimental to any structure requiring a precise compositional and/or doping profile. The main advantage of the MBE growth technique compared to other techniques is the low growth temperature, and this disappears if a high temperature anneal has to be applied. **It is of the greatest importance for MBE technology to achieve p-type doping of HgCdTe with As without using any thermal process exceeding 250°C.**

Alternative approaches have been proposed with a view to achieving arsenic activation at a temperature close to the MBE growth temperature.

8.2.2. *As-activation at low or moderate temperature*

The first alternative approach is based on HgCdTe-CdTe superlattices in which thin CdTe layers are doped with As and the HgCdTe layers are not intentionally doped.

Using the photoassisted MBE growth technique, Harper *et al.* [118] have successfully p-type doped (100)CdTe epilayers with arsenic at 180°C which is a suitable temperature to growth high quality HgCdTe. Han and co-workers [119] have grown p-type modulation-doped HgCdTe samples. These samples were obtained by using thin CdTe layers of 50 A heavily doped with arsenic and located periodically between $Hg_{1-x}Cd_xTe$ layers of 1000-1100 Å and x of 0.18-0.26. The layers were grown on a (100)CdZnTe substrate at 170°C and a p-type level of 5×10^{16} to $1\times10^{18}cm^{-3}$ were achieved. The authors proposed to consider these structures as a new quantum alloy.

The direct doping of HgCdTe with As was overcome by utilizing the fact that CdTe can be doped directly p-type. Cation stabilized conditions can be established during CdTe growth which is not the case for HgCdTe as previously discussed. Hole freeze-out does not occur in these modulation-doped structures because no acceptor ions are present in the narrow-gap regions. However, no hole mobility enhancement due to modulation doping has been observed.

This method has been used later on to fabricate p-on-n homojunction superlattice detectors operating in the 3-5 μm region [120]. In this work, it is reported that the As-doped superlattice structure can be used as it is for SL detector fabrication or interdiffused in a standard n-type anneal (the compositionally modulated structure technique [121]) resulting in p-type homogeneous HgCdTe.

The same approach has been tested by Arias *et al* [122] who have reported on p-type As-doping of CdTe and HgTe/CdTe superlattices (period of 50-180 Å) by photoassisted and conventional MBE in the (100) orientation. They have shown that at low growth temperature and under cation stabilized growth conditions, p-type doping due to arsenic can be observed on as-grown material. CdTe epilayers grown at low temperature (180°C) with photoassisted MBE are exhibing superior structural, optical and electrical properties than those grown by conventional MBE. In this work, the importance of establishing cation stabilized conditions is stressed in order to incorporate arsenic on tellurium sites. The extension of this CdTe doping process to the doping of HgTe/CdTe superlattice structures at growth temperatures below 155°C has resulted in *in situ* growth of p-type modulated doped superlattices with cut-off response at 300K out to 12.6 µm. All the p-type HgTe/CdTe samples interdiffused at 250°C for 20h under a saturated Hg environment have produced p-type HgCdTe alloys with higher hole concentrations. This indicates that even a low temperature annealing process is sufficient to increase the amount of electrically active arsenic acceptor atoms in the lattice. These experiments have been utilized to fabricate *in situ* arsenic doped p-on-n HgCdTe heterojunctions using the interdiffused superlattice process (ISP) doping approach described above. In this work [60], the n-type MBE HgCdTe, grown at 185°C on CdTe/GaAs (211)B substrate was doped with indium atoms. This epilayer was directly followed by the growth at 165°C of an As-doped (10^{17} - 10^{18}cm^{-3}) HgTe/CdTe superlattice. After the structure was grown, a Hg annealing (T=250°C) was performed (a) to interdiffuse the superlattice and form the p-type cap layer and (b) to annihilate the Hg-vacancies formed during the growth process. For LWIR diodes, a 10 min. high temperature (435°C) annealing step under a Hg-atmosphere was performed first in order to move the electrical junction (by diffusion of arsenic) away from the heterostructure interface where misfit dislocations are generated. RoA's measured at 77K were high but at lower operating temperatures, they did not increase monotonically. This deleterious effect (typically observed on LWIR HgCdTe diodes grown on GaAs substrates) was attributed to the high dislocation content in the active layer (10^6cm^{-2}).

The ISP process has also been used to form the p-type As-doped intermediate or base region of a bias-switchable dual-band HgCdTe detector. [123]

The As-doped multilayer or superlattice structure can be interdiffused in a standard n-type anneal to remove residual Hg-vacancies from the layer growth, resulting in p-type homogeneous HgCdTe (as described here above) or the superlattice can be used as it is for superlattice detector fabrication. However, it seems that in any case an anneal at a moderate (250°C) or a high temperature (435°C) which destroys partly or totally the MBE structure is used.

Puzzling results have also been reported about the p-type doping of MBE HgCdTe using arsenic [124]. In this work, p-type doping is achieved *in situ* on As-doped HgCdTe layer grown at 170-180°C on CdTe (111) substrate without any photoassistance. P-type conduction is reported to have been observed in as-grown layers of $0.28 < x < 0.35$ and after annealing under a mercury ambient. This result is attributed to the use of atomic tellurium, produced by an undescribed cracker cell, which has been found to enhance Te reactivity on the surface [125].

A full analysis of this report is not possible since some information is missing. However, the following comments can be made:

(1) layers with $x \geq 0.3$ grown in the (111) orientation are normally p-type as-grown due to stoichiometry. Doping levels can be in twinned layers much higher than what is expected from the P.T. diagram and no information on DCRC X-ray diffraction is reported. This point has been raised also by Summers *et al.*[126]

(2) No information is given about the anneal and we have seen that a high temperature anneal (435°C for 10-20 min.) is enough to activate arsenic into acceptors.

(3) No annealing results were presented on similar undoped material.

(4) No chemical analysis data was presented in either the as-grown or the annealed samples.

(5) No information is presented about the cracking efficiency of the cell.

(6) The role attributed to atomic tellurium is at least questionable. Indeed the problem in group V element doping is to substitute, As in this case, in the Te sublattice. It is stated, but not demonstrated, that by increasing the Te reactivity with atomic tellurium, conventional MBE growth conditions, which occur under Te saturation and prevent the incorporation of As in the Te site, are drastically changed.

(7) No information is given about the As effusion cell.

In conclusion, it seems that other unreported or unknown important parameters have to be considered to account for these interesting results.

The same group is using Cd_3As_2 compound in the effusion cell. In, a U.S. patent [127], it is claimed that cation-rich conditions can be achieved for $Hg_{1-x}Cd_xTe$ (x=0.22) by cadmium overpressure. If the activity of CdTe and HgTe in the $Hg_{1-x}Cd_xTe$ alloy is determined by x, which is widely accepted then (see 2.2), the cadmium pressure has no or almost no effect on the Hg-vacancy concentration (CdTe and HgTe compounds are independent), **but** it has a strong influence on the composition x.

Hence, the explanation given in the patent cannot be right. However, if indeed the effect reported is produced, two hypotheses can be proposed

1- [Cd-As] bonds are preserved during Cd_3As_2 evaporation with the very important consequence of having As in the right site or

2- As_2 molecules which are produced enhance Te reactivity on the surface [125]: This strengthens the Te-Hg bond which could allow easier As substitution. The mechanism is not understood.

8.2.3. *As-delta doping*

Another approach has been taken recently using a planar (delta) doping method [128,129]. In these experiments, $Hg_{1-x}Cd_xTe$ alloy is grown at 185°C by MBE on (211)B CdZnTe substrates. Periodically, the CdTe and Te effusion cell shutters are closed and the arsenic effusion cell shutter is opened. The periodicity interval ranges from 30 to 200 Å and the duration of the As shutter cell opening is a few seconds for an As flux in the range of $10^{15} atm^{-2}s^{-1}$. Hg flux continues to impinge on the surface which is expected to favour the HgAs bond.

The characteristics of selected As-delta doped HgCdTe epilayers including the period, electrical characteristics of as-grown and annealed epilayers, are presented in Table 10. All these As-doped layers have been grown under different growth conditions. It is interesting to note that layer #101 exhibits p-type doping in the high $10^{16} cm^{-3}$ level even before any anneal is performed (Fig.29). This is clearly one order of magnitude larger than intrinsic doping related to Hg-vacancies as expected for an undoped layer. The fact that almost no freeze-out is observed is also an evidence of a 2D character and a physical separation between holes and acceptor ions. **Therefore, this attests for the incorporation of As as an active acceptor at the growth temperature.**

Isothermal anneal at 250°C and 300°C confirm without any ambiguity that the p-character is related to the presence of As and that As has been mostly activated at 185°C which is the growth temperature. SIMS analysis has not been performed, therefore it is difficult to assess the activation

Table 10: Arsenic delta-doped MBE-grown HgCdTe epilayers

				AS GROWN				ANNEALED - 250°C			
				300 K		80K		300K		80K	
Sample #	$Hg_{1-x}Cd_xTe$ x (%)	t (µm)	Period (°A)	C.C. (cm^{-3})	µ ($cm^2/V.s$)	C.C. (cm^{-3})	µ ($cm^2/V.s$)	C.C. (cm^{-3})	µ ($cm^2/V.s$)	C.C. (cm^{-3})	µ ($cm^2/V.s$)
092	22.5	10.6	---	$2.3x10^{16}$	5690	$5.2x10^{16}$	195(p)	$2.0x10^{16}$	5223	$6.1x10^{16}$	284(p)
096	50.0	02.0	---	$7.0x10^{16}$	36(p)	$1.9x10^{16}$	10(p)	$1.2x10^{17}$	45(p)	$1.3x10^{16}$	95(p)
101	24.2	04.5	96	$2.4x10^{16}$	3159	$5.6x10^{16}$	194(p)	$1.6x10^{16}$	2080	$1.2x10^{17}$	266(p)
106	38.0	19.3	193	$5.1x10^{14}$	6667	$2.2x10^{13}$	114435	$6.1x10^{14}$	1613	$3.2x10^{15}$	217(p)
117	32.9	04.6	42	$2.5x10^{15}$	1757	$9.8x10^{14}$	536(p)	$1.1x10^{16}$	919	$9.7x10^{15}$	1473
119	41.9	02.9	97	$6.0x10^{14}$	4900	$1.2x10^{15}$	9200(p)	$9.0x10^{15}$	873(n)	$9.3x10^{15}$	10(p)
123	29.9	04.7	47	$8.0x10^{15}$	9062	$5.5x10^{14}$	87698	$2.3x10^{18}$	11(p)	$6.7x10^{16}$	130(p)
124	31.7	04.5	136	$1.9x10^{16}$	2366	$4.0x10^{16}$	478(n)	$2. 1x10^{16}$	2828	$1.9x10^{16}$	9894

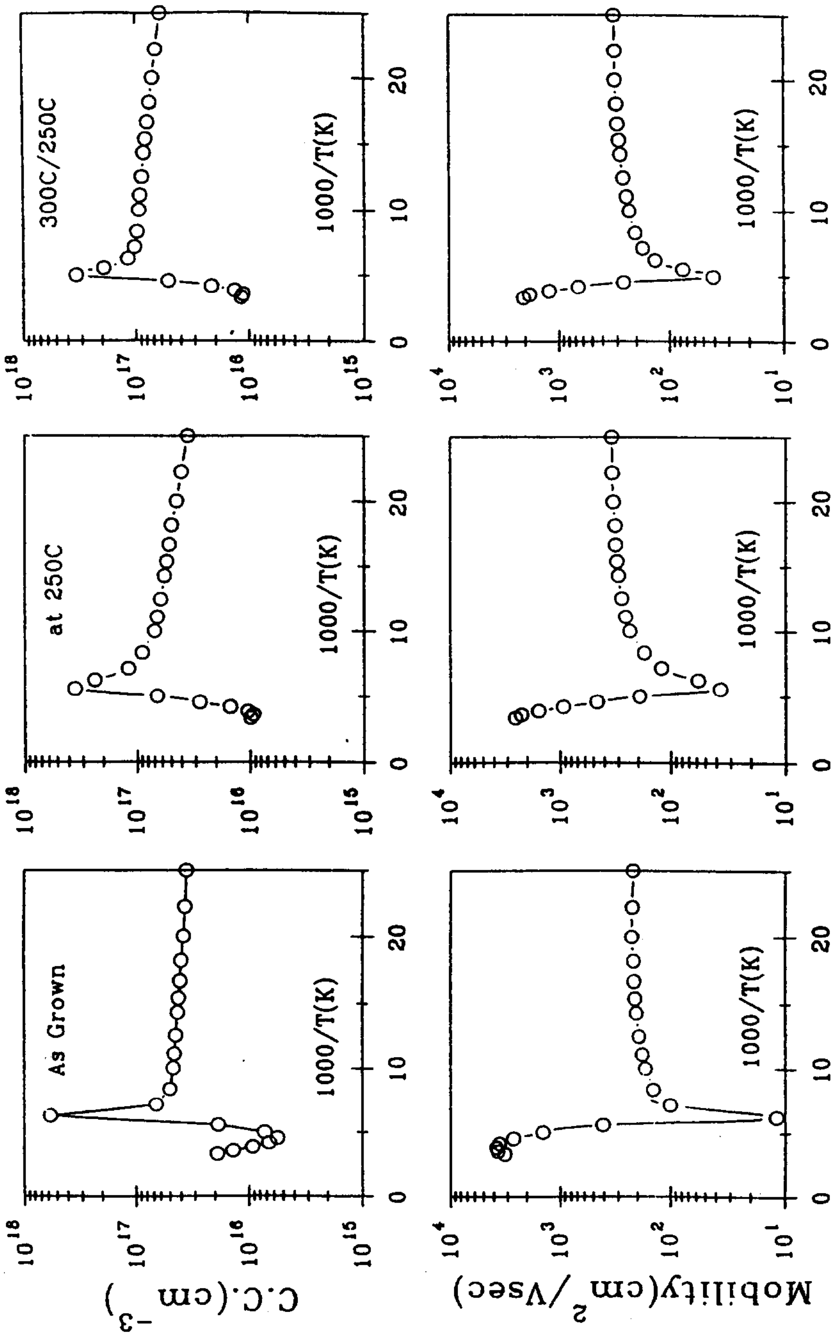

Figure 29: As-delta doped $Hg_{0.74}Cd_{0.26}Te$ layer #101

yield. However, since only a slightly increase in the carrier concentration has been observed at 250°C and no change at 300°C, this might indicate that the activation yield is high. This is supported by the fact that in the high temperature annealing experiments, required to activate As, marked changes are observed between as-grown and annealed layers [115].

P-type character has been also observed for the layers reported in Table 10. However, layer #96 has a low mobility before and after anneal, layers # 117 and 124 are p only before anneal (at 23K for layer #124) whereas layers # 106,119 and 123 exhibit very high hole mobilities in the as-grown state.

The other delta-doped layers not reported in Table 10 are n-type both in the as-grown and annnealed states. It is noteworthy that in some as-grown layers, electrons and holes have high mobility which disappear after anneal. This is very likely related to the modulation of the As doping. This should be analyzed in more detail.

In summary, 33% of the As-delta doped epilayers show p-type character related to As in the as-grown state and/or after anneal at 250°C. This is extremely encouraging and demonstrate that his approach is very promising. These preliminary results might represent the solution expected regarding *in situ* p-type doping of MBE grown HgCdTe.

However, the control of planar doping is not straightforward. The As doping profile is very critical in order to control the p-type behaviour. EPIR has not been able, so far, to determine precisely which parameters induce with certainty the p-type character. In order to achieve such a control, a thorough investigation regarding growth temperature, delta doping spacing, As flux control, As nature, i.e. As_4 vs As_2 and parameters of the growth interruption is required.

9. CONCLUSION

In this chapter, the Molecular Beam Epitaxial Growth of $Hg_{1-x}Cd_xTe$ (x=0.22) alloy has been presented and the results published since 1981 discussed in some detail. The purpose of this conclusion is to highlight the most relevant points of this activity. MBE is the growth technique using the lowest growth temperature (<200°C). Therefore, in MBE interdiffusion processes are very limited and precise control of profiles both in composition and in doping can be achieved. Very sophisticated structures such as multiquantum well lasers, multicolor detectors, smart detectors or any quantum devices can be fabricated by MBE provided that the temperature during thermal anneal and processing is not higher than the growth temperature.

MBE growth of $Hg_{1-x}Cd_xTe$ has been carried out on several growth orientations such as (111)B, (100), (111)A, (100) and (211)B and on CdTe, CdZnTe, CdTe/GaAs and CdTe/Si substrates. Lattice matched CdZnTe substrates and the (211)B orientation are currently the preferred choice for MBE. It has been found that using the (211)B orientation, twin-free epilayers with excellent structural and electrical characteristics can be grown routinely. In addition, the mercury condensation coefficient C_{Hg} is higher in the (211)B orientation than in the other orientations. C_{Hg}, which has been found in early experiments to be low and to decrease exponentially when the growth temperature increases, is currently estimated to be of 0.02-0.05 on (211)B for a growth temperature of 185°C.

It has been shown that MBE growth of HgCdTe cannot be correctly described and modelled by a pure thermodynamic approach using the mass action law since C_{Hg} is strongly influenced by the crystallographic orientation which implies that kinetics plays a role. However, regarding (211)B orientation, MBE growth-can be described with a good approximation by a quasi-equilibrium model. In particular, at 185°C, the Hg vacancy concentration compares well with that calculated for growth occurring at equilibrium under Te saturated conditions.

In order to grow device quality material, stringent control is demanded in terms of flux and susbstrate temperature stabilities. In order to achieve the requirements, the Hg, Te and CdTe flux should have a stability respectively of # 2.5%, 0.5% and 0.3% and the substrate temperature fluctuations during the growth and across the wafer should be smaller than ±0.5°C.

This is achieved in current MBE systems. Excellent thickness and composition uniformities have been measured on HgCdTe epilayers grown on substrates as large as 5-inch in diameter.

The screening of CdZnTe substrates is an essential step since it has been found that impurities diffusing from the substrate in the epilayers are highly detrimental to the control of the electrical properties.

On selected substrates, n-type doping is achieved using Indium. Very high electron mobility and excellent minority carrier lifetime have been measured on annealed In-doped layers with doping levels as low as $2\times10^{15}cm^{-3}$. Below this doping level, non-uniformity in carrier distribution, which is believed to be still associated with diffusion of impurities from the substrate, starts to be seen.

Regarding p-type doping, arsenic is the selected impurity but its incorporation at the Te site is not easy since MBE of HgCdTe occurs under Te-saturated conditions. In most of the approaches utilized so far, a high temperature anneal above 400°C has to be carried out to activate arsenic. Such an anneal invalidates the use of MBE since annealing causes alloying which destroys any sharp structure. In order to keep the integrity of MBE structures, As-delta doping has been carried out. Very interesting results have been obtained using this doping method since as-grown As related p-type HgCdTe epilayers have been obtained. However, such a doping is difficult to control and more experiments are necessary.

The focus of this paper was purposely limited to the MBE growth and characterization of $Hg_{1-x}Cd_xTe$ alloys. In conclusion, it has been shown that MBE is currently a mature growth technology which is able to produce, on a routine basis and at low cost, device quality $Hg_{1-x}Cd_xTe$ material suitable for fabrication of Focal Plane Arrays.

However, MBE has much more to offer since it is the only growth technique, with Metal-Organic MBE, which can be used to grow sophisticated structures necessary for advanced I.R. detectors and which allows also a complete *in situ* process from substrate cleaning to monolithic device processing.

REFERENCES

1. J.P. Faurie and A. Million, J. Cryst. Growth **54,** 582 (1981).

2. D. Arch, J.P. Faurie, J.L. Staudenman, M. Hibbs-Brenner and P. Chow, J. Vac. Sci. Technol.. **A4,** 2101 (1986).

3. J.L. Staudenman, R.D. Knox and J.P. Faurie, J. Vac. Sci. Technol. **A5,** 3161 (1987).

4. Y. Kim, A. Ourmazd, M. Bode and R.D. Feldmann, Phys. Rev. Lett. **63,** 636 (1989).

5. R.W. Yanka, K.A. Harris, L.M. Mohnkern, A.R. Reisinger, T.H. Myers and H. Otsuka, J. Electr. Mater. **22,** 1107 (1993).

6. R.F.C. Farrow, G.R. Jones, G.M. Williams, P.W. Sullivan, W.J.O. Boyle and J.T.M. Wotherspoon, J. Phys. D **12,** L117 (1979).

7. M.I. Abdalla and D.B. Holt, Phys. Stat. Sol (A) **17,** 2647 (1973).

8. G.J. Shimaoka, J. Cryst. Growth **45,** 313 (1978).

9. K. Zanio, Semiconductors and Semimetals, Vol.**13** (1978) Acad. Press, Ed. R.K. Willardson and A.C. Beer.

10. D.B. Holt, Thin Solid Films **24,** 1 (1974).

11. R.F. Brebrick, C.H. Su and P.K. Liao, in Semiconductors and Semimetals, Vol. **19** (1983), chap. 3, Acad. Press, Ed. R.K. Willardson and A.C. Beer.

12. K.C. Mills, Thermodynamic Data for Inorganic Sulphides, Selenides and Tellurides, Butterworths, London (1974).

13. De Nobel, Philips Res. Rept. **14,** 361 (1959).

14. R.F. Brebrick and A.J. Strauss, J. Phys. Chem. Solids, **26,** 989 (1965).

15. K. Takita, K. Masuda, M. Kudo and S. Seki, Appl. Phys. Lett. **37,** 460 (1980).

16. Tse Tung, L. Golonka and R.F. Brebrick, J. Electrochem. Soc. **128,** 45 (1981).

17. P Goldfinger and M. Jeunehomme, Trans Faraday Soc. **59,** 2851 (1963).

18. R.F. Brebrick and A.J. Strauss, J. Phys. Chem. Solids, **25,** 1441 (1964).

19. R.F. Brebrick, J. Electrochem. Soc. **118,** 2014 (1971).

20. H.R. Vydyanath and C.H. Hiner, J. Appl. Phys. **65,** 3080 (1989).

21. S. Sivananthan, X. Chu, J. Reno and J.P. Faurie, J. Appl. Phys. **60,** 1359 (1986).

22. S. Sivananthan, PhD. Thesis (1987).

23. T. Magee, DARPA IR Focal Plane Array Materials and Processing Review (1988), unpublished.

24. A. Million, L. Di Ciocco, J.P. Gaillard and J. Piaguet, J. Vac. Sci. Technol. **A6,** 2813(1988).

25. K.A. Harris, S. Hwang, D.K. Blanks, J.W. Cook Jr., J.F. Schetzina and N. Otsuka, J. Vac. Sci. Technol. **A4,** 2061 (1986).

26. B.K. Wagner, R.G. Benz, II and C.J. Summers, J. Vac. Sci. Technol. **A7,** 295 (1989).

27. D.J. Santelar, J. Vac. Sci. Technol. **A4,** 348 (1986).

28. L.H. Mohnkern, K.A. Harris, R.W. Yanka, T.H. Myers, E.M. Skelly Frame, J. Vac. Sci. Technol. **A3,** 3352 (1990).

29. CEC Wood, D. Desimone, K. Singer and G.W. Wicks, J. Appl. Phys. **53,** 4230 (1982).

30. S.C. Jackson, B.N. Baron, R.E. Rocheleau and T.W.F. Russel, J. Vac. Sci. Technol. **A3,** 1916 (1985).

31. G.L. Hansen, J.L. Schmit and T.N. Casselman, J. Appl. Phys. **53,** 7099 (1982).

32. J. Reno and J.P. Faurie, Appl. Phys. Lett. **49,** 409 (1986).

33. M. Heiblum, E.E. Mendes and L. Osterling, J. Appl. Phys. **54,** 6982 (1993).

34. W.E. Hoke, P.S. Lyman and W.H. Labossier, J. Vac. Sci. Technol. **B5,** 734 (1987).

35. M.D.Lange, PhD Thesis dissertation, University of Illinois at Chicago (1993).

36. S.L. Wright, R.F. Marks and A.E. Goldberg, J. Vac. Sci. Technol. **B6,** 842 (1988).

37. L. Di Cioccio, A. Million, J. Piaguet, G. Rolland, G. Lentz, N. Magnea and H. Mariette, J. Cryst. Growth, **95,** 552 (1989).

38. J.P. Faurie, DARPA IR Focal Plane Array Materials and Processing, (April 1989), unpublished.

39. H.A. Harris, T.H. Myers, R.W. Yarka, L.M. Mohnkern, R.W. Green and N. Otsuka, J. Vac. Sci. Technol. **A8,** 1013 (1990).

40. J.P. Faurie, R. Sporken, S. Sivananthan and M.D. Lange, J. Cryst. Growth **111,** 698 (1991).

41. J.L. Reno, P.L. Gourley, G. Monfroy and J.P. Faurie, Appl. Phys. Lett. **53,** 1747 (1988).

42. J. Cibert, Y. Gobil, K. Saminadayar, S. Tatarenko, A. Chami, G. Feuillet, Le Si Dang and E. Ligeon, Appl. Phys. Lett. **54,** 828 (1989).

43. E. Ligeon, C. Chami, R. Danielou, G. Feuillet, J. Fontenille, K. Saminadayar, A. Pouchet, J. Cibert, Y. Gobil and S. Tatarenko, J. Appl. Phys. **67,** 2428 (1990).

44. Y.P. Chen, S. Sivananthan and J.P. Faurie, J. Electr. Mater. **22,** 951 (1993).

45. Y.P. Chen, J.P. Faurie and S. Sivananthan, SPIE Vol. **2228,** 54 (1994).
46. Sivananthan, M.D. Lange, G. Monfroy and J.P. Faurie, J. Vac Sci. Technol. **B6,** 788 (1988).

47. M.E. de Souza, M. Boukerche and J.P. Faurie, J. Appl. Phys. **68,** 5195 (1990).

48. M. Boukerche, S. Sivananthan, P.S. Wijewarnasuriya, I.K. Soo and J.P. Faurie, J. Vac. Sci. Technol. **A7,** 31 (1989).

49. G.L. Destéfanis, J. Cryst. Growth **86,** 700 (1988).

50. J.P. Faurie, M. Boukerche, S. Sivananthan, J. Reno and C. Hsu, Superlattices and Microstructures **1,** 237 (1985).

51. J.R. Meyer, C.A. Hoffman, F.J. Bartoli, J.W. Han, J.W. Cook, Jr., J.F. Schetzina, X. Chu, J.P. Faurie and J.N. Schulman, Phys. Rev. **B38,** 2204 (1988).

52. R.J. Koestner, H.Y. Liu, H.F. Schaake and T.R. Hanlon, J. Vac. Sci. Technol. **A7,** 517 (1989).

53. S.M. Johnson, D.R. Ringer, J.P. Rosebeck, J.M. Peterson, S.M. Taylor and M.E. Boyd, J. Vac. Sci. Technol. **B10,** 1499 (1992).

54. R.S. List, J. Electr. Mater. **22,** 1017 (1993).

55. J.P. Faurie, Final Technical Report - DARPA Contract No F49620-91-C-0007 (Feb. 1994).

56. J.P. Faurie, A. Million, R. Bock and J.L. Tissot, J. Vac. Sci. Technol. **A1,** 1593 (1983).

57. R.J. Koestner and H.F. Schaake, J. Vac. Sci. Technol. **A6,** 2834 (1988).

58. J.M. Arias, S.H. Shin and E.R. Gertner, J. Cryst. Growth, **86,** 362 (1988).

59. T. Sasaki and N. Oda, SPIE vol. 2228, **86** (1994).

60. J.M. Arias, M. Zandian, J.G.Pasko, S.H. Shin, L.O. Bubulac, R.E. DeWames and W.E. Tennant, J. Appl. Phys. **69,** 2143 (1991).

61. J.P. Faurie and A. Million, Appl. Phys. Lett. **41,** 264 (1982).

62. M.D. Lange, S. Sivananthan, X. Chu and J.P. Faurie, Appl. Phys. Lett. **52,** 978 (1988).

63. R. Sporken, M.D. Lange and J.P. Faurie, SPIE, Vol. **1512,** 155 (1991).

64. R. Sporken, Y.P. Chen, S. Sivananthan, M.D.Lange and J.P. Faurie, J. Vac. Sci. Technol. **B10,** 1405 (1992).

65. T. Tung, L.V. De Armond, R.F. Herald, P.E. Herning, M.H. Kalisher, D.A. Olson, R.F. Risser, A.P. Stevens and S.J. Tighe, SPIE Vol. **1735,** 109 (1992).

66. J. Bajaj, J.M. Arias, M. Zandian, J.G. Pasko, L.J. Kozlowski, R.E. Dewames and W.E. Tennant, U.S. Workshop on the Physics and Chemistry of MCT, extended abstract p. 33 (1994).

67. L. Colombo and G.H. Westphal, SPIE, Vol. **2228,** 66 (1994).

68. M. Boukerche, P.S. Wijewarnasuriya, S. Sivananthan, I.K. Sou, Y.J. Kim, K.K.Mahavadi and J.P. Faurie, J. Vac. Sci. Technol. **A6,** 2830 (1988).

69. L.J. Van der Pauw, Philips Tech. Rev. **20,** 220 (1958).

70. J.P. Faurie, First Technical Report - DARPA Contract No F49620-91-C-0007 (Nov. 1991).

71. T.H. Myers, K.A. Harris, R.W. Yanka, L.M. Mohnkern, R.J. Williams and G.K. Dudoff, J. Vac. Sci. Technol. **B10,** 1438 (1992).

72. M. Boukerche, J. Reno, I.K. Sou, C. Hsu and J.P. Faurie, Appl. Phys. Lett. **48,** 1733 (1986).

73. I.K. Sou, P.S. Wijewarnasuriya, M. Botikerche and J.P. Faurie, Appl. Phys. Lett. **55,** 954 (1989).

74. M. Boukerche, S. Sivananthan, P.S. Wijewarnasuriya, S.S. Yoo, M. DeSouza, I.K. Sou, M.D. Lange and J.P. Faurie, Materials Science Forum, Vol. **65-66,** 389 (1990).

75. J.P. Faurie, S. Sivananthan and P.S. Wijewarnasuriya, SPIE, Vol. **1735,** 141 (1992).

76. H.R. Vydyanath, J. Electrochem. Soc. **128,** 2619 (1981).

77. P.M. Spencer, Br. J. Appl. Phys. **15,** 625 (1964).

78. D. Long, Phys. Rev. **176,** 923 (1968).

79. R. Finkman, J. Appl. Phys. **54,** 1883 (1983).

80. J.R. Meyer, C.A. Hoffman, F.J. Bartoli, D.A. Arnold, S. Sivananthan and J.P. Faurie, Semicond. Sci. Technol. **8,** 805 (1993).

81. D. Lang and J.L. Schmit, Semiconductors and Semimetals, edited by R.K. Willardson and A.C. Beer, Adademic, New York, Vol. **5** (1970)

82. D.L. Polla and C.E. Jones, J. Appl. Phys. **52,** 5118 (1981).

83. M.E. de Souza, Ph.D. Thesis, University of Illinois at Chicago (1991).

84. M.A. Kinch, M.T. Brau and A. Simmons, J. Appl. Phys. **44,** 1649 (1973).

85. M.C. Chen and L. Colombo, J. Appl. Phys. **72,** 4261 (1992).

86. M.Y. Pines and O.M. Stafsudd, Infrared Phys. **20,** 73 (1980).

87. J.S. Blakemore, Semiconductor Statistics, Pergamon, New York (1962).

88. R.G. Pratt, J. Hewett, P. Capper, C.L. Jones and M.T. Quelch, J. Appl. Phys. **54,** 5152 (1983).

89. G.L. Hansen and J.L. Schmit, J. Appl. Phys. **54,** 1639 (1983).

90. P.E. Peterson, J. Appl. Phys. **41,** 3465 (1970).

91. P.S. Wijewarnasuriya, M.D. Lange, S. Sivananthan and J.P. Faurie, J. Appl. Phys. **75,** 1005 (1994).

92. P.S. Wijewarnasuriya, M.D. Lange, S. Sivananthan and J.P. Faurie, accepted for publication in J. Elec. Materials (1994).

93. M.B. Reine, K.R. Maschhoff, S.P. Tobin, P.W. Norton, J.A. Mroczkowski, and R.R. Krueger, Semicond. Sci. Technol. **8,** 788 (1993).

94. P.R. Norton, Opt. Eng. **30,** 1649 (1991).

95. P.S. Wijewarnasuriya, I.K. Sou, Y.J. Kim, K.K. Mahavadi, S. Sivananthan, M. Boukerche and J.P. Faurie, Appl. Phys. Lett. **51,** 2025 (1987).

96. H.R. Vydyanath, J. Electrochem. Soc. **128,** 2609 (1981).

97. M.L. Wroge, D.J. Peterman, B.J. Morris, D.J. Leopold, J.G. Broerman and B.J. Feldman, J. Vac. Sci. Technol. **A6,** 2826 (1988).

98. M.C. Chen, L. Colombo, J.A. Dodge and J.H. Tregilgas, U.S. Workshop on the Physics and Chemistry of HgCdTe (extended abstract p. 71) (1993).

99. P. Capper, J. Cryst. Growth, **57,** 280 (1982).

100. E.S. Johnson and J.L. Schmit, J. Electron. Mater. **6,** 25 (1977).

101. P. Capper, J.A. Roberts, I. Kenworthy, C.L. Jones, J.J.G. Gosrey, C.K. Ard and W.G. Coates, J. Appl. Phys. **64,** 6227 (1988).

102. P. Capper, J. Vac. Sci. Technol. **B9,** 1667 (1991).

103. T.C. Harman, J. Electron. Mater. **8,** 191 (1979).

104. P. Herning, J. Electron. Mater. **13,** 1 (1984).

105. M.H. Kalisher, J. Cryst. Growth, **70,** 365 (1984).

106. T. Tung, J. Cryst. Growth **86,** 161 (1988).

107. H.R. Vydyanath, J.A. Ellsworth and C.M. Devaney, J. Electron. Mater. **16,** 13 (1987).

108. P. Capper, P.A.C. Whiffin, B.C. Easton, C.D. Maxey and I. Kenworthy, Mat. Lett. **6,** 365 (1988).

109. P. Capper, C.D. Maxey, P.A.C. Whiffin and B.C. Easton, J. Cryst. Growth, **97,** 833 (1989)

110. M. Boukerche, P.S. Wujewarnasuriya, S. Sivananthan, I.K. Sou, J. Kim, K.K. Mahavadi and J.P. Faurie, J. Vac. Sci. Technol. **A6,** 2830 (1988).

111. H.R. Vyvyanath, L.S. Lichtmann, S. Sivananthan, P.S. Wijewarnasuryia and J.P. Faurie, J. Electron. Mater, in press (1994).

112. H.R. Vydyanath, R.C. Abbott and D.A. Nelson, J. Appl. Phys. **54,** 1323 (1983).

113. H.R. Vydyanath, Semicond. Sci. Technol. **5,** 5213 (1990).

114. H.R. Vydyanath, J. Vac. Sci. Technol. **B9,** 1716 (1991).

115. S.H. Shin, J.M. Arias, M. Zandian, J.G. Pasko, L.O. Babulac and R.E. DeWames, J. Electron. Mater **22,** 1039 (1993).

116. J.M. Arias, S.H. Shin, J.G. Pasko; R.E. DeWames and E.R. Gertner, J. Appl. Phys. **65,** 1747 (1989).

117. J.M. Arias, J.G. Pasko, M. Zandian, S.H. Shin, G.M. Williams, L.O. Babulac, R.E. DeWames and W.E. Tennant, J. Electron. Mater. **22,** 1049 (1993).

118. R.L. Harper, Jr., S. Hwang, N.C. Giles, J.F. Schetzina, D.L. Dreifus and T.H. Myers, Appl. Phys. Lett. **54,** 170 (1989).

119. J.W. Han, S. Hwang, Y. Lansari, R.L. Harper, Z. Yang, N.C. Giles, J.W. Cook, Jr., J.F. Schetzina and S. Sen, Appl. Phys. Lett. **54,** 63 (1989).

120. K.A. Harris, T.H. Myers, R.W. Yanka, L.M. Mohnkern and N. Otsuka, J. Vac. Sci. Technol. **B9,** 1752 (1991).

121. K.A. Harris, T.H. Myers, R.W. Yanka, L.M. Mohnkern, R.W. Green and N. Otsuka, J. Vac. Sci. Technol. **A8,** 1013 (1990).

122. J.M. Arias, S.H. Shin, D.E. Cooper, M. Zandian, J.G. Pasko, E.R. Gertner, R.E. DeWames and J. Singh, J. Vac. Sci. Technol. **A8,** 1025 (1990).

123. E.R. Blazejewski, J.M. Arias, G.M. Williams, W. McLevige, M. Zandian and J. Pasko, J. Vac. Sci. Technol. **B10,** 1626 (1992).

124. O.K. Wu, G.S. Kamath, W.A. Radford, P.R. Bratt and E.A. Patten, J. Vac. Sci. Technol. **A8,** 1034 (1990).

125. J.T. Cheung, Appl. Phys. Lett. **51,** 1940 (1987).

126. C.J. Summers, R.G. Benz II, B.K. Wagner, J.D. Benson and D. Rajavel, Procs. SPIE **1106,** 1 (1989).

127. G.S. Kamath and O.K. Wu, U.S. Patent No 5,028,561.

128. J.P. Faurie, 2nd annual technical report - DARPA contract # F49620-91-C-0007 (Nov. 1992).

129. S. Sivananthan, P.S. Wijewarnasuriya and J.P. Faurie, U.S. Workshop on HgCdTe (extended abstact p.7) (1993).